2021

Robustness and Accuracy Bounds of Model-based Structural Health Monitoring

Nestor Ramon Polanco
University of Vermont

Robustness and Accuracy Bounds of Model-based Structural Health Monitoring

A Dissertation Presented

by

Néstor R. Polanco

to

The Faculty of the Graduate College

of

The University of Vermont

In Partial Fulfillment of the Requirements
for the Degree of Doctor of Philosophy
in Civil and Environmental Engineering

May, 2021

Defense Date: March 26^{th}, 2021
Dissertation Examination Committee:

Eric M. Hernandez, Ph.D., Advisor
Hamid Ossareh, Ph.D., Chairperson
David V. Rosowsky, Ph.D.
Mandar Dewoolkar, Ph.D.
Donna Rizzo, Ph.D.
Cynthia J. Forehand, Ph.D., Dean of Graduate College

Abstract

The strength and stiffness of structures degrade with time due to a combination of external forces and environmental conditions. A vehicular bridge, an offshore platform, a ship hull, or a wind turbine are examples of structures that for decades must endure cumulative degradation of their mechanical properties due to cyclic loading. Fatigue-induced damage typically starts at the exterior surface of the component unless microscopic or macroscopic imperfections are present in the material's structure. Structural Health Monitoring (SHM) provides a scientific non-destructive framework to estimate the structure's current state and remaining service life. In many model-based structural health monitoring applications, the models are linear, and commonplace is to formulate them based on modal parameters.

The research in this dissertation addresses the implications of model uncertainty to system identification and state estimation. Specifically, determining the highest achievable accuracy in the presence of noise in the measurements, unmeasured excitations, and environmental conditions. The main contributions of this dissertation are summarized as follows: i) derivation of exact mathematical expressions to compute the minimum achievable variance of the identified frequencies and damping ratios from noisy vibration measurements due to initial conditions or external forces, and ii) the development of a weighted sensitivity-based finite element model updating framework to a large scale model of a partially instrumented bridge. Additionally, the dissertation explores the robustness of the Kalman filter in structural dynamics for fatigue monitoring applications.

The dissertation presents recent developments in the feasibility of using global acceleration measurements to assess the level of composite action on operational bridge decks with unknown girder-slab connection stiffness. Our efforts focused on the 58N Bridge constructed in 1963 located on Interstate 89 in Richmond, Vermont, United States. The Bridge has a three-span continuous deck with two build-up outer girders spanning a total length of 558 feet (170.08 m). A portion of the bridge deck was monitored with uni-directional accelerometers and dynamic strain sensors distributed at various locations. Intermittently, for over two years, with measured temperatures ranging from $15°F$ to $87°F$, data was acquired. This data was used to update a finite element model of the deck. The updated model displayed improved prediction capabilities with respect to the original model. Such an updated model can be used as a baseline model for stress analysis.

Citations

Material from this dissertation has been published in the following form:

- Polanco, N. R., & Hernandez, E. M.. (2014). "Finite element model updating of bridge decks with uncertain semi-composite action using global acceleration measurements". *Mechanics Institute 2014 Conference (EMI)*. Mechanics for Sustainable and Resilient Systems. McMaster University, Hamilton, ON, Canada. Award: First place in the Dynamics Committee Student Paper Competition.
- Hernandez, E. M*. & Polanco, N. R*.. (2014). "Reliability-based fatigue monitoring of structures". *Proceedings of the European Workshop in Structural Health Monitoring*, Nantes, France.
- Hernandez, E. M*. & Polanco, N. R*.. (2014). "Uncertainty Quantification in Identified Modal Parameters using Fisher Information Criterion". Proceedings of the XXXII International Modal Analysis Conference (IMAC), Orlando, FL
- Hernandez, E. M*. & Polanco, N. R*.. (2015). "A lower bound for the variance of frequency and damping ratio identified from noisy vibration measurements". *Journal of Structural Control and Health Monitoring*, Volume 23, Issue 1.
- Polanco, N. R. & Hernandez, E. M.. (2015). "Multi-scale stress usage monitoring from global acceleration measurements: experimental validation". *ASCE Engineering Mechanics Conference*, Stanford, California, USA
- Polanco, N. R., May, G. & Hernandez, E. M.. (2016). "Finite element model updating of semi-composite bridge decks using operational acceleration measurements". *Journal of Engineering Structures*, 126, 264-277.
- Polanco, N. R., & Hernandez, E. M.. (2016). "Kalman filter robustness for fatigue usage monitoring of flexible frame structures". *American Control Conference (ACC)*, Boston, MA, USA.

*Authors contributed equally

Dedication

I dedicate my dissertation to:

My nieces and nephew;
Rosalía, Dahlia, Victoria, & Manuel.

My grandparents and grandmothers;
Monica Contreras & Ramon Almánzar; María Tavárez & Ramon Polanco.

My parents;
José M. & Mildre F.

My siblings;
Mónica M., José M., & Mariant.

My Boston Family;
Mr. Lenny, Miss Sue, Sarah, Justin, Charlotte, Shelby, Liam, Scott, Milo, Angelina, & James.

My Vermont Family;
John, C. Jane, Mara, Jessica, & Rachel.

I give my thanks to Prof. Eric M. Hernández. Your continuous guidance and support helped me to stay focused and finish up this work. Your attention to detail and high standards are abilities I will keep with me. Also to Karin, Eric Jr. & Jack, for making my stay in Vermont a bit warmer.

Lastly, and more importantly, to myself;

You struggled, you made all sort of sacrifices, and ultimately placed your Ph.D. on hold. I am so proud of you and that this dissertation is the outcome of your years in graduate school. Be jolly with your journey, be kind to yourself, and proudly step out of the ABD purgatory. Love you Néstor.

Acknowledgements

- The work in this dissertation was partially supported by the University of Vermont (UVM) through the *Graduate College Opportunity Fellowship*.
- Instrumentation and installation costs for the 58-N Bridge were funded by *The Vermont Agency of Transportation (VTrans)*.
- The work in this dissertation was partially supported by the National Science Foundation projects:
  - *BRIGE: Multiscale Model-Data Fusion for Structural Health Monitoring of Fracture Critical Structures* (**ECC-1342190**)
  - *CAREER: Structural Health Monitoring, Diagnosis and Prognosis of Minimally Instrumented Structural Systems* (**CMMI-1453502**).

Their support is gratefully appreciated and acknowledged.

Table of Contents

Citations ii
Dedication iii
Acknowledgements iv
List of Figures x
List of Tables xi

1 Introduction **1**
1.1 Structural Health Monitoring 1
1.2 Definitions 4
1.3 Motivation 8
1.4 Objective 10
1.5 Contributions 10
1.6 Bibliography 13

2 Theoretical/Mathematical Background **17**
2.1 Equation of Motion 17
2.2 Harmonic Load Response Formulas 18
2.2.1 Damped Response 18
2.3 Response to Arbitrary Loading 19
2.4 Laplace Domain Analysis 20
2.5 Fourier Domain Analysis 22
2.5.1 Fourier Transform Discrete-Time 23
2.5.2 Fast Fourier Transform (FFT) 23
2.6 Multi-Degree of Freedom System 24
2.7 Modal Analysis 25
2.8 Static Condensation of the Stiffness Matrix 29
2.9 State-Space Representation 30
2.9.1 Measurements 31
2.9.2 State-Estimation 32
2.9.3 Recursive Estimators 35
2.9.4 Discrete to continuous (d2c) Relationships 37
2.10 System Identification 39
2.10.1 Observability 40
2.11 Bibliography 42

3 Lower Bounds for the Variance of Frequency and Damping Ratio Identified from Noisy Vibration Measurements **43**
3.1 Introduction 43

3.2 Fisher Information . . . 47
3.3 Cramer-Rao Lower Bound . . . 49
3.4 Fisher Information in Free Vibration Displacement Measurements . . 50
3.4.1 Initial Velocity . . . 53
3.4.2 Initial Displacement . . . 55
3.5 Fisher Information in Free Vibration Acceleration Measurements . . . 57
3.5.1 Initial Velocity . . . 58
3.5.2 Initial Displacement . . . 59
3.6 Fisher Information in Forced Vibration Response . . . 61
3.7 Numerical Verification . . . 62
3.7.1 Single Degree of Freedom System - Free Vibration . . . 63
3.7.2 Single Degree of Freedom System - Forced Vibration . . . 64
3.7.3 Verification Using System Identification Results . . . 64
3.8 Heuristic Extension to Multi-degree of Freedom Systems . . . 69
3.9 Verification of Modal CRLB for Multidegree of freedom systems . . . 70
3.10 Conclusions . . . 73
3.11 Bibliography . . . 74

4 Finite element model updating of semi-composite bridge decks using operational acceleration measurements 78
4.1 Abstract . . . 79
4.2 Introduction . . . 79
4.3 Sensitivity-based model updating . . . 85
4.4 Model Formulation . . . 87
4.5 Two Dimensional Model - Simulated Cases . . . 90
4.6 Three Dimensional Model - Simulated Cases . . . 94
4.7 Validation Using Data from an Operational Instrumented Bridge . . . 98
4.7.1 Modeling . . . 98
4.7.2 Instrumentation . . . 99
4.7.3 System Identification . . . 101
4.7.4 Model Updating Results . . . 104
4.7.5 Validation of Updated Finite Element Model . . . 108
4.8 Conclusions . . . 110
4.9 Acknowledgments . . . 112
4.10 Bibliography . . . 113

5 Kalman filter robustness for fatigue usage monitoring of flexible frame structures 116
5.1 Abstract . . . 117
5.2 Introduction . . . 117

5.3 System of Interest 119
5.4 Mathematical Model 120
5.5 Kalman Filter 124
5.6 Strain Estimation and Uncertainty Propagation 125
5.7 Modeling Error 125
5.7.1 Physical Model 126
5.7.2 Covariance matrices 126
5.8 Estimation Results 128
5.9 Conclusions 134
5.10 Acknowledgement 135
5.11 Bibliography 135

6 Conclusions **138**
6.0.1 Intellectual Contributions 138
6.0.2 Broader Impacts 141
6.0.3 Future Work 142

List of Figures

1.1 Principle and organization of a SHM system 2
1.2 Processes of Structural Health Monitoring 3
1.3 Fracture critical structure - I-35W Bridge in Minneapolis 9

2.1 Block diagram of a continuous time classical state estimator (output only) 35
2.2 Classification of SHM methods (Figure 1. of [Shokravi, et al.; 2020] . 40

3.1 Graphical representation of derivatives necessary to compute the Fisher information matrix. In this case the particular parameters used were $x_o = 1$, $\dot{x}_o = 1$, $\omega_n = 10\pi$ and $\xi = 0.02$ 52
3.2 Noise-corrupted free vibration response of SDOF system (top), temporal variation of Fisher information for undamped frequency (middle), temporal variation of Fisher information for damping ratio (bottom) . 65
3.3 Time history of ground motion acceleration (top) and noise-corrupted system response (bottom) 66
3.4 Temporal variation of Fisher information for undamped frequency (top), temporal variation of Fisher information for damping ratio (bottom) . 67
3.5 Variation of the CoV of circular frequency (left) and damping (right) as a function of the identified order of the system. 68
3.6 Illustration of the relative importance of off-diagonal terms in the Fisher information matrix with respect to its diagonal terms and as a function of the distance between consecutive modal frequencies . . . 72

4.1 Two dimensional FEM 90
4.2 Evolution of model parameters a)Rigidity per linear meter and b) elastic modulus of concrete for Case 1 of 2D FEM 92
4.3 Evolution of model parameters a)Rigidity per linear meter and b) elastic modulus of concrete for Case 2 of 2D FEM 93
4.4 Evolution of model parameters a)Rigidity per linear meter and b) elastic modulus of concrete for Case 3 of 2D FEM 93
4.5 Three dimensional FEM of bridge deck (see Fig. 4.10 for additional dimensions) 95
4.6 Sensitivity matrix of first five eigenvalues to concrete elastic modulus and stiffness of shear links. 96
4.7 Evolution of model parameters a)Rigidity per linear meter and b) elastic modulus of concrete for Case 1 of 3D FEM 97

4.8 Evolution of model parameters a)Rigidity per linear meter and b) elastic modulus of concrete for Case 2 of 3D FEM 97
4.9 Photograph of bridge 58N located in Vermont, USA. 99
4.10 (a)Cross section of bridge deck and (b) instrumentation layout (See Fig. 4.5 for the 3D FEM) 100
4.11 Acceleration measurements at various positions along Stringer-1 during the passing of a truck on the travel lane (See Fig. 4.10b for sensor location coordinates) 102
4.12 Identified frequencies from global acceleration measurements. Mean values indicated by dotted lines 103
4.13 Frequencies of deck as a function of the effective stiffness of the shear connectors. Shown are the values of the initial stiffness (solid circle) and the updated value (solid triangle) 106
4.14 Mode shapes on the concrete slab corresponding to the updated model. On the left is the result of the constrained model updating and on the right the results of the unconstrained. 107
4.15 Comparison of maximum bending moments in various elements of the bridge deck 108
4.16 Comparison of acceleration response (updated model vs. orignal model) at stringer 1 (position P-5) when a test vehicle crosses the bridge in the travel lane at 60 mph. 109
4.17 Comparison of acceleration response (updated model vs. orignal model) at stringer 2 (position P-5) when a test vehicle crosses the bridge in the travel lane at 60 mph. 110

5.1 Dimensions of experimental structure (mm) 119
5.2 Experimental setup 120
5.3 From left-to-right: (a) The system, (b) Model M1, a frame with lumped masses and (3) Model M2, a shear-beam model with lumped masses. Dimensions in mm 121
5.4 Comparison of modal frequency and damping ratio between models and identified from vibration tests in test structure. 126
5.5 Power spectral density of the excitation (assumed unmeasured for the estimation). 127
5.6 Estimated power spectral density of the acceleration measurement noise. (According to Fig. 5.1) 128
5.7 Strain estimation Case 0: Location 1 130
5.8 Strain estimation Case 1: Location 1 130
5.9 Strain estimation Case 2a: Location 1 131
5.10 Strain estimation Case 2b: Location 1 131

5.11 Strain estimation Case 2*c*: Location 1 132
5.12 Strain estimation Case 2*d*: Location 1 132
5.13 Strain estimation Case 2*e*: Location 1 133
5.14 Strain estimation Case 3: Location 1 133

List of Tables

2.1 Summary of discrete Kalman filter equations - Gelb [Gelb; 1996] . . . 37
2.2 Summary of Discrete to Continuous (d2c) relationships 38

3.1 Comparison of System Identification Results with CRLB 68
3.2 Comparison of System Identification Results with CRLB 72

4.1 System and initial frequencies (prior to updating) for Cases 1, 2 and 3 in the 2D Model 91
4.2 System and initial model frequencies (prior to updating) for Cases 1 and 2 in the 3D Model 95
4.3 Model Parameters - Using complete data set 105
4.4 Comparison of frequencies Bridge 58N - Using complete data set . . . 105
4.5 Model Parameters - Using reduced data set 105
4.6 Comparison of frequencies Bridge 58N - Using reduced data set . . . 105

5.1 Summary of Cases 129
5.2 Strain Error RMS 134
5.3 KF Estimated Variance 134

Chapter 1

Introduction

1.1 Structural Health Monitoring

The performance of an engineering structure will degrade during its operational life. Structural Health Monitoring (SHM) aims to provide a continuous diagnosis of the "state" of the materials, the different parts, and the full assembly of these parts constituting the structure as a whole [Balageas et. al.; 2006]. In other words, SHM is the process of implementing a damage identification strategy for aerospace, civil, and mechanical engineering [Deraemaeker et. al.; 2010]. [Rytter; 1993] described four elements (or levels) of damage identification: 1) Detection: a qualitative indication that damage might have occurred; 2) Localization: the probable location of the damage; 3) Assessment: an estimate of the severity of the damage; and 4) Prediction: estimate of the future performance of the component (or structure) as damage accumulates. All these elements require various levels of data, signal and/or information processing. Signal processing is essential for implementation of any SHM technique. [Staszewski & Worden; 2009] describes six major areas where signal processing has an important

role to play in SHM: measurements and data acquisition; data processing; feature extraction, selection, and compression; pattern recognition and machine learning; reliability and statistical analysis; uncertainties and information gaps. Figure 1.1 depicts the principle and organization of a SHM system (as shown in [Balageas et. al.; 2006]).

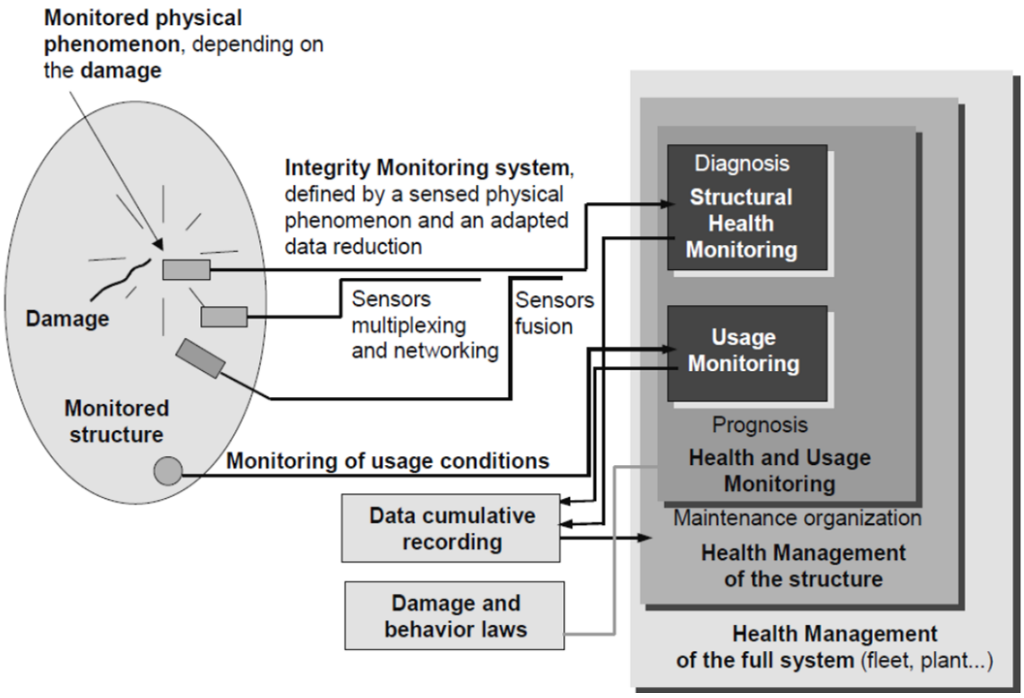

Figure 1.1: Principle and organization of a SHM system

Most SHM techniques can be classified into physics-based methods and data-based methods; though a combination of the two is common [Farrar & Lieven; 2007]. Physics-based methods, also known as model-based methods, combine the physical properties of a structure, employing a mathematical model, with sensor measurements (also known as model-data fusion). These methods are useful to predict the response of a structure to new loading conditions and new state configurations (damage). A disadvantage of these methods is that they could become computationally intensive,

so the model selection is paramount. Data-based methods purely rely on sensor measurements for damage identification, typically (but not always) through a pattern recognition technique. Although these methods can be computationally efficient and could inform that a change in the structural response as occurred, they aren't able to classify the nature of the change. In the context of this dissertation, we will follow a Model-Based offline approach (see figure 1.2 and follow the discontinuous lines).

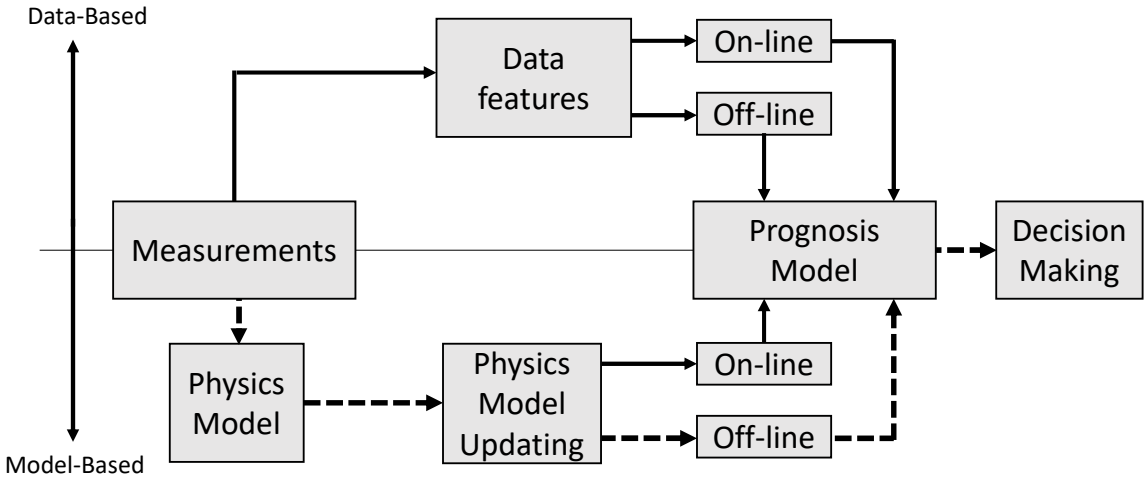

Figure 1.2: Processes of Structural Health Monitoring

In this dissertation, the author proposes several algorithms to asses and improve the robustness of model-based structural health monitoring. The proposed algorithms are validated using experiments with an increasing level of complexity: 1) model of a single degree of freedom (DOF) structure, 2) model a 30-DOF of a real small scale flexible-type frame structure in our laboratory, and 3) a large scale model of a partially instrumented bridge on I-89 (Vermont, USA) with traffic-induced data.

1.2 Definitions

The purpose of this section is to establish core terminologies and definitions used throughout the dissertation:

- *Damage:*
  - [Worden & Dulieu-Barton; 2004]: is when the structure is no longer operating in its ideal condition but can still function satisfactorily, i.e. in sub-optimal manner.
  - [Farrar & Worden; 2007]: is defined as changes to the material properties and/or geometric properties of these systems, including changes to the boundary conditions and system connectivity, which adversely affect the system's performance.
  - [Sohn, et. al.; 2004]: can be defined as changes introduced into a system that adversely affects its current or future performance. Implicit in this definition is the concept that damage is not meaningful without a comparison between two different states of the system, one of which is assumed to represent the initial, and often undamaged, state.
- *Damage Prognosis* [Sohn, et. al.; 2004]: estimates of the remaining service life of a structure given the measurement and assessment of its current damaged state and accompanying its predicted performance in the anticipated future loading environments. Every industry is interested in detecting degradation and deterioration in its structural and mechanical infrastructure at the earliest possible state and in predicting the remaining useful life of the systems. Damage

diagnosis and prognosis solutions can be used to monitor systems to confirm system integrity in normal and extreme loading environments, to estimate the probability of mission completion and personnel survivability, to determine the optimal time needed for preventive maintenance, and to develop appropriate design modifications that present observed damage propagation.

- *Fatigue:*
  - [Poncelet; 1870]: under the action of alternating tension and compression, the most perfect string may fail in fatigue.
  - [Cook & Young; 1999]: refers to the initiation and gradual propagation of cracks under cyclic loading. In parts that fail after a great many cycles of loading, cracks being with yielding on a very small scale. A flaw, inclusion, void, or surface scratch can raise local stresses high enough to produce yielding in a crystal whose planes are oriented parallel to the largest shear stress. With cycling, the crystal strain hardens and cracks. Micro-cracks grow, join, and eventually produce a macro crack, whose orientation is usually perpendicular to the maximum principal stress. The rate of crack growth increases with crack length, and can be related to stress intensity factors at the crack tip. When the crack reaches a critical length, the part suddenly breaks by brittle fracture. Most fatigue cracks begin on a surface, because it is usually where stresses are highest. Also, flaws that initiate cracks are more likely to be found on the surface than internally.
- *Fault* [Worden & Dulieu-Barton; 2004]: is when the structure can no longer operate satisfactorily. If one defines the quality of a structure or system as

its fitness for purpose or its ability to meet customer or user requirements, it suffices to define a fault as a change in the system that produces an unacceptable reduction in quality.

- *Fracture Control Plan*:
  - [McHenry & Rolfe; 1980]: engineering procedures and requirements that contribute to the prevention of fracture in metal structures. The systematic application of these practices to the prevention of fracture in a particular structure is accomplished by either the code approach or the performance specification approach to fracture control.
  - [NASA SP-8057; 1972]: set of policies and procedures intended to prevent structural failure due to the initiation or propagation of cracks or crack-like defects during fabrication, testing, and operation.
- *Fracture Critical Members (FCM)*:
  - [NASA SP-8057; 1972]: are defined as those members whose failure could result in loss of the aircraft and whose stress levels are limited by the fracture mechanics analysis requirements. In summary, fracture-critical members are identified on the basis of the consequence and likelihood of fracture.
  - [AASHTO/AWS D1.5; 2002]: are tension members or tension components of bending members (including those subject to reversal of stress), the failure of which would be expected to result in collapse of the bridge. Members and components that are not subject to tensile stress under any condition of live load shall not be defined as fracture critical.

- *Robustness*:
  - [Vander Heyden et al.; 2001]: the ability to reproduce the (analytical) method in different laboratories or under different circumstances without the occurrence of unexpected differences in the obtained result(s).
  - [Mohsen & Cekecek; 2000]: the system is expected to perform its intended function under all operating conditions (different causes of variations) throughout its intended life without necessarily eliminating noise factors (noise factors are defined as disturbance factors that cause system functional variability).
  - [Stelling et. al.; 2004]: the persistence of a system's characteristic behavior under perturbations or conditions of uncertainity.
- *State* [Kalman; 1960]: some quantitative information (a set of numbers, a function, etc.) which is the least amount of data one has to know about the past behavior of the system in order to predict its future behavior. The dynamics is then described in terms of state transitions, i.e., one must specify how one state is transformed into another as time passes.
- *Uncertainty*:
  - [Schultz et al.; 2010]: is a lack of knowledge. Input uncertainty arises from a lack of knowledge about the true value of quantities used in analyzing a decision. Often, these quantities are found in scientific models that are used to support a decision. Model uncertainty is about what variables, assumptions, and functions best characterize the processes being modeled. In practice, model uncertainties are much more difficult to deal with than

input uncertainties because they require the analyst to propose and evaluate competing models.

– [Grebici et al.; 2008]: is often considered as a lack of knowledge that may introduce risks to the outcome and execution of a process. Reducible or epistemic uncertainty can be decreased through further studies, measurements and expert consultation. However, the irreducible or stochastic variability is inherent to the physical system such as the dimensional variation in the manufactured components and cannot be reduced through additional studies or measurement.

1.3 Motivation

For structures subjected to dynamic effects such as wind loads, traffic loads, waves, shocks, etc.; fatigue induced damage is critical and accounts for over 50% of failures [Sundararajan; 1995]. In this dissertation we are interested in fatigue damage on fracture critical structures. A fracture critical structure is one in which the failure of a small number of elements (sometimes a single one) can generate systematic structural collapse; typically seen in cantilever type structures such as wind turbines, chimneys, and in non-redundant structures such as truss-type bridges, among others. These types of structures received national attention August, 1st 2007 when the I-35W steel truss bridge collapsed into the Mississippi river. The bridge is shown in figures 1.3a and 1.3b before and after the collapse respectively. The bridge was visually inspected every year since 1993 and in 2001 a report noted the presence of cracks and clear signs of fatigue [Report $MN/RC - 2001 - 10$]. After over a year of investigations,

the National Transportation Safety Board concluded that the sudden failure was originated by an undersized gusset plates (figure 1.3c). Based on the latest data from the National Bridge Inventory approximately 7.5% of all bridges in the United States and its territories are classified as "poor" condition [National Bridge Inventory; 2019]. This percentage increases to 54.7% including those with a "fair" condition assessment. The American Society of Civil Engineers scores the United States infrastructure with a sicre of **D+** [ASCE Infrastructure Report Card; 2017]. This score hasn't change since 2013.

(a) Before collapse - Side view of the bridge showing steel structural members

(b) After collapse

(c) Buckled gusset plates - National Transportation Safety Board

Figure 1.3: Fracture critical structure - I-35W Bridge in Minneapolis

In [Doebling et. al.; 1996], [Doebling et. al.; 1998], and [Sohn, et. al.; 2004] the authors provide reviews of the technical literature on vibration-based structural health monitoring. A subset of critical issues identified by the authors are: 1) Dependence on prior analytical models and/or prior test data (having a detailed FEM of the structure or presuming that a data set from the undamaged structure is available), and 2) the level of sensitivity of the modal parameters have to small flaws in a structure. The research in this dissertation addresses the implications of model uncertainty,

in the context of these issues, to system identification and state estimation. We are interested in determining the highest achievable estimation accuracy due to the presence of noise in the measurements, unmeasured excitations, and environmental conditions.

1.4 Objective

This dissertation investigates the propagation of modeling and measurement errors in system identification and state estimation. The particular application of interest is vibration-based fatigue monitoring of fracture-critical structures. The overall approach is probabilistic and the research methods employed are a combination of analytic, computational, and experimental.

1.5 Contributions

The main contributions of this dissertation are summarized below:

- Chapter 3 explores the implementation of the Fisher information and the Cramer-Rao lower bound (CRLB) as means to determine bounds for the variance of identified natural frequencies and damping ratios from noisy vibration measurements. We derive exact mathematical expressions that compute the minimum achievable bounds of the variance of identified natural frequencies and damping ratios from simulated noisy vibration measurements by initial conditions or measured excitations. The proposed bounds establish a reference level comparable to second order statistics of the system identification results. We also

demonstrate and quantify that there must be significantly more uncertainty in the identified modal damping ratios than in natural frequencies. This is a fact that stands independently of the system identification algorithm that it is employed, as long as the algorithm is unbiased.

- Chapter 4 explores a weighted sensitivity-based finite element model updating methodology. We propose a method that utilizes vertical acceleration measurements to determine the degree of composite behaviour of an operational bridge deck with unknown/uncertain installation of shear connections. The free parameters of the methodology are: the rigidity per unit length of the beam-slab interface and the elastic modulus of concrete. The proposed methodology has several key features: 1) it is intrinsically independent of the type of sensing, 2) it identifies the free parameters from noisy operational measurements, 3) it is more affordable by requiring a significant smaller number of measurements compared to those needed by traditional methodologies (dynamic strain sensors), 4) it is easy to implement to large complex finite element models, 5) it provides an insight to how the environmental conditions affects the free parameters, 6) the free parameters are based on physical and material properties making them easy to intuitively validate, 7) the updated finite element model displayed improved prediction capabilities with respect to the original model, and 8) the updated finite element model can be used as a base-line model for stress analysis. A limitation of the methodology is that although the stiffness of the deck can be assessed, no much information can be inferred regarding the deck's ultimate capacity. This is because various configurations of a shear connection can provide similar stiffness yet provide quite different post-yielding behavior.

- Chapter 5 investigates the robustness and sensitivity of the Kalman filter (KF) to estimate the stress and strain fields, and their corresponding uncertainty, throughout a building-type flexible structure from operational acceleration measurements. We investigate how these estimates are affected by varying sources of errors in the stochastic description of the measurement noise and unmeasured excitations, and in the physics of the mathematical model that describes the structure. We instrumented the structure with strain sensors in various locations and compared the measurements second order statistics with those of the strain field. In this paper we propose a formulation that transforms the KF state estimates into strain estimates and propagates their uncertainty bounds to strain field uncertainty. It was found that the propagation of the KF estimates underestimates the propagated estimation of the strain field variance. We show that, in the experimental setting, the KF's essential whiteness assumption of the parametric errors is not satisfied. Nevertheless, the KF yields in accurate mean estimates as long has no modeling error is considered. The mean estimates accuracy have a significant drop once changes in the physics of the model of the structure (modeling error) is considered. Modelling errors, that are within the range of practical engineering models, can have a significant detrimental effect in the estimation quality. To utilize more complex and detailed models is not the answer. The computational demand and accuracy of the solution of the sequential state estimation algorithm is related to the size of the model. A trade off between the detail of the representation of the physics of the structure and an acceptable estimation quality needs to be made. We need better models in the engineering practice.

1.6 Bibliography

[ASCE Infrastructure Report Card; 2017] American Society of Civil Engineers. *2017 Infrastructure Report Card*. `https://www.infrastructurereportcard.org/`

[AASHTO/AWS D1.5; 2002] Bridge Welding Code. *Report :FHWA-HIF-19-088. Infrastructure Office of Bridges and Structures*.

[Balageas et. al.; 2006] Editor(s): Balageas, D., Fritzen, C.P. & Güemes, A. (2006). *Structural Health Monitoring*. ISTE Ltd.

[Cook & Young; 1999] Cook, R. D. & Young, W. C. (1999). *Advanced Mechanics of Materials*, 2nd Edition, Pearson.

[Deraemaeker et. al.; 2010] Editor(s): Deraemaeker, A. & Worden, K. (2010).. New Trends in Vibration Based Structural Health Monitoring, *Part of the CISM Courses and Lectures book series*, (CISM, volume 520).

[Doebling et. al.; 1996] Doebling, S.W., Farrar, C.R. Prime, M.B. & Shevitz, D.W. (1996). Damage Identification and Health Monitoring of Structural and Mechanical Systems From Changes in their Vibration Characteristics: A literature Review. *Los Alamos National Laboratory report LA-13070-MS*.

[Doebling et. al.; 1998] Doebling, S. W.; Farrar, C.; Prime, M.B. & Sehvitz, D.W. (1998). A Review of Damage Identification Methods that Examine Changes in Dynamic Properties. *Shock and Vibration Digest*, 30(2):91-105.

[Eykhoff; 1974] Eykhoff, P. (1974). *System Identification: parameter and state estimation.* John Wiley and Sons Inc., New York, N.Y.

[Farrar & Lieven; 2007] Farrar, C. & Lieven, N. A. J. (2007). Damage prognosis: The future of structural health monitoring. *Philosophical transactions. Series A, Mathematical, physical, and engineering sciences*, 365(1851):623-32.

[Farrar & Worden; 2007] Farrar, C.R. & Worden K. (2007). An introduction to structural health monitoring. *Philosophical transactions. Series A, Mathematical, Physical, and Engineering Sciences*, 365(1851), 303-315.

[Friswell & Mottershead; 1995] Friswell, M.I. & Mottershead, J. E. (1995). Finite Element Model Updating in Structural Dynamics. *Kluwer Academic Publishers, Dordrecht*.

[Grebici et al.; 2008] Grebici, K., Goh, Y. M., & McMahon, C. (2008). Uncertainty and risk reduction in engineering design embodiment processes. *10th International Design Conference, Dubrovnik, Croatia, Product development models and strategies*, 143-156.

[Juang; 1994] Juang, J-N. (1994). *Applied system identification*, PTR Prentice Hall.

[Kalman; 1960] Kalman, R. E. (1960). A new approach to linear filtering and prediction problems. *Transactions of the ASME-Journal of Basic Engineering*, 82(Series D):35-45.

[Ljung; 1999] Ljung, L. (1999). *System Identification*, Prentice Hall. Upper Saddle River, NJ.

[Maia & Silva; 1997] Maia, N. M. & Silva, J. M. (Eds.). (1997). *Theoretical and Experimental Modal Analysis*. Research Studies Press Ltd. Hertfordshire, England.

[McHenry & Rolfe; 1980] McHenry, H. I. & Rolfe, S. T. (1980). *Fracture Control Practices for Metal Structures*, National Bureau of Standards Report NBSIR 79-1623.

[Mohsen & Cekecek; 2000] Mohsen, H. A. & Cekecek, E. (2000). Thoughts on the use of Axiomatic Design with the product development process. *First International Conference on Axiomatic Design*.

[National Bridge Inventory; 2019] (2019). *National Bridge Inventory* U.S. Department of Transportation. Federal Highway Administration. `https://www.fhwa.dot.gov/bridge/britab.cfm`.

[NASA SP-8057; 1972] NASA SP-8057 (1972). *Structural Design Criteria Applicable to a Space Shuttle*.

[Overschee & De Moor; 1996] Van Overschee, P. & De Moor, B. (1996). *Subspace Identification for Linear Systems: Theory.* Kluwer Academic Publications.

[Pintelon & Schoukens; 1996] Pintelon, R. & J. Schoukens (1996). *System Identification: A frequency domain approach*, 2^{nd} Edition.

[Poncelet; 1870] Poncelet, J. V. (1870). *Introduction à la mécanique industrielle physique ou expérimentale*, Paris:Gauthier-Villars.

[Report $MN/RC-2001-10$] (2001). Minnesota Department of Transportation. Fatigue Evaluation of the Deck Truss of Bridge 9340 (Report). *Report* $MN/RC-2001-10$, Minnesota Local Road Research Board.

[Rytter; 1993] Rytter, A. (1993). Vibration based inspection of civil engineering structures. *Ph.D. Dissertation*, Department of Building Technology and Structural Engineering, Aalborg University, Denmark.

[Schultz et al.; 2010] Schultz, M. T., Mitchell, K. N., Harper, B. K., & Bridges, T. S. (2010). *Decision Making Under Uncertainty*, ERDC TR-10-12. US Army Corps of Engineers - Engineer Research and Development Center.

[Sohn, et. al.; 2004] Sohn, H., Farrar, C. R., Hemez, F. M., Shunk, D. D., Stinemates, D. W., Nadler, B. R., & Czarnecki, J. J. (2004). *A Review of Structural Health Review of Structural Health Monitoring Literature 1996-2001*, United States.

[Söderström & Stoica; 1989] Söderström, T. & Stoica, P. (1989). *System Identification.* Prentice-Hall, Englewood Cliffs.

[Staszewski & Worden; 2009] Staszewski, W. J. & Worden. K. (2009). *Encyclopedia of Structural Health Monitoring*. Editors: Boller, C. Chang, Fu-Kuo. & Fujino, Y. John Wiley & Sons, Ldt.

[Stelling et. al.; 2004] Stelling, J., Sauer, U., Szallasi, Z., Doyle, F.J. 3rd, & Doyle, J. (2004). Robustness of cellular functions. *Cell*, 118(6):675-85.

[Sundararajan; 1995] Sundararajan, C. (1995). *Probabilistic Structural Mechanics Handbook: Theory and Industrial Applications*. Chapman & Hall.

[Vander Heyden et al.; 2001] Vander Heyden, Y., Nijhuis, A., Smeyers-Verbeke, J., Vandeginste, B. G., & Massart, D. L. (2001).Guidance for robustness/ruggedness tests in method validation. *Journal of pharmaceutical and biomedical analysis*, 24(5-6), 723-753.

[Worden & Dulieu-Barton; 2004] Worden, K. & Dulieu-Barton, J. M. (2004). An overview of intelligent fault detection in systems and structures. *Structural Monitoring*, 3, 85-98.

[Zárate & Caicedo; 2008] Zárate, B. A. & Caicedo, J. M. (2008). Finite element model updating: Multiple alternatives. *Engineering Structures*, 30, 3724-3730.

Chapter 2

Theoretical/Mathematical Background

2.1 Equation of Motion

The equation of motion of a linear single degree of freedom (SDoF) system is given by

$$m\ddot{x}(t) + c\dot{x}(t) + kx(t) = p(t) \tag{2.1}$$

where m is the mass (inertia element), k is the stiffness (elastic element), c is the viscous damping constant (dissipative element), and $p(t)$ represents the external load at time (t). The initial conditions consist in $x(t=0) = x_o$ and $\dot{x}(t=0) = v_o$. By defining

$$\omega_n = \sqrt{\frac{k}{m}} \tag{2.2}$$

and

$$c = 2m\omega_n\xi \tag{2.3}$$

with ξ representing the fraction of critical damping, the equation of motion can be re-written as

$$\ddot{x}(t) + 2\omega_n\xi\dot{x}(t) + \omega_n^2 x(t) = \frac{p(t)}{m} \tag{2.4}$$

2.2 Harmonic Load Response Formulas

2.2.1 Damped Response

The response of a damped SDoF system to a harmonic load ($p(t) = p_o \sin(\Omega t)$) and to arbitrary initial conditions x_o and v_o is given by

$$x(t) = Z_d \sin(\Omega t + \phi) + e^{-\omega_n\xi t}\left[E\sin(\omega_d t) + F\cos(\omega_d t)\right] \tag{2.5}$$

where Z_d is given by

$$Z_d = \frac{p_o}{k}\frac{1}{\sqrt{\left(1 - \left(\frac{\Omega}{\omega_n}\right)^2\right)^2 + \left(2\xi\frac{\Omega}{\omega_n}\right)^2}} \tag{2.6}$$

and

$$\phi = atan\left(\frac{-2\xi\frac{\Omega}{\omega_n}}{1 - \left(\frac{\Omega}{\omega_n}\right)^2}\right) \tag{2.7}$$

The coefficients E and F are given by

$$E = \frac{\xi\omega_n x_o + v_o - Z_d\left[\xi\omega_n sin(\phi) + \Omega cos(\phi)\right]}{\omega_d} \tag{2.8}$$

$$F = x_o - Z_d sin(\phi) \tag{2.9}$$

The portion of the response given by $x(t) = Z_d \sin(\Omega t + \phi)$ is usually denoted as the "steady-state response".

2.3 Response to Arbitrary Loading

The response of a SDoF system to an arbitrary loading can be computed for any time of interest t using the following convolution integral (also known as Duhamel's integral)

$$x(t) = \int_{-\infty}^{t} h(t-\tau)p(\tau)d\tau = \int_{-\infty}^{t} h(\tau)p(t-\tau)d\tau \tag{2.10}$$

If $p(t) = 0 \quad \forall t \leq 0$, then the integral simplifies to

$$x(t) = \int_{0}^{t} h(t-\tau)p(\tau)d\tau = \int_{0}^{t} h(\tau)p(t-\tau)d\tau \tag{2.11}$$

Response Spectrum

The response spectrum of a load time history $p(t)$ is defined as

$$\max r(t) \quad \forall t \quad s.t. \quad r(t) = f(x(t)) \tag{2.12}$$

where $f(x(t))$ is a function of $x(t)$ such as displacement, velocity, reaction force, etc.

2.4 Laplace Domain Analysis

The Laplace transform $\mathcal{X}(s)$ of a function $x(t)$ is defined as

$$\mathcal{X}(s) = \mathcal{L}(x(t)) = \int_0^\infty x(t)e^{-st}dt \tag{2.13}$$

It can be shown that

$$\mathcal{L}(\dot{x}(t)) = s\mathcal{L}(x(t)) = s\mathcal{X}(s) - x_o \tag{2.14}$$

Similarly

$$\mathcal{L}(\ddot{x}(t)) = s^2\mathcal{L}(x(t)) + sx_o + v_o = s^2\mathcal{X}(s) - sx_o - v_o \tag{2.15}$$

Applying these results to the equation of motion of linear SDoF systems we obtain

$$ms^2\mathcal{X}(s) + cs\mathcal{X}(s) + k\mathcal{X}(s) = \mathcal{P}(s) + x_o\,(1+s) + v_o \tag{2.16}$$

The solution, in the Laplace domain is given by

$$\mathcal{X}(s) = \frac{\mathcal{P}(s) + x_o\,(1+s) + v_o}{ms^2 + cs + k} \tag{2.17}$$

In the special case of zero initial conditions

$$\mathcal{X}(s) = \mathcal{P}(s)\frac{1}{ms^2 + cs + k} = \mathcal{P}(s) \cdot \mathcal{H}(s) \tag{2.18}$$

which turns out to be an algebraic equation. One of the advantages of working in the Laplace domain is that one can turn a linear differential equation into an algebraic equation. The function $\mathcal{H}(s)$ is known in control literature as the Transfer function.

The transfer function can be re-written as

$$\mathcal{H}(s) = \frac{1}{ms^2 + cs + k} = \frac{1}{m(s^2 + 2\omega_n\xi s + \omega_n^2)} = \frac{1}{m(s - s_1)(s - s_2)} \tag{2.19}$$

where

$$s_{1,2} = -\omega_n\xi \pm i\omega_d \tag{2.20}$$

The values $s_{1,2}$ are known as the poles of the transfer function. It is trivial to show that $\forall\ 0 < \xi < 1$

$$|s_{1,2}| = \omega_n \tag{2.21}$$

i.e. the poles of the transfer function lie in a circle of radius ω_n.

In order to return to the time domain, one must apply an inverse Laplace transform to $\mathcal{X}(s)$. This involves using the Bromwich formula

$$x(t) = \lim_{R\to\infty} \int_{a-iR}^{a+iR} \frac{1}{2\pi i}\mathcal{X}(s)e^{st}ds \tag{2.22}$$

where a is taken to the right of all the singularities of $\mathcal{X}(s)$. There are also many

available tables of Laplace transform pairs, which can be very useful and save time.

2.5 Fourier Domain Analysis

Fourier analysis of a periodic function refers to the extraction of the series of sines and cosines (continuous time) or coefficients (discrete time) which when superimposed will reproduce the function. This transformation is a mathematical method of a function in the time into a function in the frequency domain.

The Fourier transform is the Laplace transform evaluated along the imaginary axis, so $s = i\omega$.

$$\mathcal{X}(i\omega) = \int_{-\infty}^{\infty} x(t)e^{-i\omega t}dt \tag{2.23}$$

The inverse Fourier transform is given by

$$x(t) = \frac{1}{2\pi}\int_{-\infty}^{\infty} \mathcal{X}(i\omega)e^{i\omega t}d\omega \tag{2.24}$$

The relationship between force and displacement in the Fourier domain (also commonly referred to as frequency domain) is given by

$$\mathcal{X}(\omega) = \mathcal{P}(\omega)\frac{1}{-m\omega^2 + i\omega c + k} \tag{2.25}$$

A useful result is

$$\mid \mathcal{X}(\omega) \mid = \mid \mathcal{P}(\omega) \mid \frac{1/m}{\sqrt{(\omega_n^2 - \omega^2)^2 + 4\omega_n^2\omega^2\xi^2}} = \mathcal{P}(\omega) \cdot \mathcal{H}(\omega) \tag{2.26}$$

2.5.1 Fourier Transform Discrete-Time

In SHM, measurements are sampled points from the vibrations of the structure of interest in the time domain. By transforming these signals into the frequency domain, we get insightful characteristics of the dynamics of the system.

$$X_k = \sum_{n=0}^{N-1} x_n e^{-i2\pi kn/N}$$

where X_k is called the frequency spectrum of the signal, $n = 0, \ldots, N-1$, N is the length of the signal, and k refers to the kth sample.

To calculate the transform, by taking a look to the expression above, we can see that it is nothing more than a straight forward linear operation of $X_{Nx1} = \mathbf{F_{NxN}} x_{Nx1}$, where $\mathbf{F}_{NxN}$ is called the Fourier Matrix and $\mathbf{F_{kn}} = e^{-i2\pi kn/N}$

2.5.2 Fast Fourier Transform (FFT)

[Cooley & Tukey; 1965] shows that we can split the computation of the DTF into two smaller parts. They separated the DTF into even and odd indexed sub-sequences

$$\begin{cases} n = 2m & if\, even \\ n = 2m+1 & if\, odd \end{cases}$$

where $m = 1, 2, \ldots, \frac{N}{2} - 1$. After some algebra manipulation, we end up with the summation of two terms that can be computed simultaneously

$$
\begin{aligned}
X_k &= \sum_{n=0}^{N-1} x_n e^{-i2\pi kn/N} \\
&= \sum_{m=0}^{N/2-1} x_{2m} e^{-i2\pi k(2m)/N} + \sum_{m=0}^{N/2-1} x_{2m+1} e^{-i2\pi k(2m+1)/N} \\
&= \sum_{m=0}^{N/2-1} x_{2m} e^{-i2\pi km/(N/2)} + e^{-i2\pi km/(N)} \sum_{m=0}^{N/2-1} x_{2m+1} e^{-i2\pi km/(N/2)} \\
&= x_{even} + e^{-i2\pi km/(N)} x_{odd}
\end{aligned}
$$

The advantage in solution time is related to the number of operations that the DTF needs vs the FFT. DTF requires $O(N^2)$ (operations) = N (multiplications) $\times$ N (additions). The FFT reduces the number of computations from $O(N^2)$ to $O(N \log_2 N)$.

2.6 Multi-Degree of Freedom System

In a structural system with n interconnected masses it is necessary to account for the forces being transmitted through the connections. The equation of motion of every mass will include coupling terms that involve the motion of one or more of the remaining masses. In the case of linear viscous damping, the m equation of motions can be written in matrix form as

$$\mathbf{M}\ddot{x}(t) + \mathbf{H_c}\dot{x}(t) + \mathbf{K}x(t) = f(t) \tag{2.27}$$

The three resulting matrices are typically denoted as: $\mathbf{M}$, the mass matrix, $\mathbf{H_c}$ damping matrix, and $\mathbf{K}$ is the stiffness matrix. The time varying vector $\mathbf{x(t)}$ is the

displacement of the **m** masses at time **t**. The right hand side $f(t)$ is the load vector at time t applied at the corresponding masses.

2.7 Modal Analysis

The objective of modal analysis is to decouple the equations of motion. We wish to transform the set of m interdependent equations to m independent equations that can be solved independently. To begin, consider the undamped equation of motion

$$\mathbf{M}\ddot{x}(t) + \mathbf{K}x(t) = 0 \tag{2.28}$$

Assume a solution of the form

$$x(t) = A\phi \sin(\omega t) \tag{2.29}$$

and second derivative given by

$$\ddot{x}(t) = -A\phi\omega^2 \sin(\omega t) \tag{2.30}$$

where A is a scalar, ϕ is a vector, and ω is a circular frequency. Substituting this *ansatz* into the equation of motion we obtain

$$-\mathbf{M}\phi\omega^2 \sin(\omega t) + \mathbf{K}A\phi \sin(\omega t) = 0 \tag{2.31}$$

Eliminating common terms we get

$$\mathbf{K}\phi = \mathbf{M}\phi\lambda \tag{2.32}$$

This can be re-written in two common equivalent forms, such as

$$(\mathbf{K} - \mathbf{M}\lambda)\,\phi = 0 \tag{2.33}$$

$$\mathbf{M}^{-1}\mathbf{K}\phi = \phi\lambda \tag{2.34}$$

These equations mean that if you can find any ϕ and λ that satisfy these equations, then the ansatz is correct. Eq.2.33 can be useful when trying to determine an analytical expression to find λ.

$$(\mathbf{K} - \mathbf{M}\lambda)\,\phi = 0 \Rightarrow det\,(\mathbf{K} - \mathbf{M}\lambda) = 0 \tag{2.35}$$

This results in a polynomial of degree n with n roots. Each one of these roots is a solution with a corresponding vector ϕ. The corresponding ϕ is a vector in the null-space of the matrix $(\mathbf{K} - \mathbf{M}\lambda)$. The scalar λ is known as *eigenvalue* and the corresponding vector ϕ is known as an eigenvector.

Orthogonality Property

It can be shown that eigenvectors of the undamped system satisfy the following orthogonality property for $i \neq j$

$$\phi_i^T \mathbf{M} \phi_j = 0 \tag{2.36}$$

Similarly

$$\phi_i^T \mathbf{K} \phi_j = 0 \tag{2.37}$$

Mass-normalized modes

If ϕ is a mode shape (arbitrarily scaled), then $\alpha\phi$ is also a mode shape, where α is a scalar. Thus it is possible to find scalars α_i for each mode i such that

$$\psi_i^T \mathbf{M} \psi_i = 1 \tag{2.38}$$

where $\psi = \alpha\phi$. The scaled modes ψ are known as mass-normalized modes. The corresponding normalizing scalars for each mode are given by

$$\alpha_i = \frac{1}{\sqrt{\phi_i^T \mathbf{M} \phi_i}} \tag{2.39}$$

For mass-normalized modes, the following equality holds

$$\psi_i^T \mathbf{K} \psi_i = \lambda_i \tag{2.40}$$

Classical Damping

Any viscous damping matrix that satisfies the following orthogonality property is known as classical damping for $i \neq j$

$$\psi_i^T \mathbf{H_c} \psi_j = 0 \tag{2.41}$$

Popular examples of classical damping matrices

$$\mathbf{H_c} = \alpha\mathbf{M} \qquad \mathbf{H_c} = \beta\mathbf{K} \qquad \mathbf{H_c} = \alpha\mathbf{M} + \beta\mathbf{K} \tag{2.42}$$

Modal Analysis

For systems with classical damping

$$\mathbf{M}\ddot{x}(t) + \mathbf{H_c}x(t) + \mathbf{K}x(t) = f(t) \tag{2.43}$$

One can define the following linear transformation of the displacement vector

$$x(t) = \Psi z(t) \tag{2.44}$$

where

$$\Psi = [\psi_1 \quad \psi_2 \quad ... \quad \psi_n] \tag{2.45}$$

then

$$\mathbf{M}\Psi\ddot{z}(t) + \mathbf{H_c}\Psi\dot{z}(t) + \mathbf{K}\Psi z(t) = f(t) \tag{2.46}$$

premultiplying by Ψ^T we obtain

$$\Psi^T\mathbf{M}\Psi\ddot{z}(t) + \Psi^T\mathbf{H_c}\Psi\dot{z}(t) + \Psi^T\mathbf{K}\Psi z(t) = \Psi^T f(t) \tag{2.47}$$

Using the aforementioned orthogonality properties

$$\ddot{z}(t) + \Xi\dot{z}(t) + \Lambda z(t) = \Psi^T f(t) \tag{2.48}$$

these are independent set of equations and hence can be solved individually for each mode i.

$$\ddot{z}_i(t) + 2\omega_i \xi_i \dot{z}_i(t) + \omega_i^2 z_i(t) = \psi_i^T f(t) \tag{2.49}$$

The dynamic response in physical coordinates can be found by simply applying the linear transformation

$$x(t) = \Psi z(t) = \sum_i \psi_i z_i(t) \tag{2.50}$$

2.8 Static Condensation of the Stiffness Matrix

The mass matrix formulation for many structural dynamics problems only include inertia (mass) terms corresponding to translational (vertical and horizontal) degrees of freedom (DoF) . Static condensation is used to condense the DoFs that have zero mass assigned to them from dynamic equations without affecting the innate structural response characteristics of the system. By looking at Eq. 2.27 and setting $\mathbf{H_c} = \mathbf{0}$:

$$\begin{bmatrix} \mathbf{K_{pp}} & \mathbf{K_{ps}} \\ \mathbf{K_{sp}} & \mathbf{K_{sp}} \end{bmatrix} \begin{bmatrix} \mathbf{P} \\ \mathbf{S} \end{bmatrix} = \begin{bmatrix} \mathbf{F_p} \\ \mathbf{F_s} \end{bmatrix} = \begin{bmatrix} \mathbf{F_p} \\ \mathbf{0} \end{bmatrix} \tag{2.51}$$

where $\mathbf{P}$ stands for primary DoF and $\mathbf{S}$ stands for secondary DoF. Both P and S are sub-vectors of the DoFs to be retained and condensed out, respectively. The sub-matrices $\mathbf{K_{pp}}$, $\mathbf{K_{ps}}$, $\mathbf{K_{sp}}$, and $\mathbf{K_{sp}}$ and the force sub-vectors $\mathbf{F_p}$ and $\mathbf{F_s}$ correspond

to the displacement sub-vectors $\mathbf{P}$ and $\mathbf{S}$. $\mathbf{F_s} = \mathbf{0}$ means no elastic rotational forces are acting on the system. After some matrix manipulation we get that:

$$\mathbf{K_{cc}} = \mathbf{K_{pp}} - \mathbf{K_{ps}}\mathbf{K_{ss}}^{-1}\mathbf{K_{sp}} \tag{2.52}$$

where $\mathbf{K_{cc}}$ is the condensed stiffness matrix. The stiffness matrix is now suitable for used with lumped mass matrix (translational elements only). It is possible to express the displacement of the condensed DoF by $\mathbf{S} = -\mathbf{K_{22}}^{-1}\mathbf{K_{sp}}\mathbf{P}$. It is worth noting the size of the system can be further reduced by condensing additional DoFs that we aren't necessarily interested in or that don't contribute to the dynamics of the system. These DoFs can be vertical or redundant horizontal DoF. The mass matrix shall be modified to lump the masses of neighboring DoF.

2.9 State-Space Representation

The state-space representation provides a map from input to state and from state to output. In finite dimensional models, the state is the smallest collection of variables that, known at given time, can be projected into the future with the use of a structure and the input acting on the system. By considering the auxiliary equation of $\dot{q}(t) = \dot{q}(t)$ the equation of motion can be written in first order form:

$$\begin{Bmatrix} \dot{q}(t) \\ \ddot{q}(t) \end{Bmatrix} = \begin{bmatrix} \mathbf{0_{n\times n}} & \mathbf{I_{n\times n}} \\ -\mathbf{M}^{-1}\mathbf{K} & -\mathbf{M}^{-1}\mathbf{H_c} \end{bmatrix} \begin{Bmatrix} q(t) \\ \dot{q}(t) \end{Bmatrix} + \begin{bmatrix} \mathbf{0_{n\times m}} \\ \mathbf{M}^{-1}\mathbf{b_2} \end{bmatrix} u(t) + \begin{bmatrix} \mathbf{0_{n\times (n-m)}} \\ \mathbf{M}^{-1}\mathbf{b_1} \end{bmatrix} w(t) \tag{2.53}$$

this system of equations can be rewritten as

$$\dot{x}(t) = \mathbf{A_c}x(t) + \mathbf{B_c}u(t) + \mathbf{L_c}w(t) \tag{2.54}$$

where $x(t) = \left\{ \begin{array}{c} q(t) \\ \dot{q}(t) \end{array} \right\} \in \Re^{2n\times 1}$ is the state vector, $\mathbf{A_c} \in \Re^{2n\times 2n}$ is the state matrix, $\mathbf{B_c} \in \Re^{2n\times m}$ is the known input to state matrix, and $\mathbf{L_c} \in \Re^{2n\times(n-m)}$ is the unknown input to state matrix. The known excitation are defined in the vector $u(t) \in \Re^{m\times 1}$ with $\mathbf{b_2} \in \Re^{\ n\times m}$ its a Boolean force distribution matrix that indicates which DoF has a known loading and m is the number of independent excitations. The unknown excitation are denoted by the vector $w(t) \in \Re^{(n-m)\times 1}$ and a its Boolean force distribution matrix $\mathbf{b_1} \in \Re^{\ n\times(n-m)}$. The subscript c means that the equations are in continuous time.

The state-space representation of a structure can be achieved with the geometrical and material properties of the structure or by estimating the matrices using a system identification scheme. It is worth noting that by rewriting second order equations of motion to a first order formulation, the new system needed to be solved has doubled in size. As the number of degrees of freedom increases, the solution becomes more computationally expensive limiting its applicability to small size models (low number of Dofs). Additionally these equations, with its boundary conditions, can not be solved analytically (except for very simple cases) so an approximate solution can be obtained by a discretization of the system in both space and time.

2.9.1 Measurements

Measurements of the response of the system are represented by

$$y(t) = \mathbf{C_c}x(t) + \mathbf{D_{c2}}p(t) + \mathbf{D_{c1}}w(t) + v(t) \tag{2.55}$$

where $y(t) \in \Re^{n\times 1}$, $\mathbf{C_c} \in \Re^{n\times 2n}$ is the output matrix, $\mathbf{D_{c1}}$ and $\mathbf{D_{c2}} \in \Re^{n\times m}$ are the feed-through (or direct transmission) matrices and $v(t)$ is the measurement noise (associated to the sensor technology). For displacement or velocity measurements, the $\mathbf{D}$ matrix is zero and C_c has the following form:

$$\mathbf{C_{dis}} = \mathbf{c_2}\,[\,\mathbf{I} \quad \mathbf{0}\,] \qquad \mathbf{C_{vel}} = \mathbf{c_2}\,[\,\mathbf{0} \quad \mathbf{I}\,] \tag{2.56}$$

where $\mathbf{c_2} \in \Re^{r\times n}$ maps the state to the measurements where every row of it has a one at the column corresponding to the measured degree of freedom of that row and zero elsewhere. If the measurements consists of accelerations:

$$\mathbf{C_{accel}} = \mathbf{c_2}\,[\,-\mathbf{M}^{-1}\mathbf{K} \quad -\mathbf{M}^{-1}\mathbf{C_D}\,] \tag{2.57}$$

and the $\mathbf{D}$ matrices are given by:

$$\mathbf{D_{c2}} = \mathbf{c_2}\mathbf{M}^{-1}\mathbf{b_2} \qquad \mathbf{D_{c1}} = \mathbf{c_2}\mathbf{M}^{-1}\mathbf{b_1} \tag{2.58}$$

2.9.2 State-Estimation

In some SHM applications, it is desirable to estimate unmeasured (or ummeasurable) quantities of the structural response by blending a mathematical model and with an usually incomplete characterization of the input forces. Furthermore, there are instances where the input forces have a complex distribution, e.g wind acting on large

structures, waves clashing on maritime structures, etc. These provide additional difficulties for the state-estimation problem. As a way to mitigate unavoidable errors, the measurements are used to improve the estimation. In the context of this dissertation measurements are modeled as shown in Eq. 2.55. In Control theory, a system that processes input/output signals and estimates the states of the system is referred to as an observer. In general, the output only state estimates provided by an observer can be written in first order state-space form as:

$$\dot{\hat{x}}(t) = \mathbf{A_c}\hat{x}(t) + \mathbf{G_c}\left[y(t) - \mathbf{H_c}\hat{x}(t)\right] \tag{2.59}$$

where $\hat{x}(t)$ is the state estimate. As can be seen from Eq. 2.59, the observer state estimate is the response of the system subjected to excitations consisting of the weighted difference between measured response ($y(t)$) and model's response estimate $\hat{x}(t)$ (see Fig. 2.1). Discrepancy between measured response and model predictions can arise mainly from a combination of four different sources: model error, unmeasured excitations, measurement error, and unknown initial conditions. In most applications, these cannot truly be distinguish one from the other. The feedback gain matrix $\mathbf{G_c}$ is the essence of any observer design and it is chosen based on the assumption of which source of error is responsible for the output discrepancy and the selection of an objective function to be minimized.

Let's look at the state-space representation of the estimates:

$$\begin{Bmatrix} \dot{\hat{q}}(t) \\ \ddot{\hat{q}}(t) \end{Bmatrix} = \begin{bmatrix} \mathbf{0_{n\times n}} & \mathbf{I_{n\times n}} \\ -\mathbf{M^{-1}K} & -\mathbf{M^{-1}H_c} \end{bmatrix} \begin{Bmatrix} \hat{q}(t) \\ \dot{\hat{q}}(t) \end{Bmatrix} + \begin{bmatrix} \mathbf{G_1} \\ \mathbf{G_2} \end{bmatrix} \Delta y(t) \tag{2.60}$$

where $\Delta y(t) = y(t) - \mathbf{H_c}\hat{x}$ is the output discrepancy at time t. To satisfy the top partition it is necessary that $\mathbf{G_1}\Delta y(t) = 0$ which means that either $\mathbf{G_1} = 0$ or $\Delta y(t) \in \mathcal{N}(\mathbf{G_1})\forall\ t$. Since in general $\mathbf{G_1}$ does not have a right null space and moreover, even if it did, $\Delta y(t)$ does not need no remain in the same space for all times, so $\mathbf{G_1} = 0$. Thus for any observer of the form given by Eq. 2.59 to be realizable in second order form its feedback gain matrix needs to have the following internal structure:

$$\mathbf{G_c} = \begin{bmatrix} \mathbf{0} \\ \mathbf{G_2} \end{bmatrix} \tag{2.61}$$

where $\mathbf{G_2}$ is still free to be selected. This result was first shown by [Balas; 1998].

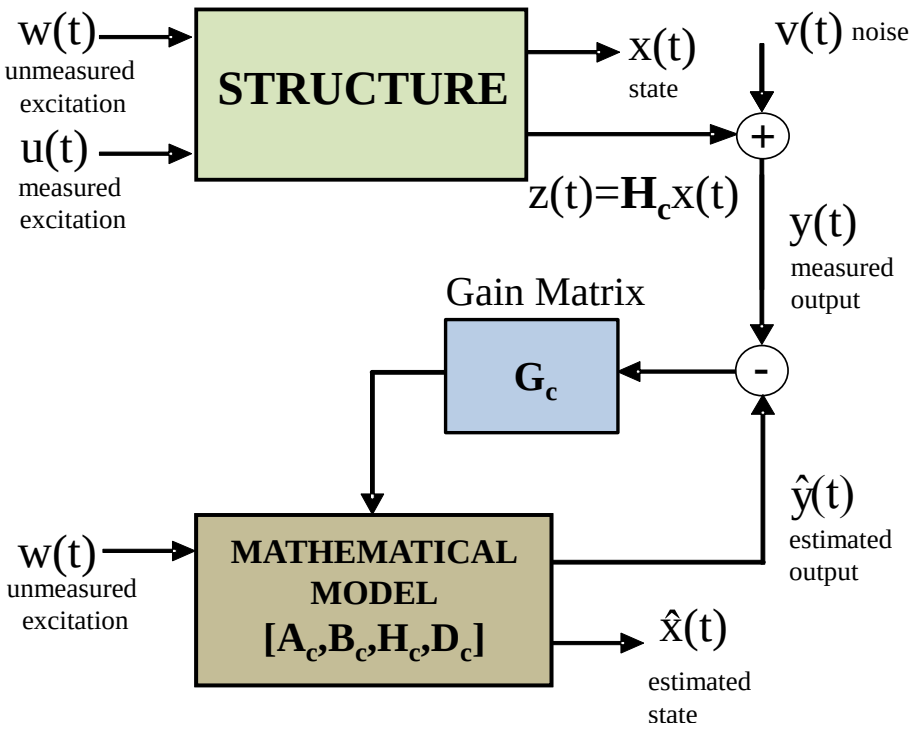

Figure 2.1: Block diagram of a continuous time classical state estimator (output only)

2.9.3 Recursive Estimators

Recursive estimators are mostly based on Bayes' theorem

$$P(X|Y) = \frac{P(Y|X) \times P(X)}{P(Y)} \tag{2.62}$$

where X is the state and Y is the measurements. This form describes how the knowledge of the system state is combined with the measurement information to get a better estimate of the state. The knowledge of the system state is given with the "a priori" probability of the state $P(X)$. The measurement information is the likelihood

probability $P(Y|X)$ which depends on the state. The likelihood and the "a priori" probability are multiplied and normalized through the evidence $P(Y)$, which is a normalization factor. The resulting new probability of the state $P(X|Y)$ is known as the "a posteriori" estimate. When the next measurement is processed the former "a posteriori" state probability is the new "a priori" probability. It is desirable to use a distribution where the "a priori" probability and the likelihood probability yields to "a posteriori" distribution of the same class. In other words, the family of the probability distribution is not changing in the recursive process.

Bayesian linear state estimation has been applied by many researchers on various fields of science, with the contribution from Kalman [Kalman; 1960] being the most celebrated. In classical Kalman filtering it is assumed that the model is correct but that the excitations and measurement noise are realizations of a Gaussian white random process with zero mean and known covariance matrix $\mathbf{Q}$ and $\mathbf{R}$, respectively. A related problem is where no disturbances are acting on the system and we have a correct model but the dynamic response is uncertain due to lack of knowledge of the initial conditions. The seminal contribution to solve this problem is the work done by Luenberger [Luenberger; 1964].

The basic equations of the Kalman filter algorithm are given on Table 2.1.

Table 2.1: Summary of discrete Kalman filter equations - Gelb [Gelb; 1996]

System Model	$x_k = \mathbf{A}x_{k-1} + w_{k-1}$	$w_k \sim \mathcal{N}(0, \mathbf{Q}_k)$
Measurement Model	$z_k = \mathbf{H}x_k + v_k$	$v_k \sim \mathcal{N}(0, \mathbf{R}_k)$
Initial Conditions	$\mathbb{E}\left[x(0)\right] = \hat{x}_0$, $\mathbb{E}\left[(x(0) - \hat{x}(0))(x(0) - \hat{x}(0))^T\right] = \mathbf{P}_0$	
Other Assumptions	$\mathbb{E}\left[w_k v_j^T\right] = 0$ for all j,k	
State Estimate Extrapolation	$\hat{x}_k^{(-)} = \mathbf{A}\hat{x}_{k-1}^{(+)}$	
Error Covariance Extrapolation	$\mathbf{P}_0 = \mathbf{A}\mathbf{P}_{k-1}\mathbf{A}^T + \mathbf{Q}_{k-1}$	
State Estimate Update	$\hat{x}_k^{(+)} = \hat{x}_k^{(-)} + \mathbf{K}_k[z_k - \mathbf{C}\hat{x}_k^{(-)}]$	
Error Covariance Update	$\mathbf{P}_k^{(+)} = [\mathbf{I} - \mathbf{K}_k\mathbf{H}]\mathbf{P}_k^{(-)}$	
Kalman Gain Matrix	$\mathbf{K}_k = \mathbf{P}_k^{(-)}\mathbf{H}^T[\mathbf{H}\mathbf{P}_k^{(-)}\mathbf{H}^T + \mathbf{R}_k]^{-1}$	

2.9.4 Discrete to continuous (d2c) Relationships

All previous equations are presented in continuous time. In practice, vibration signals are obtained in a digital fashion so we need to convert the continuous system matrices to discrete time matrices.

The solution of the continuous time state-space representation is well known, [Kailath; 1980], and can be expressed by:

$$x(t) = x_0 e^{\mathbf{A_c}t} + \int_0^t e^{-\mathbf{A_c}(t-\tau)}\mathbf{B_c}u(\tau)d\tau \tag{2.63}$$

and by taking $t = k\Delta t$ the previous equation can be expressed as

$$x_{k+1} = \mathbf{A_d}x_k + \mathbf{A_d}\int_0^{\Delta t} e^{-\mathbf{A_c}\Delta t}\mathbf{B_c}u(\tau)d\tau \tag{2.64}$$

where τ has the origin at the start of each time step and $\mathbf{A_d}$ is the state-space

matrix in discrete time (see Table 2.2 for details). To convert equation 2.64 into an algebraic form, the integral that is related to the excitation needs to be resolved. The solution of the integral is governed by how the intra sampling behavior of the input is considered. The reader is referred to [Bernal; 2007] for more details. The author discusses the discrete to continuous relationships of the state-space representation matrices. The inter sampling behavior for analysis is based on the nature of the input that is exciting the system. Bellow is a summary of these relationships:

Table 2.2: Summary of Discrete to Continuous (d2c) relationships

	Matrices in continuous time			
Method	$\mathbf{A_d}$	$\mathbf{B_d}$	$\mathbf{C_d}$	$\mathbf{D_d}$
BLH	$e^{\mathbf{A_c}\Delta t}$	$\mathbf{A_d}\mathbf{B_c}\Delta t$	$\mathbf{C_c}$	$\mathbf{D_c}$
ZOH	$e^{\mathbf{A_c}\Delta t}$	$\left[\mathbf{A_d}-\mathbf{I}\right]\mathbf{A_c}^{-1}\mathbf{B_c}$	$\mathbf{C_c}$	$\mathbf{D_c}$
FOH	$e^{\mathbf{A_c}\Delta t}$	$\left[\mathbf{A_d}-\mathbf{I}\right]^2\mathbf{A_c}^{-2}\mathbf{B_c}1/\Delta t$	$\mathbf{C_c}$	$\mathbf{D_c}-\mathbf{C_c}\mathbf{A_c}^{-1}\ldots$ $\left[\mathbf{I}-\mathbf{A_c}^{-1}\left(\mathbf{A_d}-\mathbf{I}\right)1/\Delta t\right]\mathbf{B_c}$
SZOH	$e^{\mathbf{A_c}\Delta t}$	$\mathbf{A_d}^{0.5}\left[\mathbf{A_d}-\mathbf{I}\right]\mathbf{A_c}^{-1}\mathbf{B_c}$	$\mathbf{C_c}$	$\mathbf{D_c}+\mathbf{C_c}\mathbf{A_c}^{-1}\left[\mathbf{A_d}^{0.5}-\mathbf{I}\right]\mathbf{B_c}$

After selecting the inter step consideration, the state-space representation and the measurements of the system can be expressed as:

$$x_{k+1} = \mathbf{A_d}x_k + \mathbf{B_d}p_k + \mathbf{G_k}w_k \tag{2.65}$$

$$y_k = \mathbf{C_d}x_k + \mathbf{D_{d2}}p_k + \mathbf{D_{d1}}w_k + v_k \tag{2.66}$$

where the subscript d means discrete and k means the values of the state, excitations and noise at the kth step.

2.10 System Identification

System identification deals with the estimation of a model that better explains, in some predefined sense, observed data on a dynamical system ([Eykhoff; 1974], [Söderström & Stoica; 1989], [Juang; 1994], [Overschee & De Moor; 1996], [Pintelon & Schoukens; 1996], and [Ljung; 1999]). The search space is typically constrained to a certain family or class of models and within that class optimal parameters are sought. Due to the presence of noise in the measurements and unmeasured excitations, the identified parameters are not optimal. The objective is to arrive at some practical description of the dynamical system by processing the input (if any) and outputs (measurements). The form of the dynamical model is chosen depending its application: *parametric* models belongs to a class where each model is differentiated by specific values of the parameter space and *non-parametric* models are those described in terms of functions e.i., frequency response functions, impulse response functions, etc. Broadly speaking, identification entitles: 1) collection of outputs, 2) selection of the type of dynamical model, and 3) a criteria to select such model.

We implemented Subspace Identification (SUBID) and Eigensystem Realization Algorithm (ERA) techniques to estimate model parameters from measurements in this dissertation. The reader is referred to chapters 3 and 4 for more details on these. [Shokravi, et al.; 2020] provides an extensive overview of SHM methods that apply to system identification (see Fig. 2.2).

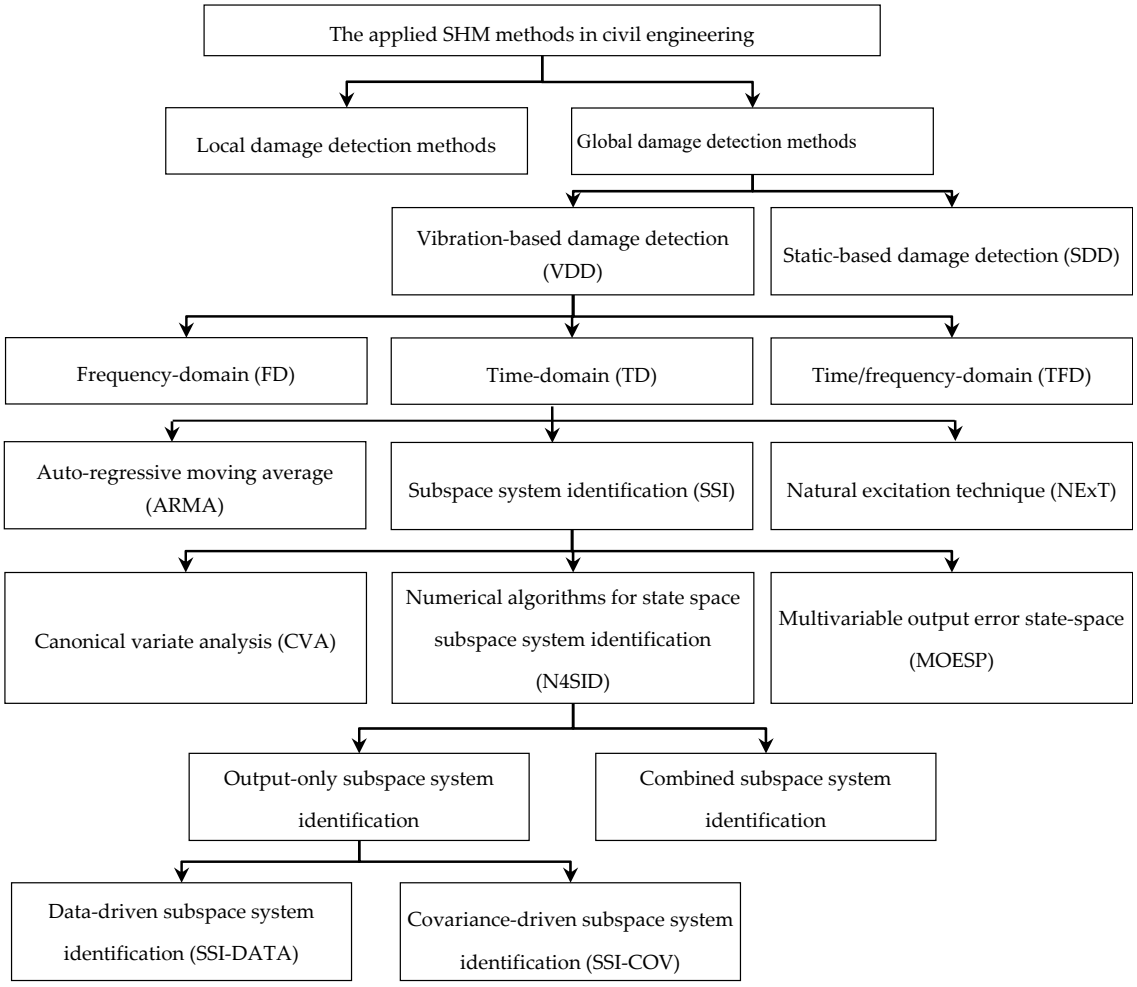

Figure 2.2: Classification of SHM methods (Figure 1. of [Shokravi, et al.; 2020]

2.10.1 Observability

A state, $x(t_o)$, is observable if it can be determined from knowledge of the system state-space matrices and the output $y(t)$ for $t > t_o$. In structural dynamics, if every mode shape has at least one measurement coordinate with non-zero amplitude the system is called fully observable (other wise it is defined as partially observable). For example, consider a simply supported beam under any type of dynamic loading with

a single sensor in the middle of the span. In this example, regardless of the number of mode shapes of the beam that are excited only the odd number mode shapes are going to be captured by the sensor (even mode shapes have no contribution in the middle span of a simply supported beam). In summary, a state is observable if you can back track the initial values of the state by having knowledge system matrices and measured output response.

There are different ways to determine the observability of a system. One way is evaluate the rank of the observability block $\mathbf{O}_p$:

$$\mathbf{O}_n = \begin{bmatrix} \mathbf{C_d} \\ \mathbf{C_d A_d} \\ \vdots \\ \mathbf{C_d A_d}^{n-1} \end{bmatrix} = n \tag{2.67}$$

where n is the order of the system (2 times the number of DoFs).

A more quantitative measure of the observability is through the Observability Grammian $\mathbf{W}_o(t_f, t_o)$ defined by:

$$\mathbf{W_o}(t_f, t_o) = \int_{t_o}^{t_f} e^{\mathbf{A}^T(\tau - t_o)} \mathbf{C}^T \mathbf{C} e^{\mathbf{A}(\tau - t_o)} d\tau \tag{2.68}$$

where t_f is the final time of observations. By examining the condition number of $\mathbf{W_o}$ we can get a measure of the observability of the system. Given two sensor configurations, one could infer that the one with the lowest condition number of $\mathbf{W}_o$ is more desirable since it is more robust to measurement noise or changes in the input.

2.11 Bibliography

[Balas; 1998] Balas, M. J., (1998) *Do all linear flexible structures have convergent second-order observers?*, AIAA J. Guidance Control Dyn., 4, 2319-2323,

[Bernal; 2007] Bernal, D. (2007), *Optimal discrete to continuous transfer for band limited inputs*, Journal of Engineering Mechanics, 133(12), 1370-1377

[Cooley & Tukey; 1965] Cooley, James W. & Tukey, John W. (1965). *An algorithm for the machine calculation of complex Fourier series*. Math. Comput., 19-(90), 297-301.

[Gelb; 1996] Gelb, A. (Ed.) (1996), *Applied Optimal estimation*, Fourteenth ed., The M.I.T Press, Cambridge,

[Kailath; 1980] Kailath, T. (1980), *Linear Systems* Prentice Hall Inc

[MATLAB] `https://www.mathworks.com/help/signal/ref/pwelch.html`

[Luenberger; 1964] Luenberger, D. (1964), *Observing the state of a linear system*. IEEE Transactions on Military Electronics, 74-80

[Shokravi, et al.; 2020] Shokravi, H., Shokravi, H., Bakhary, N., Rahimian Koloor, S.S., Petrů, M. (2020), *Health Monitoring of Civil Infrastructures by Subspace System Identification Method: An Overview*. Applied Sciences, 10, 2786

[Welch; 1967] Welch, P. D. (1967), *The use of fast Fourier transforms for the estimation of power spectra: A method based on time averaging over short modified periodograms*,IEEE Transactions on Audio and Electroacoustics, 15, 70-73

Chapter 3

Lower Bounds for the Variance of Frequency and Damping Ratio Identified from Noisy Vibration Measurements

3.1 Introduction

System identification deals with the estimation of a model that better explains, in some predefined sense, observed data on a dynamical system [1–6]. The search space is typically constrained to a certain family or class of models and within that class optimal parameters are sought. Due to the presence of noise in the measurements and unmeasured excitations, the identified parameters are not optimal. The mathematical form in which model parameter estimates are presented range from point

estimates to a joint probability density function [7]. As an intermediate and common compromise, various researchers have proposed methods that aim to estimate only the mean and variance of the desired model parameters. Under some restrictions these methodologies allow for the computation of confidence intervals with specified probability [8].

In many structural engineering applications, the models are linear and it is commonplace to formulate them on the basis of modal parameters, i.e. mode shapes, frequencies and modal damping ratios [9]. Various authors have performed experimental uncertainty quantification studies with the objective of gaining insight into the origin and relative magnitude of the various factors that give rise to uncertainty in the identification of dynamic models from measured data [10,11]. In [10] it is reported that sources of uncertainty in the identification of modal frequencies and damping can be divided into: test-setup uncertainty, measurement uncertainty and data analysis uncertainty. It was found that there is significantly more variation in the identified modal damping ratios that in the identified modal frequencies. In [11] two different laboratory experiments were conducted and the statistics of the frequency response functions measured at different points were obtained for a range of frequencies. It was reported that more variability is present at the high-frequency range than in the low-frequency range.

On the theoretical side we can point out to the work of Gersch [12] as one of the pioneers on the subject of uncertainty quantification of identified models in structural dynamics. Gersch developed expressions that relate auto-regressive coefficients (AR) of auto-regressive moving average (ARMA) models to eigenvalues of the system, and thus with modal frequency and damping ratios. He used these expressions

together with the Cramer-Rao lower bound (CRLB) theorem to compute the maximum achievable accuracy of the modal frequency and damping ratio based on the maximum likelihood estimates (MLE) of identified AR coefficients. Another fundamental development can be found in [13], where a methodology for optimal sensor placement for system identification was developed on the basis of determining the sensing locations that maximize the Fisher information matrix for a fixed number of possible measurements. Implicit integral expressions were derived to evaluate the Fisher information of linear multi-degree of freedom systems with mass and (or) stiffness proportional damping. More recent developments on the subject of uncertainty quantification of identified modal parameters have been reported in [14–17].

In [14] it was shown that in the case of output-only system identification it is possible to obtain an estimate of the covariance of the normalized modal parameters from knowledge of the mean and covariance of the parameters that define a common denominator rational transfer function matrix, which in principle can be identified from the structural response measurements. In [15] an algorithm is proposed that efficiently estimates the covariance of modal parameters obtained from multi-setup subspace identification. Multi-setup system identification refers to an algorithm capable of merging data from different sensor locations and different test setups. The algorithm was validated using ambient vibration data of the Z24 bridge. In [16] an algorithm is proposed to remove bias errors from system identification results and estimating the variance errors from a single ambient vibration test. The bias removal procedure makes use of a stabilization diagram. The variance estimation procedure uses the first-order sensitivity of the modal parameter estimates to perturbations of the measured output-only data. In [18] an algebraic relationship between the variance

of the natural frequency and the damping ratio was derived on the basis of assuming the location of the eigenvalue in the complex plane to be random within a circle where the variance of the real part equals the variance of the imaginary part. From examination of the existing literature we can deduced that modal damping ratios are significantly more difficult to estimate than modal frequencies. Although most of the studies regarding identification of damping and its uncertainty operate under the basis of assuming viscous modal damping, other models for damping have been proposed and methods to estimate it have been developed and summarized by [19].

In a recent paper by S.K. Au [17] the problem of maximum achievable accuracy in operational modal analysis was investigated using a frequency domain Bayesian approach. In similar fashion to our research, classical damping and well separated modes were assumed. Our research differs from the work of [17] in various ways: (i) all derivations are in the time domain as opposed to the frequency domain; (ii) we are interested in signals resulting from initial conditions or known excitations and the only source of uncertainty is the measurement noise and (iii) our approach is based on Fisher information and CRLB as opposed to Bayes' theorem. Despite these differences, it is interesting to note that general result trends are preserved. These will be discussed within the body of this chapter.

In the following pages, we derive of exact mathematical expressions which allow for the computation of the minimum achievable variance of identified modal frequency and damping ratio from noisy vibration measurements induced by either initial conditions or measured excitations. Derived bounds establish a reference level to which the second order statistics of system identification results can be compared. We also demonstrate and quantify that there must be significantly more uncertainty in iden-

tified modal damping ratios than in natural frequencies. This is a fact which stands independent of the system identification algorithm that is employed, as long as the algorithm is unbiased. The mathematical background of the proposed expressions is rooted in the CRLB theory.

We begin with an examination of the Fisher information matrix and the CRLB theory. Following this we proceed to derive exact expressions for the CRLB for natural frequency, damping ratio, and initial conditions under free vibration conditions and arbitrary excitations in single degree of freedom systems. Using the SDOF results and modal analysis we extend the results to classically damped multi-degree of freedom systems with well separated modal frequencies. We illustrate the results numerically and confirms them by means of simulated system identification results. The close the chapter with a section summarizing the main findings.

3.2 Fisher Information

The Fisher information is a measure of the amount of information that an observable random variable X carries about an unknown parameter θ upon which the probability of X depends. The probability function for X, which is also the likelihood function for θ, is a function $f(X;\theta)$; is the probability mass (or probability density) of the random variable X conditional on the value of θ. The Fisher information is defined as

$$I(\theta) = -E\left[\frac{\partial^2 \ln f(X,\theta)}{\partial \theta^2}\right] \tag{3.1}$$

or alternatively as

$$I(\theta) = E\left[\left(\frac{\partial \ln f(X,\theta)}{\partial \theta}\right)^2\right] \tag{3.2}$$

To gain some insight, one can use eq.3.1 to verify that the Fisher information of the mean of a Gaussian random variable is equal to the inverse of the variance. This is consistent with basic statistics which states that given a fixed number of samples of a Gaussian random variable the uncertainty (lack of information) in the estimate of the mean increases with the variance. An important property of the Fisher information is that, given n independent measurements x_i of the random variable X, the Fisher information is additive, such that

$$I_n(\theta) = \sum_{i=1}^{n} I_i(\theta) \tag{3.3}$$

where I_i is the Fisher information of the i^{th} measurement. It was shown in [22] that the Fisher information matrix of a scalar discrete signal $s(t)$ dependent on multiple parameters θ_i and corrupted by additive Gaussian white noise with variance σ^2 is given by

$$I_{ij}(\theta) = \frac{1}{\sigma^2} \sum_{n=0}^{N-1} \frac{\partial s(n;\theta)}{\partial \theta_i} \frac{\partial s(n;\theta)}{\partial \theta_j} \tag{3.4}$$

where $s(n;\theta)$ is value of the signal at time $t = n\Delta t$ and Δt is the time step between measurements. A dimensional analysis of the previous equation indicates that the units of the Fisher information are $[P]^{-2}$ where P is the unit of the parameter being investigated. Therefore, the corresponding Fisher information of two different parameters, with different units, can not be compared directly. For the cases of interest in our research, the Fisher information of circular frequency has units of

s^2/rad^2 while the Fisher information of damping ratio has no units.

3.3 Cramer-Rao Lower Bound

If $f(X;\theta)$ satisfies the regularity condition

$$E\left[\frac{\partial \ln(f(X;\theta))}{\partial\theta}\right] = 0 \quad \forall\theta \tag{3.5}$$

where the expectation is taken with respect to $f(X;\theta)$, then the variance of any unbiased estimator $\hat{\theta}$ must satisfy

$$Var(\hat{\theta}) \geq CRLB = \frac{1}{I(\theta)} \tag{3.6}$$

This lower limit is known as the Cramer-Rao lower bound (CRLB). For the case of multiple parameters $\theta \in \mathbb{R}^{n\times 1}$, the Fisher information becomes a matrix and the CRLB is given by

$$CRLB = \mathbf{I}(\theta)^{-1} \tag{3.7}$$

The proof of this theorem can be found in [22]. From the previous discussion it is clear that the Fisher information is always positive (by definition) and that the minimum achievable variance of θ will shrink as the number of measurements increases. By definition, if we denote $\mathbf{R} = \mathbf{I}(\theta)^{-1}$, then

$$Var(\hat{\theta}_i) \geq CRLB(\theta_i) = \mathbf{R}_{i,i} \tag{3.8}$$

It is possible to use the previous result to compute the minimum coefficient of

variation (CoV) induced by the CRLB. This is given by

$$CoV(\hat{\theta}_i) \geq \frac{\sqrt{CRLB(\theta_i)}}{E[\theta_i]} \tag{3.9}$$

Since the CoV is unitless, this criteria will be used for the remainder of the chapter to compare the maximum achievable accuracy among different parameters.

3.4 Fisher Information in Free Vibration Displacement Measurements

In this section we develop the Fisher information theory and the CRLB in the context of single degree of freedom (SDOF) elastic systems with velocity proportional damping subjected initial conditions. The free vibration response of a SDOF with additive noise ($\nu(t)$) is given by

$$s(t) = e^{-\xi\omega_n t}\left[\left(\frac{\dot{x}_o + \xi\omega_n x_o}{\omega_d}\right)\sin\omega_d t + x_o\cos\omega_d t\right] + \nu(t) \tag{3.10}$$

where ξ is the damping ratio, ω_n is the undamped circular frequency, $\omega_d = \omega_n\sqrt{1-\xi^2}$, x_o is the initial displacement and $\dot{x}_o$ is the initial velocity. The derivatives necessary to compute the Fisher information (eq. 3.4) can be found, after some

differentiation and algebraic manipulations, to be given by

$$\frac{\partial s}{\partial \omega_n} = e^{-\xi\omega_n t}[-\xi t \left(\frac{\dot{x}_o + \xi\omega_n x_o}{\omega_d}\right) \sin\omega_d t + \ldots \\ + t\left(\frac{\dot{x}_o + \xi\omega_n x_o}{\omega_d}\right)\sqrt{1-\xi^2}\cos\omega_d t - \frac{\dot{x}_o}{\omega_n\omega_d}\sin\omega_d t + \ldots \\ - x_o\xi t\cos\omega_d t - x_o t\sqrt{1-\xi^2}\sin\omega_d t] \tag{3.11}$$

$$\frac{\partial s}{\partial \xi} = e^{-\xi\omega_n t}[-\omega_n t \left(\frac{\dot{x}_o + \xi\omega_n x_o}{\omega_d}\right) \sin\omega_d t + \ldots \\ + \left[\xi\left(\frac{\dot{x}_o}{\omega_n} + \xi x_o\right)\left(1-\xi^2\right)^{-\frac{3}{2}} + \frac{x_o}{\sqrt{1-\xi^2}}\right]\sin\omega_d t + \ldots \\ - \left(\frac{\dot{x}_o + \xi\omega_n x_o}{\omega_d}\right)\left(\frac{\omega_n\xi t}{\sqrt{1-\xi^2}}\right)\cos\omega_d t - x_o\omega_n t\cos\omega_d t + \ldots \\ + x_o\left(\frac{\omega_n\xi t}{\sqrt{1-\xi^2}}\right)\sin\omega_d t] \tag{3.12}$$

$$\frac{\partial s}{\partial \dot{x}_o} = \frac{e^{-\xi\omega_n t}}{\omega_d}\sin\omega_d t \tag{3.13}$$

$$\frac{\partial s}{\partial x_o} = \frac{\xi}{\sqrt{1-\xi^2}}e^{-\xi\omega_n t}\sin\omega_d t + e^{-\xi\omega_n t}\cos\omega_d t \tag{3.14}$$

For illustration purposes Fig. 1 depicts the shape of each of the derivatives given above for the particular case of a system with $\omega_n = 10\pi$ and $\xi = 0.02$. The derivatives can be evaluated at discrete times consistent with the signal sampling rate and inserted into eq.3.4 to compute the sum and obtain the Fisher information. Since we are investigating four parameters, the Fisher information matrix will be 4×4.

Evaluation of eq.3.4 using the previously shown derivatives in discrete time can

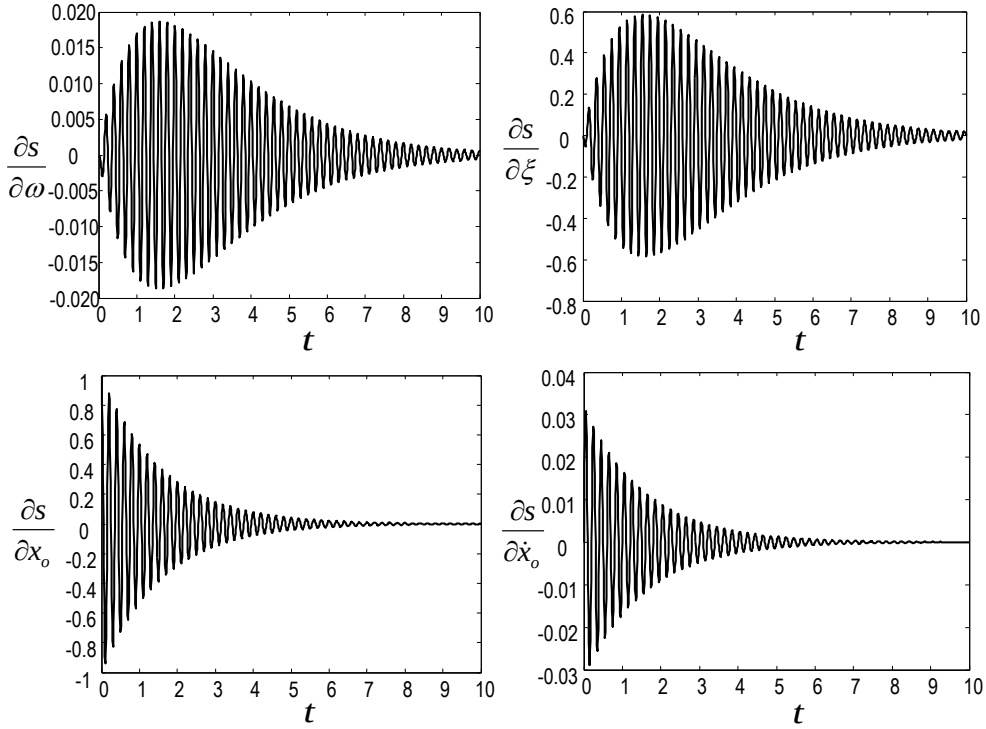

Figure 3.1: Graphical representation of derivatives necessary to compute the Fisher information matrix. In this case the particular parameters used were $x_o = 1$, $\dot{x}_o = 1$, $\omega_n = 10\pi$ *and* $\xi = 0.02$

only be done numerically within the context of a particular example, however it proves useful to examine the Fisher information in the limiting case where the sampling rate goes to zero and the observation time goes to infinity, i.e.

$$\lim_{\substack{\Delta t \to 0 \\ t \to \infty}} I_{ij} = \lim_{\substack{\Delta t \to 0 \\ t \to \infty}} \frac{1}{\Delta t \sigma^2} \sum_{n=0}^{N-1} \frac{\partial s(n;\theta)}{\partial \theta_i} \frac{\partial s(n;\theta)}{\partial \theta_j} \Delta t = \frac{1}{\sigma_d^2} \int_0^\infty \frac{\partial s(t;\theta)}{\partial \theta_i} \frac{\partial s(t;\theta)}{\partial \theta_j} dt \qquad (3.15)$$

where σ_d^2 is the displacement measurement noise variance per unit of time (in a Brownian motion sense). Eq.3.15 can be evaluated in closed form for any SDOF system with initial velocity ($\dot{x}_o$) and displacement (x_o). Eq.3.15 is an upper bound on

the Fisher information, since all possible information is being used. The CRLB computed from the asymptotic Fisher information represents the lowest possible bound on the variance of the estimated parameters.

Some particular results are of special practical interest, namely, estimating the Fisher information regarding circular frequency (ω) and damping ratio (ξ) in noise contaminated free vibration measurements induced by an initial velocity or displacement. These are explored in the following sections.

3.4.1 Initial Velocity

Substituting $x_o = 0$ and $\dot{x}_o = v_o$ into eq.3.11 and solving the integral in eq.3.15 we obtain the upper bound on the Fisher information regarding circular frequency (ω_n) in noise contaminated free vibration displacement measurements with additive white Gaussian noise. The resulting expression is

$$\lim_{\substack{\Delta t \to 0 \\ t \to \infty}} I_{\omega_n} = \frac{1}{\sigma_d^2} \int_0^\infty \left(\frac{\partial s}{\partial \omega_n} \right)^2 dt = \frac{1 + 5\xi^2}{8\sigma_d^2 \xi^3 \omega_n^5} v_o^2 \tag{3.16}$$

Similarly, the upper bound for the Fisher information regarding the damping ratio (ξ) is given by

$$\lim_{\substack{\Delta t \to 0 \\ t \to \infty}} I_{\xi} = \frac{1}{\sigma_d^2} \int_0^\infty \left(\frac{\partial s}{\partial \xi} \right)^2 dt = \left(\frac{1}{8\sigma_d^2 \xi^3 \omega_n^3} \right) v_o^2 + H.O.T \tag{3.17}$$

where $H.O.T$ are higher order terms where the damping ratio appears in the numerator with powers higher than two. The previous integrals, although not necessarily difficult, are numerous and cumbersome to compute. The authors resorted to the software MATHEMATICA [29] to compute them in a time efficient manner.

Their validity was confirmed using numerical integration. All other integrals to follow were computed in a similar fashion.

By the CRLB theorem (eq.3.8) the minimum variance that can be achieved whenever using an unbiased estimator of the natural circular frequency (ω_n) of a SDOF system from noisy displacement response measurements is

$$Var(\omega_n) \geq I_{\omega_n} = \frac{8\sigma_d^2 \xi^3 \omega_n^5}{(1+5\xi^2)\, v_o^2} \tag{3.18}$$

From this expression, the induced lower bound for the coefficient of variation of ω_n is

$$CoV_{\omega_n} \geq \sqrt{\frac{8\sigma_d^2 \xi^3 \omega_n^3}{(1+5\xi^2)\, v_o^2}} \tag{3.19}$$

Similarly, the minimum variance that can be achieved whenever using an unbiased estimator of the damping ratio ξ of a SDOF system from noisy displacement measurements is given by

$$Var(\xi) \geq \frac{8\sigma_d^2 \xi^3 \omega_n^3}{v_o^2} \tag{3.20}$$

From this expression, the induced lower bound for the coefficient of variation of ξ is

$$CoV_{\xi} \geq \sqrt{\frac{8\sigma_d^2 \xi \omega_n^3}{v_o^2}} \tag{3.21}$$

Fom eq.3.19 and 3.21 one can obtain an expression for the ratio between the minimum coefficient of variation of damping and the minimum coefficient of variation

of circular frequency

$$\frac{\min(CoV_\xi)}{\min(CoV_{\omega_n})} = \frac{\sqrt{1+5\xi^2}}{\xi} \tag{3.22}$$

From the previous expression it is evident that the coefficient of variation that can be expected when identifying viscous damping is significantly higher that the one for identified frequency. This is in agreement with system identification results in civil and mechanical engineering practice. For small values of damping, i.e. $\xi << 1$, the previous expression can be reduced to

$$\frac{\min(CoV_\xi)}{\min(CoV_{\omega_n})} \approx \frac{1}{\xi} \tag{3.23}$$

In [17] it was found that this ratio is given by

$$\frac{\min(CoV_\xi)}{\min(CoV_{\omega_n})} = \frac{1}{\xi}\sqrt{\frac{B_f}{B_\xi}} \tag{3.24}$$

where B_f and B_ξ are constants that depend on the size of bandwidth around the resonant frequency. If the bandwidth is large, then both of the previous expressions coincide.

3.4.2 Initial Displacement

In this section we examine the case where the free vibration is induced by an initial displacement. All other conditions, i.e. measurement time and noise model remain the same as in the previous section. Using eq.3.11 with $\dot{x}_o = 0$ and substituting into eq.3.15 with $\theta = \omega_n$ we obtain

$$\lim_{\substack{\Delta t\to 0\\ t\to\infty}} I_{\omega_n} = \frac{1}{\sigma_d^2}\int_0^\infty \left(\frac{\partial s}{\partial \omega_n}\right)^2 dt = \frac{1}{8\sigma_d^2\xi^3\omega_n^3\left(1-\xi^2\right)}x_o^2 + H.O.T. \tag{3.25}$$

where the minimum coefficient of variation for ω_n is given by

$$CoV_{\omega_n} \geq \sqrt{\frac{8\sigma_d^2\xi^3\left(1-\xi^2\right)\omega_n}{x_o^2}} \tag{3.26}$$

Similarly, for the Fisher information regarding damping ratio (ξ) we use eq.3.12 with $\dot{x}_o = 0$ and substitute into eq.3.15 with $\theta = \xi$ to obtain

$$\lim_{\substack{\Delta t\to 0\\ t\to\infty}} I_{\xi} = \frac{1}{\sigma_d^2}\int_0^\infty \left(\frac{\partial s}{\partial \xi}\right)^2 dt = \frac{1+2\xi^2}{8\sigma_d^2\xi^3\omega_n\left(1-\xi^2\right)^2}x_o^2 + H.O.T \tag{3.27}$$

where the minimum coefficient of variation for ξ is given by

$$CoV_{\xi} \geq \sqrt{\frac{8\sigma_d^2\omega_n\xi\left(1-\xi^2\right)^2}{\left(1+2\xi^2\right)x_o^2}} \tag{3.28}$$

For the case of vibration induced by an initial displacement, the quotient of the coefficient of variation of damping ratio to the coefficient of variation of circular frequency is given by

$$\frac{\min(CoV_{\xi})}{\min(CoV_{\omega_n})} = \sqrt{\frac{1-\xi^2}{\xi^2\left(1+2\xi^2\right)}} \approx \frac{1}{\xi} \tag{3.29}$$

For small values of damping, typically found in structures, eq.3.23 and eq.3.29 are identical. It is interesting to note that for any given initial displacement it is possible to find a corresponding initial velocity such that the asymptotic value of the Fisher information for frequency or damping is identical.

Up to this point we have derived the Fisher information and the minimum attainable coefficient of variation by a unbiased estimator for circular frequency (ω_n) and damping ratio (ξ). We have also proved that for $\xi << 1$ and independently of the excitation source (initial displacement or initial velocity), the natural frequency of the structure and the level of noise; the ratio between the CoV of damping ratio versus the CoV of circular frequency is a constant and approximately equal to the inverse of the damping ratio.

3.5 Fisher Information in Free Vibration Acceleration Measurements

In the previous section we have obtained results in the case of displacement measurements, in this section we investigate the Fisher information and CRLB in the case of acceleration measurements. The measured signal in the case of acceleration response of a single degree of freedom with additive measurement noise is given by

$$s(t) = e^{-\xi\omega_n t}\left[\left(\frac{\left(2\xi^2-1\right)\omega_n v_o + \xi\omega_n^2 x_o}{\sqrt{1-\xi^2}}\right)\sin\omega_d t - \left(2\xi\omega_n v_o + \omega_n^2 x_o\right)\cos\omega_d t\right] + v_a(t) \tag{3.30}$$

This is found by taking two derivatives of the deterministic portion of eq.3.10 and adding acceleration measurement noise. Note that the measurement noise is different in both cases. Again, two cases are of particular interest, initial displacement

excitations and initial velocity excitations. For both cases we will examine the Fisher information and determine the minimum variance of identified frequency and damping ratio.

3.5.1 Initial Velocity

If the system is excited by an initial velocity and noise contaminated acceleration measurements are used, then the upper limit of the Fisher information on circular frequency is given by

$$\lim_{\substack{\Delta t\to 0\\ t\to\infty}} I_{\omega_n} = \frac{1}{\sigma_a^2}\int_0^\infty \left(\frac{\partial s}{\partial \omega_n}\right)^2 dt = \frac{(1+\xi^2)}{8\sigma_a^2\omega_n\xi^3}v_o^2 + H.O.T \tag{3.31}$$

and its corresponding minimum CoV is

$$CoV_{\omega_n} \geq \sqrt{\frac{8\sigma_a^2\xi^3}{(1+\xi^2)\,\omega_n v_o^2}} \tag{3.32}$$

Similarly, the Fisher information regarding damping ratio (ξ) is given by

$$\lim_{\substack{\Delta t\to 0\\ t\to\infty}} I_{\xi} = \frac{1}{\sigma_a^2}\int_0^\infty \left(\frac{\partial s}{\partial \xi}\right)^2 dt = \left(\frac{\omega_n\,(1+2\xi^2)}{8\sigma_a^2\xi^3\,(1-\xi^2)^2}\right) v_o^2 + H.O.T \tag{3.33}$$

and its corresponding minimum CoV is

$$CoV_{\xi} \geq \sqrt{\frac{8\sigma_a^2\xi\,(1-\xi^2)^2}{\omega_n\,(1+2\xi^2)\,v_o^2}} \tag{3.34}$$

If the corresponding coefficient of variations are computed for frequency and damping, their ratio is given by

$$\frac{\min(CoV_\xi)}{\min(CoV_{\omega_n})} = \sqrt{\frac{(1-\xi^2)^2(1+\xi^2)}{\xi^2(1+2\xi^2)}} \approx \frac{1}{\xi} \tag{3.35}$$

which not surprisingly, coincides with the case of displacement measurements with low damping ratio.

3.5.2 Initial Displacement

If the system is excited by an initial displacement, the upper limit on the Fisher information is given by

$$\lim_{\substack{\Delta t\to 0\\ t\to\infty}} I_{\omega_n} = \frac{1}{\sigma_a^2}\int_0^\infty \left(\frac{\partial a}{\partial \omega_n}\right)^2 dt = \frac{\omega_n(1+5\xi^2)}{8\sigma_a^2\xi^3}x_o^2 + H.O.T \tag{3.36}$$

and its corresponding minimum CoV is

$$CoV_{\omega_n} \geq \sqrt{\frac{8\sigma_a^2\xi^3}{(1+5\xi^2)\omega_n^3 x_o^2}} \tag{3.37}$$

Similarly, the Fisher information for the damping ratio (ξ) is given by

$$\lim_{\substack{\Delta t\to 0\\ t\to\infty}} I_\xi = \frac{1}{\sigma_a^2}\int_0^\infty \left(\frac{\partial a}{\partial \xi}\right)^2 dt = \left(\frac{\omega_n^3(1-2\xi^2)}{8\sigma_a^2\xi^3(1-\xi^2)^2}\right)x_o^2 + H.O.T \tag{3.38}$$

and its corresponding minimum CoV is

$$CoV_\xi \geq \sqrt{\frac{8\sigma_a^2\xi(1-\xi^2)^2}{\omega_n^3(1-2\xi^2)x_o^2}} \tag{3.39}$$

If the corresponding coefficient of variations are computed for frequency and damping, their ratio is given by

$$\frac{\min(CoV_\xi)}{\min(CoV_{\omega_n})} = \sqrt{\frac{(1-\xi^2)^2(1+5\xi^2)}{\xi^2(1-2\xi^2)}} \approx \frac{1}{\xi} \tag{3.40}$$

which also coincides with the case of displacement measurements with small damping ratios.

In the previous expressions σ_a^2 is the acceleration measurement noise variance per unit of time and it differs from σ_d^2. The relationship between these will depend on the type of sensors that are used. If one is interested in a criteria for equality of Fisher information regardless of the measurement type (displacement vs. acceleration), then it is necessary to equate the expressions of the corresponding Fisher information and solve for the σ_d in terms of σ_a. As an example, equating eq.3.16 and eq.3.31 we can find that

$$\frac{\sigma_a^2}{\sigma_d^2} = \left(\frac{1+\xi^2}{1+5\xi^2}\right)\omega_n^4 \tag{3.41}$$

which means that in order to obtain the same Fisher information regarding natural frequency from free vibration signals generated by an initial velocity; the variance of the noise in the acceleration (σ_a^2) and the variance of the noise in the displacement (σ_d^2) need to satisfy the above relationship. The previous result can be understood intuitively as follows: If a system is very slow, then it is much better to measure displacements because one can tolerate a higher level of noise. On the other hand, if the system is very fast, then it is better to measure accelerations. Although this is conceptually intuitive, the formula provides a quantification of the concept.

3.6 Fisher Information in Forced Vibration Response

In the case of forced vibrations, the noise contaminated measured response of the SDOF to an arbitrary input $u(t)$ is given by the convolution integral

$$s(t) = \int_0^t h(t-\tau)u(\tau)d\tau + \nu(t) \tag{3.42}$$

where $h(t)$ is the impulse response function. By using Leibnitz's rule of differentiation of integrals, we can find that the required derivative of the signal is given by

$$\frac{\partial s(t)}{\partial \theta_i} = \int_0^t \frac{\partial h(\tau)}{\partial \theta_i} u(t-\tau)d\tau \tag{3.43}$$

By definition (eq.3.4) the Fisher information after N observations is given by

$$\begin{aligned} I_{ij}(N) &= \frac{1}{\sigma^2}\sum_{n=0}^{N-1} \frac{\partial s(n;\theta)}{\partial \theta_i}\frac{\partial s(n;\theta)}{\partial \theta_j} \\ &= \frac{1}{\sigma^2}\sum_{n=0}^{N-1} \left(\int_0^{n\Delta t} \frac{\partial h(n\Delta t-\tau)}{\partial \theta_i} u(\tau)d\tau\right)\left(\int_0^{n\Delta t} \frac{\partial h(n\Delta t-\tau)}{\partial \theta_j} u(\tau)d\tau\right) \end{aligned} \tag{3.44}$$

If we examine the limiting case where the sampling rate goes to infinity, we obtain the following expression for the upper bound of the Fisher information at time T

$$\lim_{\Delta t \to 0} I_{ij}(T) = \frac{1}{\sigma_d^2} \int_0^T \left[\int_0^t \frac{\partial h(\tau)}{\partial \theta_i} u(t-\tau) d\tau \right] \left[\int_0^t \frac{\partial h(\tau)}{\partial \theta_j} u(t-\tau) d\tau \right] dt \tag{3.45}$$

Notice that since the impulse response $h(t)$ of a SDOF system is the response due to an initial velocity $\dot{x}_o = 1/m$, where m is the mass, we have

$$h(t) = e^{-\xi \omega_n t} \left(\frac{1}{m \omega_d} \right) \sin \omega_d t \tag{3.46}$$

where the necessary derivatives of the impulse response have already been computed in a previous section and in the case of frequency and damping ratio are given by eq.3.11 and 3.12 substituting $x_o = 0$ and $\dot{x}_o = 1/m$. In general, the integral in eqs.3.44 depends explicitly on the time history of the excitation force ($u(t)$). Once the Fisher information is computed, the CRLB in eq.3.6 can be used to compute the minimum achievable variance of the estimated parameters.

3.7 Numerical Verification

In this section we proceed to simulate the theoretically exact Fisher information and corresponding CRLB given in the previous sections for circular frequency and damping ratio. We will examine a single degree of freedom system in free vibration and in forced vibration.

3.7.1 Single Degree of Freedom System - Free Vibration

Consider a SDOF with $m = 1$, $\omega_n = 2\pi$, $\xi = 0.2$ subjected to an initial velocity of $v_o = 1m/s$. The total simulation time is $12s$ with a $\Delta t = 0.01s$ and the displacement measurement noise variance is $\sigma^2 = 0.01m^2$. Fig. 3.2 illustrates the noise corrupted free vibration response ($s(t)$), the computed temporal evolution of the Fisher information regarding circular frequency and damping ratio using eq.3.4. In a dotted line, the figure also shows the limiting values computed using eqs.3.16 and 3.17 (in this case $\lim I_\omega = 1,914$ and $\lim I_\xi = 62,911$). As expected, the Fisher information is a non-decreasing function that flattens out after the vibration ends and only noise is left in the signal ($s(t)$). The results shown in Fig. 3.2 confirm that the derived asymptotic values are indeed correct.

Based on the CRLB, the minimum variance that any unbiased estimator can achieve in estimating frequency and damping is $\min Var_{\omega_n} = 5.22\times10^{-4}$ and $\min Var_\xi = 1.59 \times 10^{-5}$. The respective coefficient of variations being $\min CoV_{\omega_n} = 0.0037$ and $\min CoV_\xi = 0.02$. The ratio of the coefficients of variation is 5.41 which is close to the result given by evaluating eq.3.22 (5.47). The small discrepancy results from neglecting higher order terms.

3.7.2 Single Degree of Freedom System - Forced Vibration

Consider a SDOF with $m = 1$, $\omega_n = 2\pi$, $\xi = 0.05$ subjected to a ground motion. In this case the total observation time is $T = 60s$ with $\Delta t = 0.02$. The displacement measurement noise variance was selected as $\sigma^2 = 5 \times 10^{-7} m^2/g^2$. Figure 3.3 shows the ground motion that was applied and the noise corrupted measured response.

The Fisher information for undamped circular frequency and damping ratio computed using eq.3.44 is shown in Fig. 3.4. In both cases the Fisher information basically flattens after $30s$ which is the point at which the response dies out and mostly measurement noise remains. In this case the CRLB for the minimum coefficient of variation of identified circular frequency and damping is computed using the total Fisher information and is $\min CoV_{\omega_n} = 0.00031$ and $\min CoV_{\xi} = 0.0062$.

3.7.3 Verification Using System Identification Results

In this section we examine the performance of a particular system identification algorithm with respect to the asymptotic results previously derived. Specifically, we will test how close is the minimum variance of estimated modal parameters to the CRLB. We will employ subspace identification (SUBID) [30] and will implement it using the MATLAB system identification toolbox [31]. To perform all simulations we will use the same system and measurement noise model used in the previous section.

A linear state space model of the following form was identified from input-output

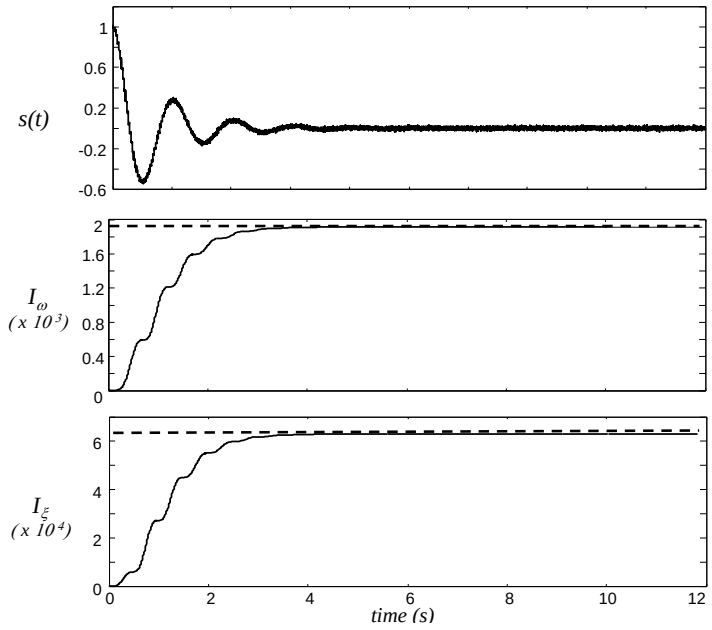

Figure 3.2: Noise-corrupted free vibration response of SDOF system (top), temporal variation of Fisher information for undamped frequency (middle), temporal variation of Fisher information for damping ratio (bottom)

data

$$x(k+1) = \mathbf{A}(k) + \mathbf{B}u(k) \tag{3.47a}$$

$$y(k) = \mathbf{C}x(k) + \mathbf{D}u(k) \tag{3.47b}$$

where $x(k)$ is the internal state at time $t = k\Delta t$, $u(k)$ is the input, $y(k)$ is the output. The matrices $\mathbf{A}$, $\mathbf{B}$, $\mathbf{C}$, and $\mathbf{D}$ result from the implementation of the system identification algorithm. The complex eigenvalues of the SDOF (λ) can be calculated from the eigenvalues of $\mathbf{A}$, which here we denote as α. Both λ and α come in complex conjugate pairs and each one satisfies

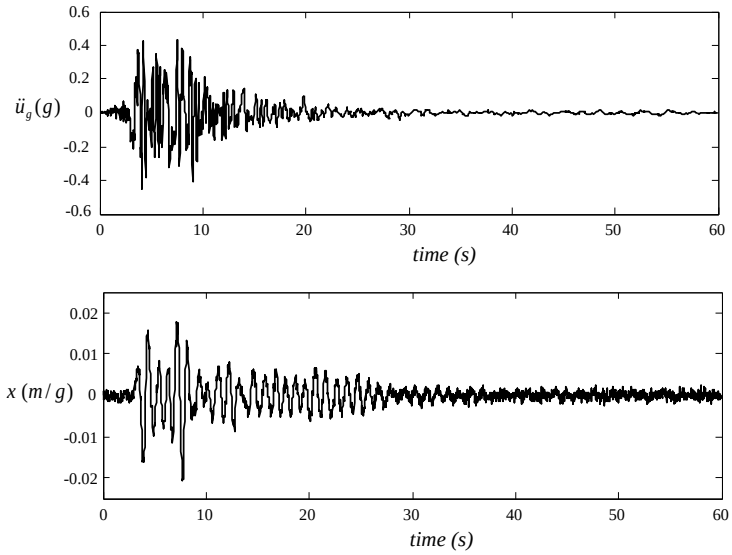

Figure 3.3: Time history of ground motion acceleration (top) and noise-corrupted system response (bottom)

$$\lambda = \frac{\log(\alpha)}{\Delta t} \tag{3.48}$$

The undamped frequency (ω_n) and damping ratio (ξ) can be computed from λ by using the expression

$$\lambda = -\xi\omega_n + i\sqrt{1-\xi^2}\omega_n \tag{3.49}$$

We performed 500 realizations of the noise contaminated system response and proceeded to identify the state space matrices and extract the modal circular frequency and damping ratio. It is essential to note that the identified linear model does not explicitly account for the presence of noise and thus in order to indirectly account for it, the size of the model has to be artificially increased to leave "space"

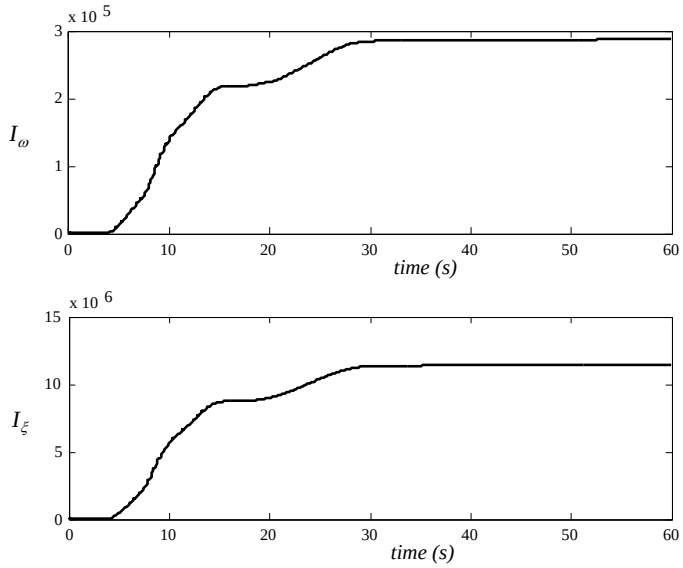

Figure 3.4: Temporal variation of Fisher information for undamped frequency (top), temporal variation of Fisher information for damping ratio (bottom)

for the noise to project.

The results of the identified modal parameters are summarized in Table 3.1. These results were obtained using a system order of 20 and extracting only the mode of interest. As expected, it was found that the statistical properties of the identified circular frequency and damping are influenced by the assumed order of the system. Figure 3.5 illustrates the variation of the CoV of the identified parameters as a function of the order of the identified state-space model (eq.3.47). The larger the identified order, the more accurate the estimation of the true mode becomes. One logical explanation for this is that by artificially enlarging the size of the identified system, more space is provided for the noise to project, which effectively cleans the identified mode of interest.

As can be seen, the SUBID results are unbiased and thus the CRLB should

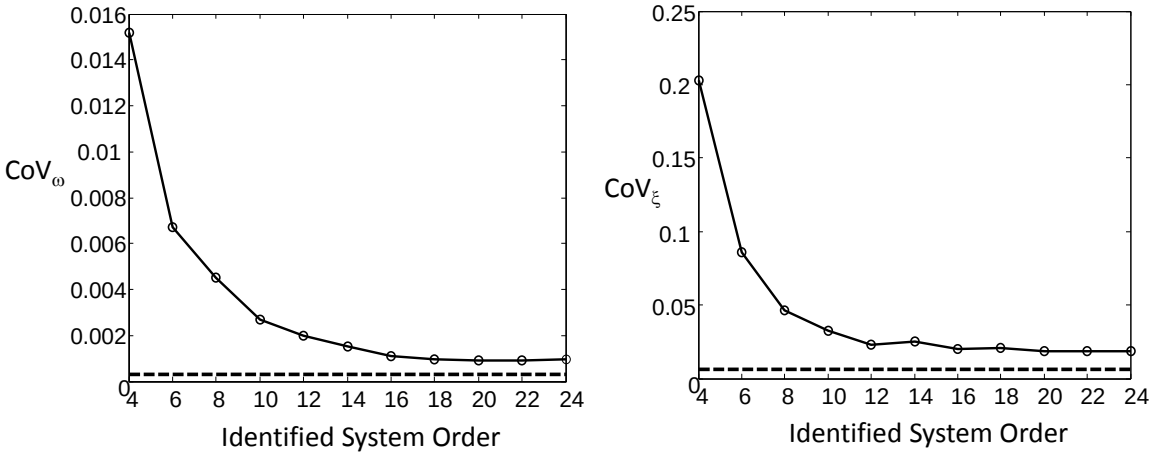

Figure 3.5: Variation of the CoV of circular frequency (left) and damping (right) as a function of the identified order of the system.

apply. The CRLB for circular frequency and damping was computed from the final value of the Fisher information shown in Fig. 3.4 and recorded in Table 3.1. It is verified that the CRLB provides a bound for the CoV of both identified parameters that was not reached by SUBID.

Table 3.1: Comparison of System Identification Results with CRLB

	Circular Freq.		Damping ratio	
	Sample Ave.	CoV	Sample Ave.	CoV
CRLB	6.2832	0.0003	0.0500	0.0062
SUBID	6.2830	0.0009	0.0500	0.0185

3.8 Heuristic Extension to Multi-degree of Freedom Systems

All the results so far correspond to SDOF systems. For multi-degree of freedom (MDOF) systems with N degrees of freedom and classical damping the response at any point p in the structure is given by

$$z(p,t) = \sum_{i=1}^{N} \phi_i(p) x_i(t) \tag{3.50}$$

where $\phi_i(p)$ is the amplitude of the i^{th} mode at p and $x_i(t)$ is the response of the i^{th} mode. If a sensor is present at p, then in the presence of additive noise, the measured signal at p will be given by $s(t) = z(p,t) + \nu(t)$.

The results for SDOF systems can be heuristically extended by analyzing every mode individually. Due to the orthogonality property of mode shapes, the derivative with respect to any modal parameter of a particular mode only depends on that mode, while the terms corresponding to other modes cancel out. Thus the block diagonal terms in the Fisher information matrix $\mathbf{I}(\theta)$ remain unchanged as the results are extended from SDOF to MDOF systems.

The cross modal terms in the Fisher information matrix, namely

$$I(\omega_i, \omega_j) = \frac{1}{\sigma^2} \sum_{n=0}^{N-1} \frac{\partial s(n;\theta)}{\partial \omega_i} \frac{\partial s(n;\theta)}{\partial \omega_j} \tag{3.51}$$

and

$$I(\omega_i, \xi_j) = \frac{1}{\sigma^2} \sum_{n=0}^{N-1} \frac{\partial s(n;\theta)}{\partial \omega_i} \frac{\partial s(n;\theta)}{\partial \xi_j} \tag{3.52}$$

for modes i and j can not be eliminated by simple inspection, since they will not be zero in general. In the special case where modes are well separated, the cross terms involve sums of products of enveloped sines and cosines with different frequencies. Figure 3.6 illustrates that these sums decay rapidly as the distance between the modal frequencies increase. Therefore it is expected that the magnitude of the off-diagonal block matrices in the Fisher information will diminish with respect to the block diagonals. This implies that the inverse of the Fisher information matrix, i.e. the Cramer-Rao lower bound matrix will be mostly block diagonal. Consequently the CRLB of each mode can be computed independently without significant error if the modes are well separated. The validity of this heuristic claim will be tested in the following section.

3.9 Verification of Modal CRLB for Multidegree of freedom systems

Consider a shear-beam system with the following mass and stiffness matrices

$$\mathbf{M} = \begin{bmatrix} 1 & 0 \\ 0 & 1 \end{bmatrix} \tag{3.53}$$

$$\mathbf{K} = \begin{bmatrix} 30 & -20 \\ -20 & 20 \end{bmatrix} \tag{3.54}$$

The circular frequencies of this system are $\omega_{n,1} = 2.09$ rad/s and $\omega_{n,2} = 6.75$ rad/s. The damping of the system is classical with $\xi = 0.05$ for every mode. The mass-normalized modal matrix is given by

$$\Phi = \begin{bmatrix} -0.6154 & -0.7882 \\ -0.7882 & 0.6154 \end{bmatrix} \tag{3.55}$$

The equation of motion in the modal space when the system is subject to a ground motion ($\ddot{u}_g(t)$) are given by

$$\begin{bmatrix} 1 & 0 \\ 0 & 1 \end{bmatrix} \begin{bmatrix} \ddot{x}_1(t) \\ \ddot{x}_2(t) \end{bmatrix} + \begin{bmatrix} 0.2094 & 0 \\ 0 & 0.6754 \end{bmatrix} \begin{bmatrix} \dot{x}_1(t) \\ \dot{x}_2(t) \end{bmatrix} + \dots$$
$$+ \begin{bmatrix} 4.3845 & 0 \\ 0 & 45.6155 \end{bmatrix} \begin{bmatrix} x_1(t) \\ x_2(t) \end{bmatrix} = \begin{bmatrix} -1.4036 \\ -0.1728 \end{bmatrix} \ddot{u}_g(t) \tag{3.56}$$

We performed 500 stochastic realizations with the ground motion shown in Fig. 3.3(top) and with displacement measurements at the first degree of freedom, contaminated with an additive Gaussian white noise with $\sigma^2 = 5 \times 10^{-7} m^2/g^2$. For each realization we implemented SUBID and identified modal frequencies and damping ratios. The order of the identified system was 50. The second order statistics of the results are shown in Table 3.2.

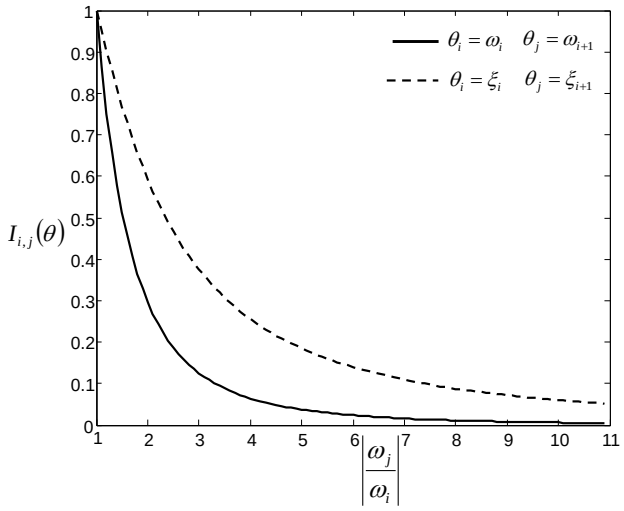

Figure 3.6: Illustration of the relative importance of off-diagonal terms in the Fisher information matrix with respect to its diagonal terms and as a function of the distance between consecutive modal frequencies

Table 3.2: Comparison of System Identification Results with CRLB

	Circular Freq.		Damping ratio	
	Sample Ave.	CoV	Sample Ave.	CoV
CRLB-Mode1	2.0939	0.0001	0.0500	0.0018
SUBID-Mode 1	2.0939	0.0004	0.0480	0.0048
CRLB-Mode 2	6.7539	0.0026	0.0500	0.0327
SUBID-Mode 2	6.7541	0.0050	0.0522	0.0601

From the results shown in Table 3.2 one can see that in the case of well separated modes, the heuristic extension of the CRLB computed mode-by-mode provides effective bounds for the CoV of circular frequency and damping ratio. It is also of

interest to note that the two modes have very different bounds. This is driven mainly by the difference in modal forces. From the right-hand side of eq. 3.56 one can see that mode 1 has a much higher load factor than mode 2, this means that the response of that mode will be much higher and thus the signal-to-noise ratio of mode 1 will be higher that for mode 2. Higher signal-to-noise ratio leads to better estimation accuracy.

3.10 Conclusions

We presented the derivations of exact expressions to compute the lowest achievable variance by any unbiased estimator of modal frequency and damping ratio from free vibration and forced vibration signals contaminated by additive Gaussian white noise. These limits are found through the CRLB theory. The results were obtained for displacement or acceleration measurements contaminated with zero-mean additive Gaussian white noise.

The expressions were derived for single degree of freedom systems and extended to classically damped MDOF systems with well-separated modes. It was proved that the CoV of identified modal damping ratio must be significantly higher that the CoV of identified modal frequency by factor approximately equals to the inverse of the damping ratio. The analytical results were illustrated via simulated system identification using SUBID methods.

3.11 Bibliography

[1] L. Ljung (1999). System Identification. Prentice Hall. Upper Saddle River, NJ.

[2] Jer-Nan Juang (1994). Applied system identification. PTR Prentice Hall.

[3] P. Eykhoff (1974). System Identification: parameter and state estimation. John Wiley and Sons Inc., New York, N.Y.

[4] T. Söderström and P. Stoica (1989). System Identification, Prentice-Hall, Englewood Cliffs.

[5] P. Van Overschee and B. De Moor (1996). Subspace Identification for Linear Systems: Theory. Kluwer Academic Publications.

[6] R. Pintelon and J. Schoukens (1996). System Identification: A frequency domain approach, 2^{nd} Edition 2012.

[7] J.L. Beck and L.S. Katafygiotis (1998). Updating models and their uncertainties I: Bayesian statistical framework. ASCE Journal of Engineering Mechanics 124(4):455-461

[8] M. Dohler, F. Hille, X. Lam, L. Mevel and W. Rucker (2011). Confidence intervals of modal parameters during progressive damage test. Proc. Soc. Exp. Mech. 2011, 237-250.

[9] N.M. Maia and J.M. Silva (Eds.) (1997). Theoretical and Experimental Modal Analysis. Research Studies Press Ltd. Hertfordshire, England.

[10] D.T. Griffith and T.G. Carne (2007). Experimental uncertainty quantification of modal test data. Proc. of the XXV International Conference in Modal Analysis.

[11] S. Adhikari, M.I. Friswell, K. Lonkar and A. Sarkar (2009). Experimental case studies for uncertainty quantification in structural dynamics. Probabilistic Engineering Mechanics 24:473-492

[12] W. Gersch (1974). On the achievable accuracy of structural system parameter estimates. Journal of Sound and Vibration 34(1) 63-79

[13] F. E. Udwadia (1994). Methodology for Optimum Sensor Locations for Parameter Identification in Dynamic Systems. ASCE Journal of Engineering Mechanics.120(2):368-390.

[14] R. Pintelon, P. Guillaume and J. Schoukens (2007). Uncertainty calculation in operational modal analysis. Mechanical Systems and Signal Processing 21(6) 2359-2373.

[15] M. Dohler, X-B Lam and L. Mevel (2013). Uncertainty quantification for modal parameters from stochastic subspace identification on multi-setup measurements. Mechanical Systems and Signal Processing 36(2):562-581

[16] E. Reynders, R. Pintelon and G. De Roeck (2008). Uncertainty bounds on modal parameters obtained from stochastic subspace identification. Mechanical Systems and Signal Processing 22(4) 948-969.

[17] S.K. Au (2014). Uncertainty law in ambient modal identification-Part I: Theory. Mechanical Systems and Signal Processing 48(1-2) 15-33.

[18] D. Bernal, M. Dohler, S. Mozaffari-Kojidi, K. Kwan and Y. Liu (2013). First mode damping ratios for buildings. Earthquake Spectra, doi: 10.1193/101812EQS311M

[19] S. Adhikari and J. Woodhouse (2001). Identification of Damping: Part 1, Viscous Damping. Journal of Sound and Vibration 243(1):43-61

[20] C.E. Shannon (1948). A Mathematical Theory of Communication. The Bell System Technical Journal 27:379-423.

[21] J.G. Proakis and M. Salehi (2005). Fundamentals of Communication Systems. Pearson, Prentice Hall. Upper Saddle River, NJ.

[22] S. M. Kay (1993). Fundamentals of Statistical Signal Processing: Estimation theory. Prentice Hall. Upper Saddle River, NJ.

[23] E.Karlsson, T. Söderström and P. Stoica (2000). The Cramer-Rao lower bound for noisy input-output systems. Signal Processing 80:2421-2447.

[24] E.M. Hernandez, N.R. Polanco (2014). Uncertainty Quantification of Identified Modal Parameters Using the Fisher Information Criterion. XXXII Proceedings of the International Conference in Modal Analysis - Model Validation and Uncertainty Quantification, Volume 3, 177-184

[25] R.K. Mehra (1974). Optimal inputs or linear systems input identification. IEEE Trans. Autom. Control 19(3): 192-200.

[26] R.K. Mehra (1974). Optimal input signals for parameter estimation in dynamical systems - Survey and results . IEEE Trans. Autom. Control 19(6): 753-768.

[27] K. Erazo, E.M. Hernandez (2013). A model-based observer for state and stress estimation in structural and mechanical systems: Experimental validation, Mech. Syst. Signal Process. 43(1-2):141-152

[28] T. Wigren and A. Nehorai (1991). Asymptotic Cramer-Rao bounds for estimation of the parameters of damped sine waves in noise. IEEE Transactions on Signal Processing 39(4) 1017-1020.

[29] Wolfram Research, Inc., Mathematica, Version 8.0, Champaign, IL (2010).

[30] P. van Overschee, and B. De Moor. Subspace Identification of Linear Systems: Theory, Implementation, Applications. Springer Publishing: 1996.

[31] http://www.mathworks.com/products/sysid/

Chapter 4

Finite element model updating of semi-composite bridge decks using operational acceleration measurements

Néstor Polanco[1], Geoffrey May[2], Eric M. Hernandez[1]

[1]Dept. of Civil and Env. Engineering. University of Vermont. 103 Votey Hall, 33 Colchester Ave., Burlington VT 05405, USA

[2]OBEC Consulting Engineers

Journal: *Journal of Engineering Structures*, 126, 264-277.

4.1 Abstract

Composite bridge decks provide higher flexural moment capacity and stiffness compared to their non-composite counterparts. In order to achieve composite behavior, differential slip between the steel member and the concrete slab must be restrained by means of shear connectors. In older bridge decks composite behavior is uncertain. Uncertainty arises, among other things, due to lack of knowledge regarding the type of shear connector used (if any), cumulative damage due to fatigue, and aging effects. In this paper the authors propose the use of sensitivity-based finite element model updating to determine the degree of composite behavior of operational bridge decks with uncertain shear connectors. The free parameters of the models are: rigidity per unit length of the beam-slab interface and the elastic modulus of the concrete slab. The features used in the model updating procedure are the identified modal frequencies from operational acceleration measurements. A sequential sensitivity-based weighted least-squares solution was implemented. The proposed methodology is verified in various simulated bridge deck structures and validated in an operational and partially instrumented bridge deck with uncertain composite action.

4.2 Introduction

Based on data from the National Bridge Inventory approximately 24% of all multi-span bridges in the United States are constructed using steel girders and a concrete slab [National Bridge Inventory; 2019]. This percentage is higher in the Northeast where it reaches approximately 63%. One important component in this type of deck

construction is shear connectors. Shear connectors enable composite behavior by transferring horizontal shear stresses between the steel beam and the concrete slab. Composite decks possess a significantly larger flexural strength and stiffness with respect to non-composite ones [2]. Shear connectors are typically constructed by welding vertical steel studs to the top face of the top flange in steel girders prior to pouring of the concrete slab. The design of shear connectors is governed by two criteria; static strength and fatigue. Shear connectors are first designed for fatigue loads due to moving vehicles and then checked for static ultimate strength. Girders are checked for static ultimate strength assuming full composite action, i.e. the number of shear connectors is enough to transfer the horizontal shear force at the interface that results when the steel girder has fully yielded and the concrete slab has simultaneously reached its maximum compressive capacity. AASHTO LRFD Specifications require that steel girder/concrete slab decks be designed as fully composite [8]. If a beam does not have enough connectors to guarantee fully-composite behavior, then it is categorized as partially composite and its ultimate load capacity is typically governed by the failure of shear connectors.

Whenever the structural integrity of an existing bridge deck needs to be assessed; the presence and effectiveness of shear connectors becomes a central issue. In older bridges with unknown construction practices, lack of as-built drawings and(or) cumulative damage effects such as fatigue, the effectiveness of shear connectors is uncertain. The most widely used approach in the practice of structural assessment of bridge decks with uncertain composite action consists in assuming no interaction between the concrete deck and the steel beam. This practice typically results in a diagnosis that is not cost effective and inconsistent with the fact that over the years

of service some of these decks have withstood traffic loading beyond the strength provided by the non-composite assumption. An overly conservative diagnosis regarding a bridge deck could result in an unnecessary decision to replace, retrofit, or to reduce the load rating of the deck. Development of technologies capable of assessing the effectiveness of shear connectors and the degree of composite action in uncertain bridge decks would prove useful for engineers and public transportation decision makers.

A reasonable approach to assess the effectiveness of composite action in a deck is to instrument it with sensors capable of measuring the strains in the vicinity of the steel-concrete interface. If the strain measurements in the steel and concrete near the interface are close, then one can infer that there is negligible relative slip between the two surfaces and composite behavior is verified (at least within the range of loading consistent with the measurements). As an alternative, one can measure the strain at various points along the depth of the steel girder and interpolate (or extrapolate) the location of the neutral axis. Using principles from structural mechanics, the level of composite action can be inferred from the estimated location of the neutral axis. This last approach is only valid if no net axial force is present in the deck. One drawback of strain-based approaches is that they require significant instrumentation and can only assess composite action at a local level, i.e. at the section where the strain is measured.

Recent examples of the strain measurement approach can be found in the literature. In [4] Breña et al. present results from monitoring an I-girder type highway overpass under a controlled live load test. A total of 60 strain measurements were used to estimate load distribution factors and these results were compared with the results from a finite element model (FEM). The researchers found that although the

deck was designed as non-composite, the strain measurements across the cross section (assuming Bernoulli's hypothesis of linear strain distribution) were consistent with the condition of I-girders acting as composite with the reinforced concrete slab. In [5] Chakraborty and DeWolf developed and implemented a continuous strain monitoring system on a three-span composite I-girder overpass. The instrumentation consisted of 20 uniaxial strain gages. The study reported on data over a period of 5 months. Among other things, the study included the determination of the location of the height of the neutral axes of various structural members when large trucks travel across the bridge. One of the conclusions of this study was that the measured strain levels are typically significantly below those recommended by AASHTO. The authors stated that this is a byproduct of conservative simplifications typically used in conventional designs, such as not including redundancies, connection restraints, and the way in which loads are distributed to different parts of the structure. This conclusion is in agreement with a previous study [6].

Jauregui et al. [7] conducted a series of controlled field loading tests on a standard I-girder bridge built in the late $1950's$ and assigned for decommission. Measurements consisted of strains and vertical deformations at various points. Results of the investigation show that the deck behaved as if partially composite right up to the onset of yielding. Partial composite action occurred in spite of the lack of shear connectors between the girders' top flange and the concrete slab. This suggests that partially composite action of the girders can be attributed to friction due to the slab bearing down on the girder top flange and mechanical interlock at the girder-deck interface. Jauregui et al. argued that these two forms of shear restraint are dependable if not overcome and thus may be used to arrive at a better measure of the bending stiffness

and resistance of the deck.

The main hypothesis of this paper is that global acceleration measurements induced by traffic can be used to estimate the stiffness provided by the presence of partial composite action in bridge decks. Specifically, free vibration response shortly after the vehicle leaves the deck. Laboratory experiments conducted by various researchers on isolated composite beams provide encouraging results which indicate that this approach might be scalable to operational bridge decks [9, 10].

Morassi et al. [9], performed a theoretical and experimental laboratory investigation into the behavior of isolated, free-free steel beams-concrete slab composite beams. They found that if shear connectors are damaged, then their effect can be seen in the changes in vibration frequencies. It is expected that their general conclusions extrapolate to cases with different boundary conditions. Finally, Kwon et al. [10] performed a series of controlled laboratory experiments aimed at testing the effectiveness of post-installed shear connectors. After examination of their experimental results, it is possible to conclude that steel girders with concrete slabs that do not possess explicit shear transfer mechanisms in the form of shear connectors; exhibit a flexural stiffness that lies between the fully-composite and non-composite assumptions. It can also be concluded that the difference between the overall stiffness of a composite beam with shear connectors versus an identical one without shear connectors can be observed even within the range of linear stresses.

The use of acceleration measurements presents several advantages with respect to localized strain monitoring: (i) the overall integrated behavior of the deck can be assessed as opposed to a more local examination provided by the strains measurements (ii) a smaller number of sensors could be used to perform the assessment, making

instrumental monitoring of these type of structures more affordable. We propose the use of a sensitivity-based weighted finite element model updating to determine the degree of composite behavior in operational bridge decks with unknown/uncertain installation of shear connectors. The free parameters of the model are the rigidity per unit length of the beam-slab interface and the elastic modulus of the concrete slab. The features used in the model updating procedure are the identified modal frequencies and their corresponding mode shapes extracted from global acceleration measurements. A sequential weighted least-squares solution was implemented with a diagonal weighting matrix on which each element is inversely proportional to the variance of the identified modal features.

From the perspective of model updating, the fundamental challenges addressed in this paper are to determine if: (a) the concrete modulus of elasticity and the interface stiffness are independently identifiable from a subset of modal frequencies and (b) the sensitivity of frequencies to changes in the free parameters is large enough to overcome the "noise" in the identified modal parameters. The identification noise is important because bridges are subjected to variations in environmental conditions that affect boundary conditions and stiffness properties of the material, which in turn get reflected as changes in modal properties.

The proposed approach is verified in the context of numerical simulations and validated in an operational and partially instrumented bridge deck located in the state of Vermont, USA. The bridge was built in 1963 and it supports two lanes of traffic. The deck consists of a concrete slab supported on three inner longitudinal stringers and two exterior girders. The interior stringers are supported on transverse floor beams simply connected to the two main longitudinal girders. The bridge spans

a total of 170.08 m ($558ft$). A portion of the bridge deck was instrumented with a total of 10 vertical accelerometers distributed along the length of stringers.

The paper begins with a section describing the sensitivity-based model updating procedure to be employed. The procedure uses eigenvalue sensitivity in order to set up the linear set of equations. It also includes a weighting matrix to account for the relative variance in the identification of the modal features. The paper continues with a section describing the various models and assumptions to be used through the rest of the paper. This is followed by sections describing two-dimensional and three-dimensional numerical simulations aimed at verifying the proposed methodology. A section describing the application in the context of an operational bridge deck concludes the computational portion of the paper. The paper ends with a section highlighting the main findings, limitations and potential future work.

4.3 Sensitivity-based model updating

Finite element model updating can be defined as a series of computational steps, in which a preselected set of model parameters within a particular model class are modified to minimize a function of the difference between response measurements of the system and model predictions [20,23]. More formally this can be stated as: Given a model class $\mathcal{M}(\theta)$ with response feature vector $y_{\mathcal{M}} \in \mathbb{R}^m$ and corresponding system response feature vector $y_{\mathcal{S}} \in \mathbb{R}^m$, modify an f-dimensional subset $\theta_f \subset \theta$ such that a local minimum of the function $J = g(\Delta y)$ is attained, where $\Delta y = y_{\mathcal{S}} - y_{\mathcal{M}}$. The subset θ_f is typically referred to as the free parameter space. In general, the response features and model parameters exhibit a non-linear relationship. The relation between

the response features and perturbations in the free model parameters $\Delta\theta_f$ can be written as

$$y_{\mathcal{M}}(\theta_f + \Delta\theta_f) - y_{\mathcal{M}}(\theta_f) = \mathbf{S}\Delta\theta_f + H.O.T. \tag{4.1}$$

where $H.O.T$ represents higher order terms in $\Delta\theta_f$, the matrix $\mathbf{S} \in \mathbb{R}^{m\times f}$ and each component of it is defined as

$$S_{ij} = \frac{\partial y_{\mathcal{M},i}}{\partial \theta_{f,j}} \tag{4.2}$$

The objective function J is typically selected as a quadratic form

$$J = \epsilon^T \mathbf{W} \epsilon \tag{4.3}$$

where

$$\epsilon = \Delta y - \mathbf{S}\Delta\hat{\theta}_f \tag{4.4}$$

$\mathbf{W} \in \mathbb{R}^{m\times m}$ is a weighting matrix and $\Delta\hat{\theta}_f$ is the estimated change in the free parameters. If $m \geq f$ then the solution that minimizes J is obtained by

$$\Delta\hat{\theta}_f = \alpha \left(\mathbf{S}^T\mathbf{W}\mathbf{S}\right)^{-1} \mathbf{S}^T\mathbf{W}\{\Delta y\} = \mathbf{F}\{\Delta y\} \tag{4.5}$$

where $0 < \alpha \leq 1$ is a scalar. The purpose of α is to reduce the estimated change in the model parameters to avoid unrealistic variations (overshooting) byproduct of the linearization in eq.4.1. The covariance of the estimates in each step of the updating is given by

$$COV\left[\Delta\hat{\theta}_f\right] = \mathbf{F}COV\left[\{\Delta y\}\right]\mathbf{F}^T \tag{4.6}$$

In this study the measurement features will consist of a subset of modal frequencies and(or) their corresponding mode shape amplitudes at sparse locations. Analytical closed-form expressions of the sensitivity of eigenvalues and mode shapes in undamped multi-degree of freedom systems can be found in the literature [19, 21]. The sensitivity of eigenvalues to parameters that define the mass and(or) stiffness is given by

$$\frac{\partial\lambda_j}{\partial\theta_k} = \phi_j^T\left[-\lambda_j\frac{\partial\mathbf{M}}{\partial\theta_k} + \frac{\partial\mathbf{K}}{\partial\theta_k}\right]\phi_j \tag{4.7}$$

This expression is very convenient because it only involves the mode shape corresponding to the frequency of interest. In cases where the computation of closed-form sensitivities becomes computationally expensive or prohibitive, one can always resort to a less elegant computation given by

$$S_{ij} \approx \frac{\Delta y_{\mathcal{M},i}}{\Delta\theta_{f,j}} \tag{4.8}$$

This requires careful selection of $\Delta\theta_{f,j}$ and the solution of multiple eigenvalue problems in order to compute the changes in eigenvalues and eigenvectors.

4.4 Model Formulation

The mathematical theory describing the behavior of composite beams with weak shear connectors subjected to unidirectional bending on a symmetry plane has been

studied in depth by various researchers [11], [12], [13] and [14]; just to mention a few. More recently, Dall′Asta [16] developed a more complete theoretical formulation for three-dimensional cases. The author included out-of-plane bending and torsion based on Kirchhoff bending theory and Vlasov torsion theory. Ranzi et al. [17] performed a two-dimensional comparative study using four different formulations to analyze partially composite two-layer beams subject to symmetric bending, namely; the exact analytical solution, direct stiffness method, the finite element method and finite differences. The authors concluded that the direct stiffness method, formulated using basis functions from the exact solution, provides the best accuracy followed by the finite element method and the finite differences. This paper focuses on complex three-dimensional structures and does not assume prior knowledge of the basis functions from the exact solution, therefore a finite element model (FEM) formulation is preferred.

All finite element models (FEM) to be considered in this paper are linear, elastic with lumped mass and classical damping. The set of parameters θ consist of all the material properties necessary to formulate the stiffness, mass and damping matrices. The set of free parameters θ_f will be the elastic modulus of the reinforced concrete slab and the stiffness of the connecting elements representing the rigidity per linear unit of length of the interface between the steel girder and the concrete slab. The stiffness of the connecting elements will provide an indication of the overall degree of composite action between steel and concrete. In both cases the parameters represent homogenized averaged properties.

As mentioned previously the two fundamental problems to address are: (i) identifiability of parameters, i.e. Is it possible to separately identify the elastic modulus

of concrete and the stiffness of the interface?, and (ii) Can these parameters be identified in the presence of noise or bias in the identified modal features? To investigate these two aspects, various scenarios and models with increasing complexity will be examined.

We begin with the simplified model of one of the stringers by considering it as a simply supported 2-dimensional continuous beam. The model has analogous sections and dimensions to the stringers (W18x60) and tributary area of the concrete slab. This model consists of two parallel longitudinal rows of frame-type elements for concrete slab (top) and the steel stringer (bottom); as shown in Fig. 4.1a. The longitudinal elements are interconnected at intermediate nodes by massless perpendicular vertical elements that represent the stiffness of the interface that enables the composite behavior, Fig. 4.1b. The model was implemented using a code developed by the third author in MATLAB environment. Figure 4.1a shows the dimensions and general details of the specific model considered. The mass of the model is lumped at the nodes and the stiffness matrix is for horizontal and vertical degrees of freedom (rotations where condensed out).

We also study a 3-dimensional model analogous to the portion of the bridge deck that is instrumented as indicated in Fig. 4.10. The model explicitly includes the main girders, floor beams, girders, bracings, and slab. The model has $83,026$ DOF, 932 frame members that represent the steel elements (girder, stringers, floor beams, bracings) and shear connectors, and 13,120 shell areas to model the concrete slab. The model was formulated using the software SAP2000 and it is shown in Figures 4.5a, 4.5b, and 4.5c.

4.5 Two Dimensional Model - Simulated Cases

This section describes the simulation results corresponding to the application of sensitivity-based model updating to the 2-D semi-composite beam shown in Fig. 4.1a. The main interest is to determine if the two free parameters θ_1= elastic modulus of concrete and θ_2= shear connector stiffness per linear meter are distinguishable based on the first five flexural modal frequencies of the deck.

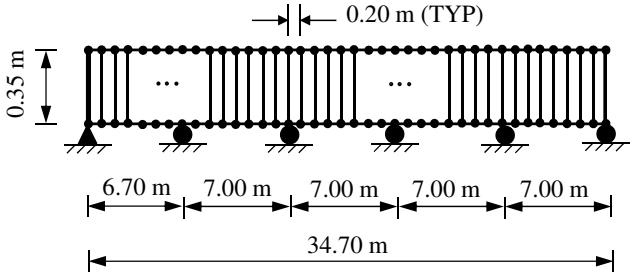

(a) Longitudinal section of two dimensional FEM of composite beam

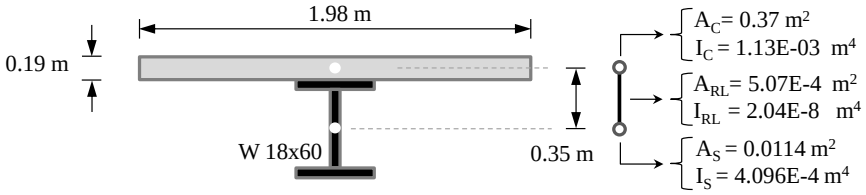

(b) Transverse section of two dimensional FEM of composite beam

Figure 4.1: Two dimensional FEM

Various cases where considered:

1. CASE 1: Identify a simultaneous increase of 20% in the rigidity per unit length of the vertical connectors and in the elastic modulus of concrete.

2. CASE 2: Identify a 20% decrease in the rigidity per unit length of the vertical connectors and an increase of 20% in the elastic modulus of concrete.

3. CASE 3: Identify an increase of 100% in the rigidity per unit length of the vertical connectors while the elastic modulus of concrete remains unchanged. This was induced by reducing the separation of vertical connectors in half while keeping the stiffness of the individual connectors the same. This case involves the presence of model error since the model does not match the system used to generate the "identified" modal features.

Table 4.1: System and initial frequencies (prior to updating) for Cases 1, 2 and 3 in the 2D Model

Frequency (#)	**SYSTEM (Hz)**	**CASE 1 (Hz)**	**CASE 2 (Hz)**	**CASE 3 (Hz)**
1	16.24	16.80	16.17	17.20
2	17.40	18.042	17.30	18.63
3	20.28	21.13	20.21	21.85
4	22.86	24.13	22.84	24.92
5	25.79	27.05	25.58	28.39

The first two cases are intended to investigate the capability of the methodology to distinguish separate changes in the free parameters. For both cases the separation between the vertical connectors was selected as $s_m = 0.20\ m$. Case 3 examines the effect of model error. Here the separation of the connectors is inconsistent with the model and it is necessary to verify if the correct stiffness per unit length can

still be estimated. For this case the system had a separation of vertical connectors $s_\lambda = 0.10\ m$ and the model $s_m = 0.20\ m$. For all cases, the sensitivity approach was implemented using only the discrepancies in the first six eigenvalues. In all cases the initial values of the free model parameters are $3,630$ kN/m/m for the rigidity per unit meter of the rigid connectors and 28 GPa for the elastic modulus of concrete.

Figures 4.2, 4.3 and 4.4 show the evolution of the free model parameters as the number of iterations increases for cases 1, 2 and 3 respectively. It can be seen that in all cases, despite some initial overshooting, the selected free parameters converge to the target values. This suggests that the parameters are independently identifiable from changes in modal frequencies.

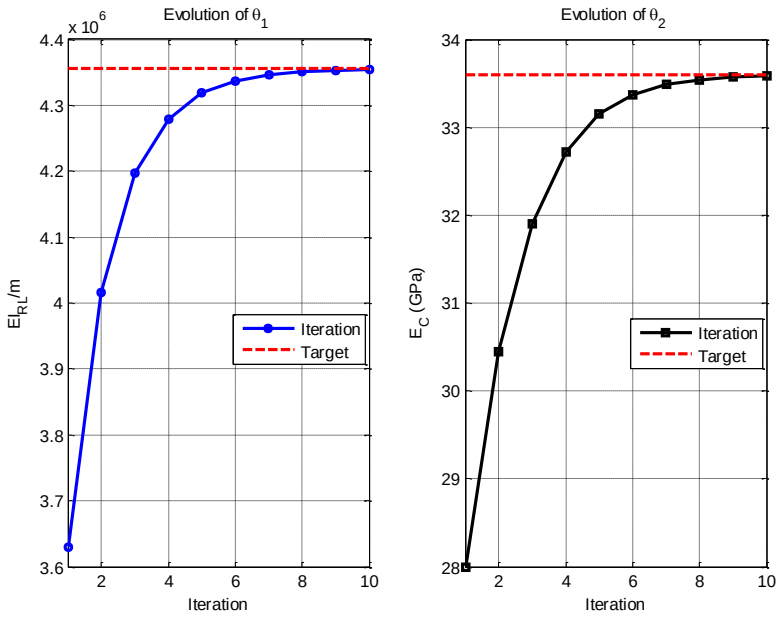

Figure 4.2: Evolution of model parameters a)Rigidity per linear meter and b) elastic modulus of concrete for Case 1 of 2D FEM

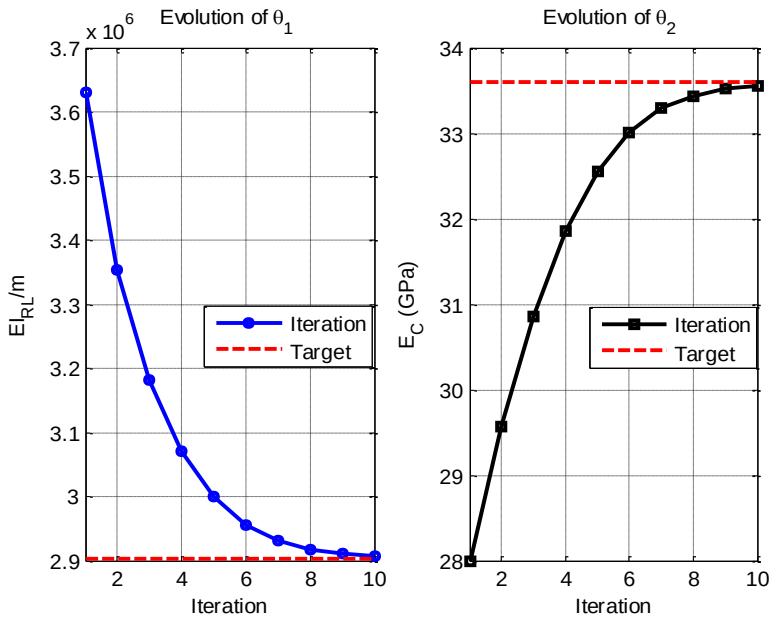

Figure 4.3: Evolution of model parameters a)Rigidity per linear meter and b) elastic modulus of concrete for Case 2 of 2D FEM

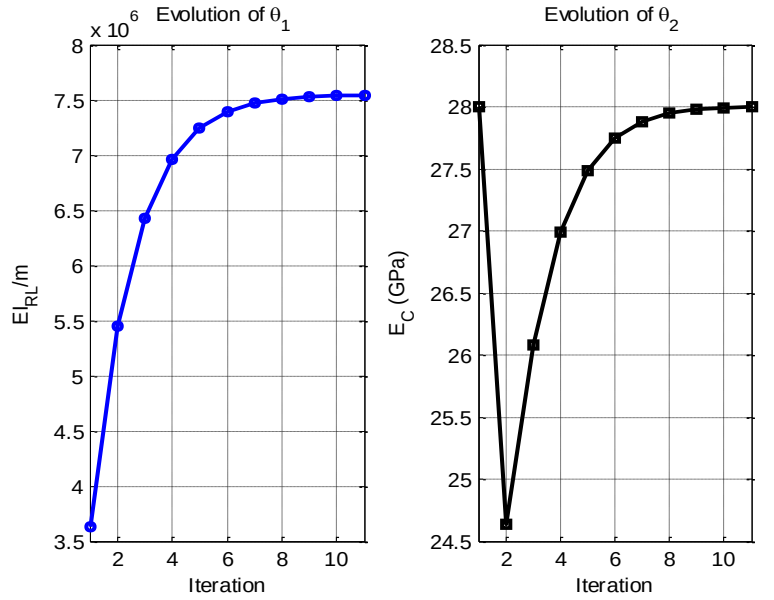

Figure 4.4: Evolution of model parameters a)Rigidity per linear meter and b) elastic modulus of concrete for Case 3 of 2D FEM

4.6 Three Dimensional Model - Simulated Cases

Following encouraging results from updating a 2D FEM of an isolated stringer, verification of the sensitivity approach using a 3D FEM is investigated. This model simulates the instrumented portion of the bridge deck shown in Fig. 4.5. Cases 1 and 2 from the previous section are investigated, namely

1. CASE 1: Identify a simultaneous increase of 20% in the rigidity per unit length of the vertical connectors and in the elastic modulus of concrete.

2. CASE 2: Identify a 20% decrease in the rigidity per unit length of the vertical connectors and an increase of 20% in the elastic modulus of concrete.

Table 4.2 shows the five modal frequencies used to perform the model updating. The table also shows the initial values of the frequencies prior to updating corresponding to each case. The sensitivity matrix was approximated using eq.4.8. The value of $\Delta\theta_f$ to compute the changes in modal parameters was selected as $0.01\theta_f$. The sensitivity matrix is shown in Fig. 4.6. As expected the eigenvalues are more sensitive to changes in the concrete modulus, however the sensitivity due to changes in the stiffness of the shear links is not negligible.

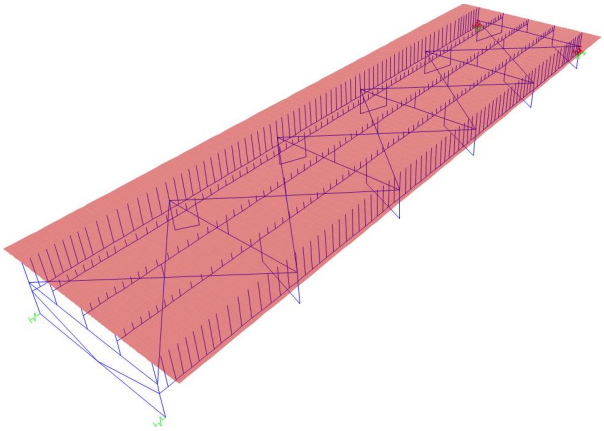

(a) Three dimensional FEM of bridge deck

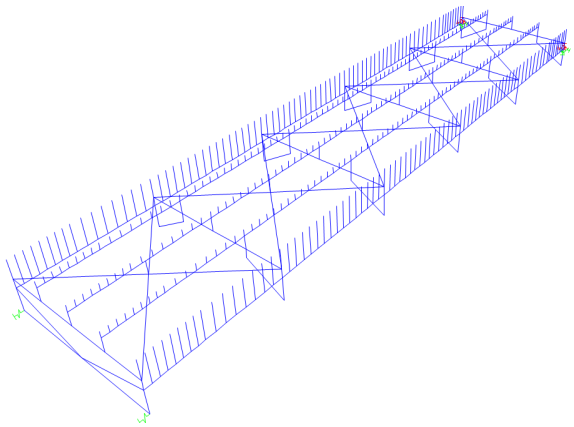

(b) Three dimensional FEM of bridge deck (no slab)

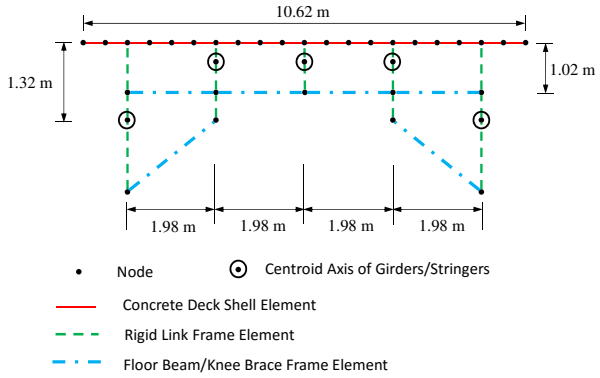

(c) Cross section of three dimensional FEM

Figure 4.5: Three dimensional FEM of bridge deck (see Fig. 4.10 for additional dimensions)

Table 4.2: System and initial model frequencies (prior to updating) for Cases 1 and 2 in the 3D Model

Frequency (#)	**SYSTEM (Hz)**	**CASE 1 (Hz)**	**CASE 2 (Hz)**
1	14.05	14.35	14.30
2	17.16	17.69	17.58
3	18.15	18.80	18.67
4	18.83	19.51	19.37
5	22.19	19.51	19.37

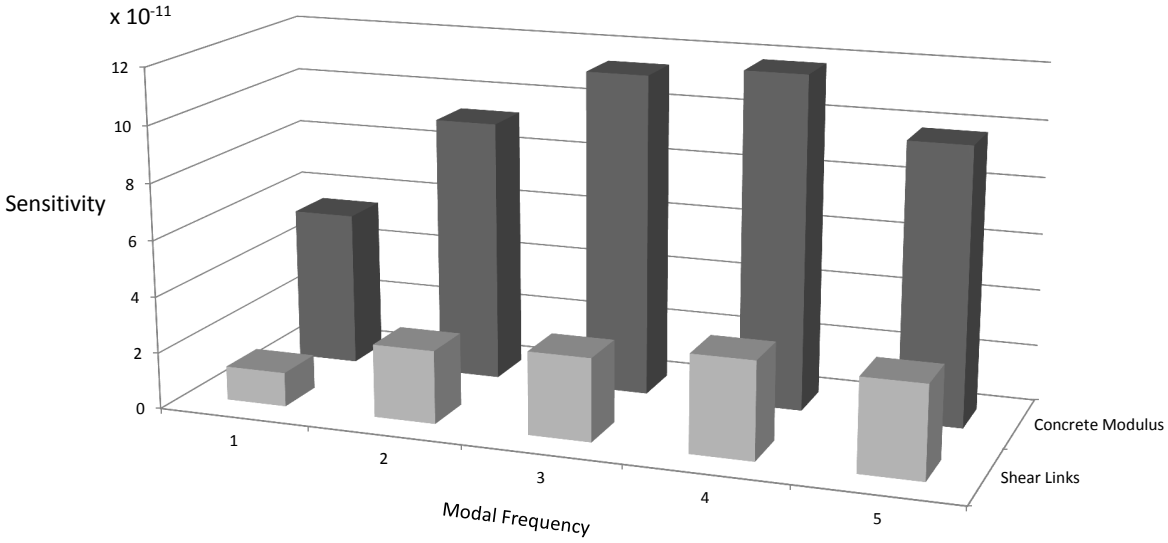

Figure 4.6: Sensitivity matrix of first five eigenvalues to concrete elastic modulus and stiffness of shear links.

Figures 4.7 and 4.8 show the results for Cases 1 and 2 respectively. In similar fashion to the 2D FEM, the modal features and the model parameters converge to the target values.

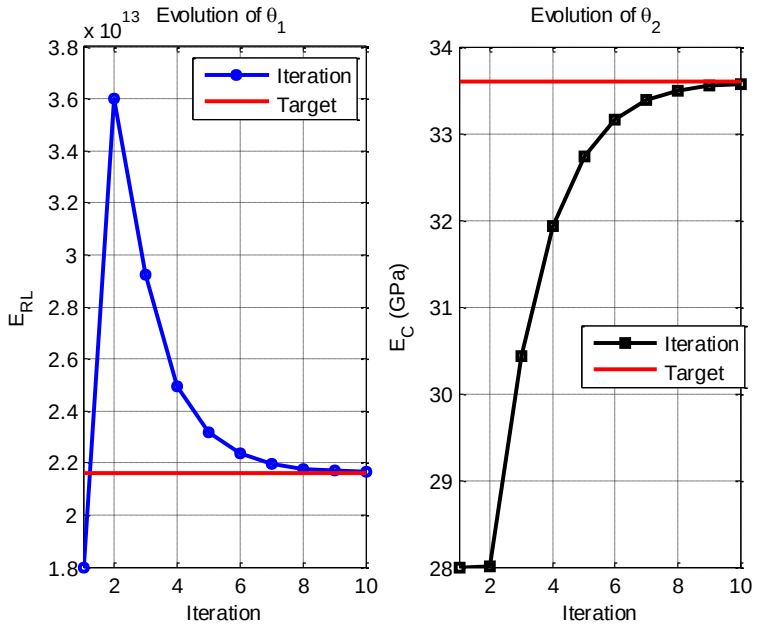

Figure 4.7: Evolution of model parameters a)Rigidity per linear meter and b) elastic modulus of concrete for Case 1 of 3D FEM

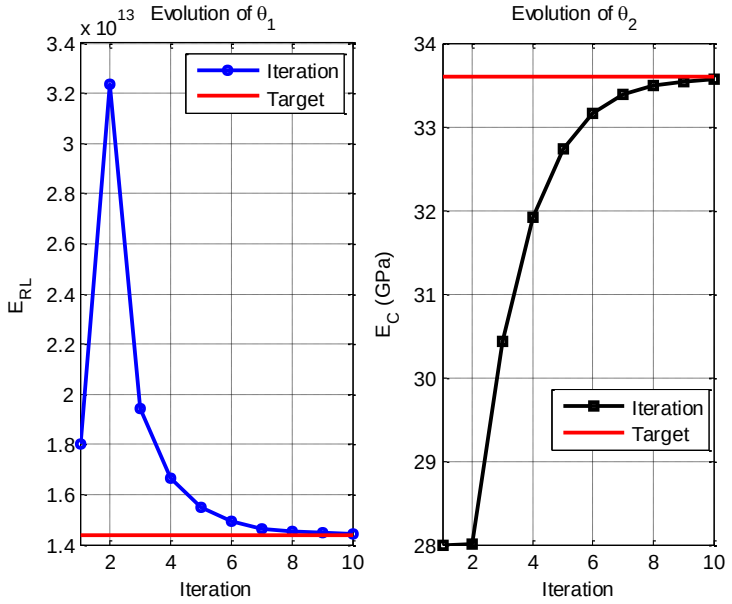

Figure 4.8: Evolution of model parameters a)Rigidity per linear meter and b) elastic modulus of concrete for Case 2 of 3D FEM

4.7 Validation Using Data from an Operational Instrumented Bridge

Having established that it is possible to distinguish between stiffness changes in shear connectors and the concrete slab based on changes in modal frequencies, it is appropriate to proceed and apply the proposed method in the context of an instrumented and operational bridge deck. Bridges 58N & S are twin bridges along interstate 89 in Vermont, USA. For this study, only the two-lane north-bound bridge was instrumented. The bridge was designed in 1961 and built in 1963. As can be seen from Fig. 4.9 the deck is supported on two longitudinal built-up I-girders, which rest upon two intermediate reinforced concrete piers and at the ends on reinforced concrete abutments.

A typical cross section of the deck is depicted in Fig. 4.10. The reinforced concrete slab (190mm thick) is supported at the ends on the main longitudinal girders (with variable depth between 2.44 m (at the midspan) and 4.27 m (at the supports) and on continuous intermediate stringers (W18x60) parallel to the main girders. The stringers are supported on a transverse floor beam (W36 x 170) which itself is simply supported on the main girders. The transverse floor beams are spaced at 7.01 m on-center.

4.7.1 Modeling

As can be seen from Fig. 4.5a, the model is a substructure of the bridge. The boundary conditions of the model are as follows: (i) rigid vertical supports at the abutment,

Figure 4.9: Photograph of bridge 58N located in Vermont, USA.

(ii) longitudinal spring supports at the abutment (representing the horizontal rigidity of the support at the abutment) and (iii) springs and masses at the opposite end, these represent the stiffness and mass necessary to achieve the static displacement, the fundamental vertical and torsional modal frequencies of the complete bridge deck. The free parameters of the model are the stiffness per unit length of the shear connectors between the slab and the stringer, and the elastic modulus of the concrete deck.

4.7.2 Instrumentation

Instrumentation on the bridge deck consists of 10 accelerometers (PCB Model 393A03) as shown in Fig. 4.10b. The deck was also instrumented with dynamic strain sen-

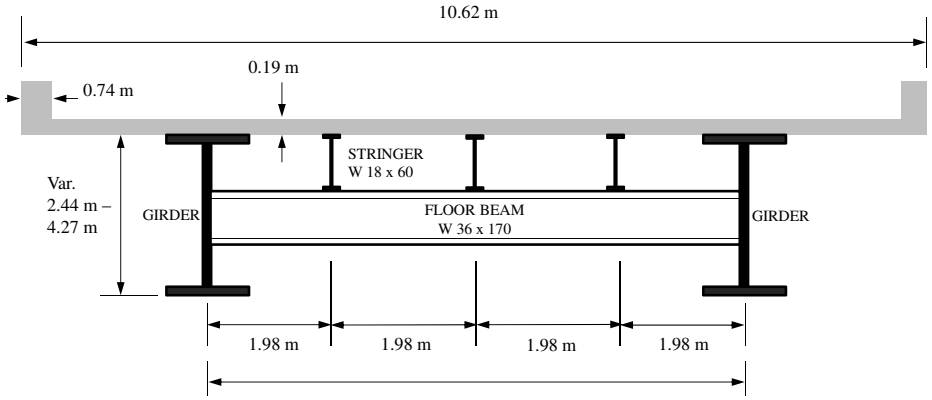

(a) Cross section of bridge deck

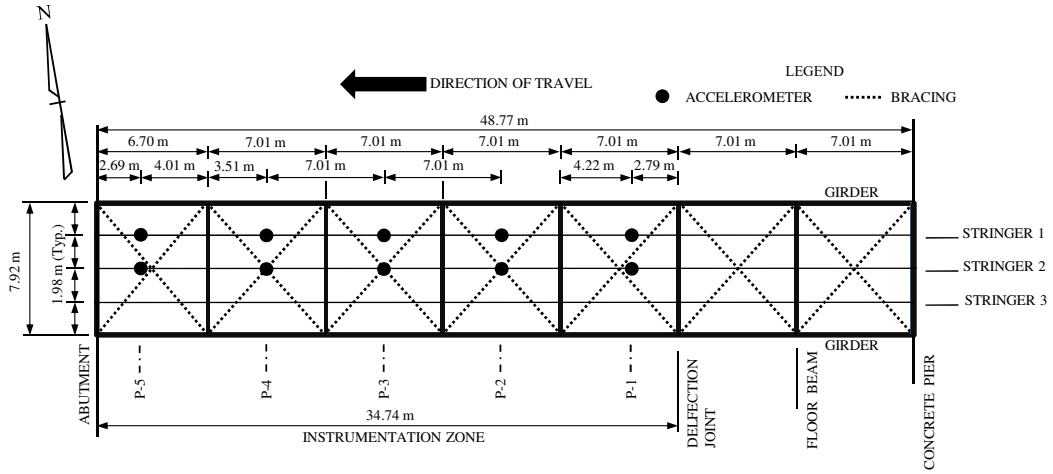

(b) Instrumentation layout

Figure 4.10: (a)Cross section of bridge deck and (b) instrumentation layout (See Fig. 4.5 for the 3D FEM)

sors, but those measurements will not be used for the purposes of this paper, for more information regarding the strain measurements see [18]. The location of the accelerometers was selected to capture the maximum expected structural response of the stringers while at the same time minimizing the required number of sensors (due to budgetary constraints). It is worth noting that the main interest in the instrumentation is to capture the structural behavior of the stringers, however due to the

interconnected nature of the structural system, some aspects of the global structural response will also be captured. To perform the data acquisition the LMS SCADAS MOBILE SCM05 with a uniform sample rate of 200 Hz was used. The data collection presented in this study begins April 12, 2012 and concludes November 20, 2013, with a hiatus between August 27, 2012 and August 28, 2013. Therefore, the data spans between April and November of a nominal year. Measurements consist of 1-hour long records recorded sporadically during this interval. To reduce the effect of input uncertainty (weight, speed or lane of travel of the vehicles) only free vibration measurements were used in this analysis. A total of 184 free vibration intervals were selected from the measured data. The criteria for selection was that the length of the record be longer than 10 seconds after the vehicle left the bridge while no other vehicle entered the bridge during that time. The measured temperature during the selected intervals ranged from $15°F$ to $87°F$. Typical acceleration measurements during the passing of a heavy truck are shown in Fig. 4.11.

4.7.3 System Identification

Knowledge of the characteristics of the traffic experienced by the bridge, vehicle speed, weight and traveling lane, is rarely available. As a way to reduce uncertainty related to the traffic induced excitation, free vibration responses are used for the system identification. This is only possible because of the low average daily traffic on this bridge, for bridges with constant traffic more advanced methods are necessary. The acceleration intervals were processed using the Eigensystem Realization Algorithm

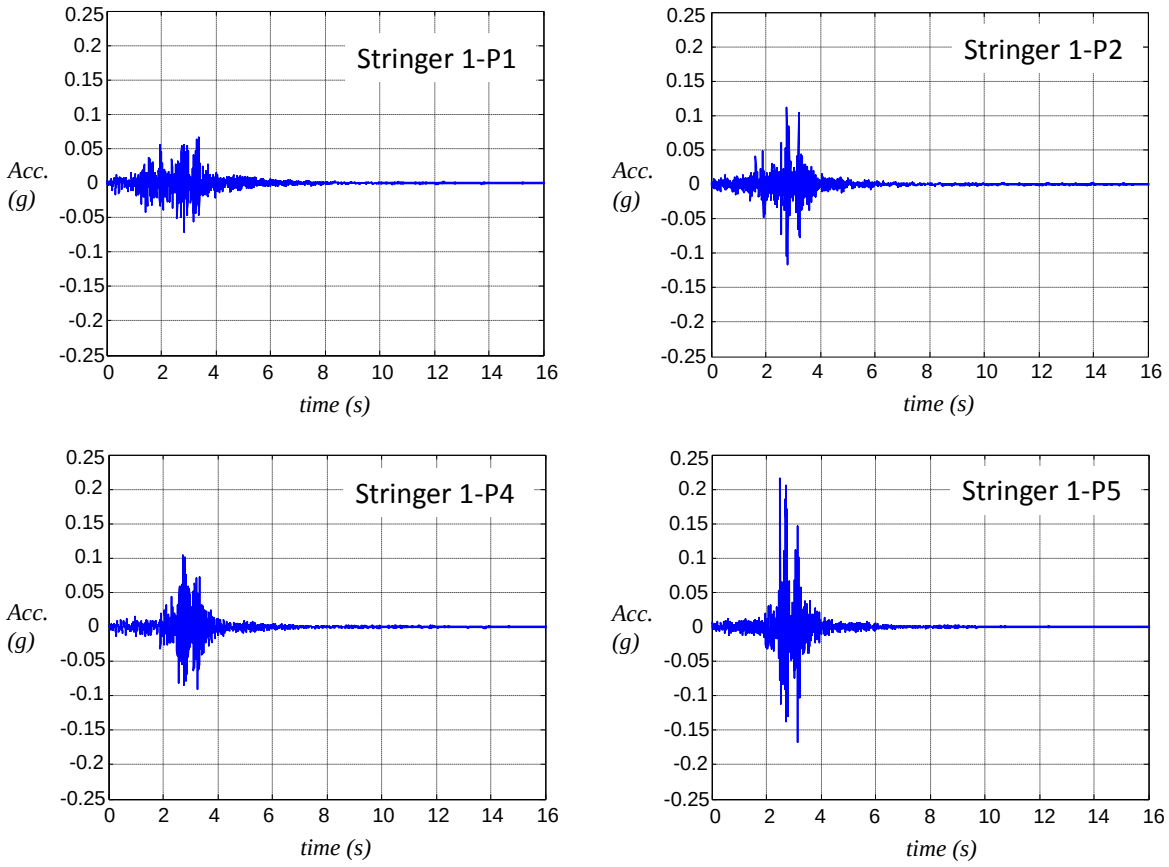

Figure 4.11: Acceleration measurements at various positions along Stringer-1 during the passing of a truck on the travel lane (See Fig. 4.10b for sensor location coordinates)

(ERA) [22]. The ERA identifies a linear model of the form

$$x(k+1) = \mathbf{A}x(k) + \mathbf{B}u(k) \tag{4.9a}$$

$$y(k) = \mathbf{C}x(k) + \mathbf{D}u(k) \tag{4.9b}$$

where $x(k)$ is the internal state at time $t = k\Delta t$, $u(k)$ is the input, $y(k)$ is

the output. The **A** matrix, also known in control literature as the state transition matrix, and it carries information about the system eigenvalues. The mathematical formulation to extract the system frequencies from the eigenvalues of **A** can be found in [22]. A summary of the identified modal frequencies from the selected data set is shown on Fig. 4.12.

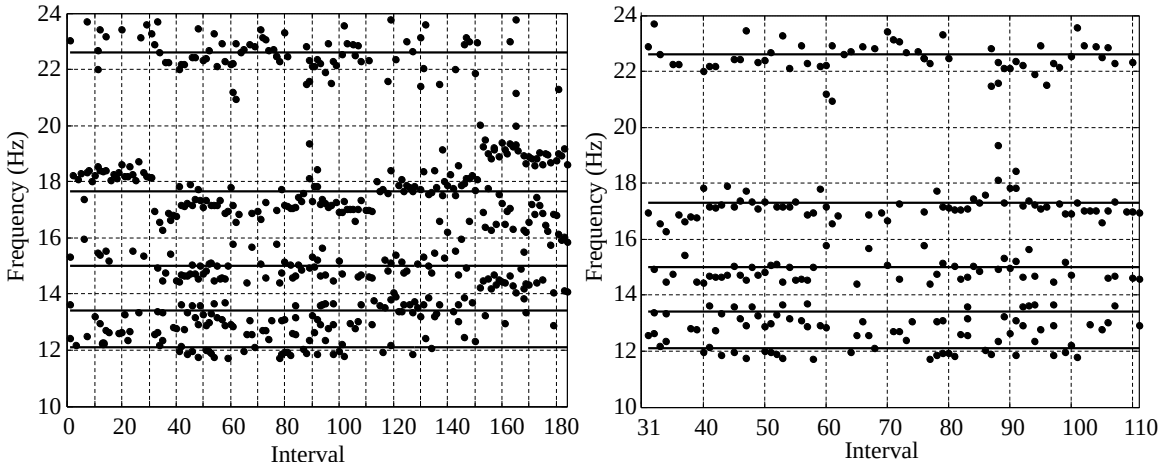

(a) Identified frequencies between April and November

(b) Identified frequencies between July and October

Figure 4.12: Identified frequencies from global acceleration measurements. Mean values indicated by dotted lines

From Fig. 4.12 it can be observed that during colder months the natural frequencies experience an increase with respect to the warmer summer months. This change occurs in all mode shapes and it appears to be reversible, so it can not be attributed to a structural damage. We attribute it to temperature and humidity variations which affect the mechanical properties of the deck and boundary conditions.

4.7.4 Model Updating Results

This section presents a summary of the results from the implementation of the finite element model updating procedure described in Section 4.3. Two scenarios are compared: (i) using all identified frequencies across the complete time interval of measurements and (ii) using only the subset of the data corresponding to the summer months.

In both cases the variance of the identified frequencies is computed and a diagonal weighting matrix is computed. The i^{th} diagonal element of the weighting matrix is the inverse of the variance of the i^{th} identified frequency. For convenience purposes, the weighting matrix is scaled in such manner that the diagonal of the weighting matrix adds to unity. This is an arbitrary choice since the weighting matrix can be multiplied by any scalar without changing the result of the weighted least-squares solution. For each case, two different procedures were implemented. In the first one, the model updating algorithm was unconstrained while in the second one, the algorithm was constrained to operate within reasonable limits for the variables,specially the concrete modulus of elasticity. The selected lower and upper bound for the concrete elastic modulus were 21.37 GPa and 27.59 GPa respectively, this corresponds to a lower bound of a compressive strength of concrete of 20.68 MPa(3 ksi) and an upper bound of 34.47 MPa(5 ksi). The expression used to link concrete strength and elastic modulus was $E_c = 4700\sqrt{f'c}(MPa)$ [8].

The model updating results for the scenario where all the data was used is presented in Tables 4.3 and 4.4. The model updating results for the scenario where only a subset of the data was used is presented in Tables 4.5 and 4.6.

Table 4.3: Model Parameters - Using complete data set

Parameter	**Initial**	**Unconstrained**	**Constrained**
$\theta_1 = E_c(GPa)$	28	10.08	21.5
$\theta_2 = k_L(MN/m/m)$	516.6	2,857.7	4.2

Table 4.4: Comparison of frequencies Bridge 58N - Using complete data set

Frequency (#)	**ID (Hz)**	σ^2	**W**	**Initial (Hz)**	**Unconstrained (Hz)**	**Constrained (Hz)**
1	12.04	0.65	0.09	14.04	12.64	12.94
2	13.37	0.14	0.43	17.16	14.90	14.40
3	15.02	0.30	0.28	18.15	15.58	14.52
4	17.80	0.69	0.08	18.83	16.24	14.84
5	22.57	0.42	0.11	22.19	19.58	19.72

Table 4.5: Model Parameters - Using reduced data set

Parameter	**Initial**	**Unconstrained**	**Constrained**
$\theta_1 = E_c(GPa)$	28	15.3	21.5
$\theta_2 = k_L(MN/m/m)$	516.6	26,889.8	5.9

Table 4.6: Comparison of frequencies Bridge 58N - Using reduced data set

Frequency (#)	**ID (Hz)**	σ^2	**W**	**Initial (Hz)**	**Unconstrained (Hz)**	**Constrained (Hz)**
1	12.15	0.11	0.26	14.04	13.33	12.96
2	13.20	0.10	0.29	17.16	16.08	14.49
3	14.86	0.16	0.22	18.15	16.86	14.60
4	17.21	0.21	0.13	18.83	17.56	14.94
5	22.49	0.30	0.10	22.19	21.08	19.76

Fig. 4.13 shows a semi-log plot depicting the variation of the main vertical frequencies of the deck as a function of the stiffness per unit length of the shear connectors. The plots shows the frequencies corresponding to the initial model and to the updated model (using a subset of the data shown in Fig. 4.12b).

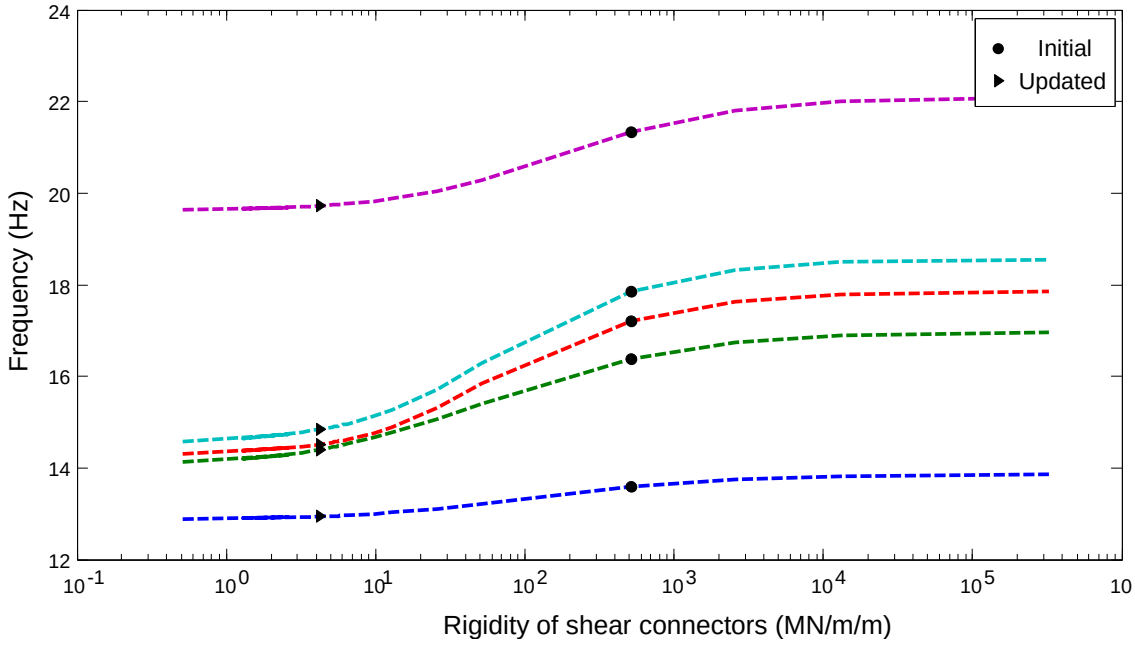

Figure 4.13: Frequencies of deck as a function of the effective stiffness of the shear connectors. Shown are the values of the initial stiffness (solid circle) and the updated value (solid triangle)

Fig. 4.14 shows the mode shapes (in the concrete slab) corresponding to the constrained and unconstrained model updating. For both cases the reduced data set was used. As can be seen, significant differences exist between the unconstrained and constrained model updating results.

Fig. 4.15 presents a comparison between the maximum bending moments in the stringers and outer girders as a function of the updated composite behavior of

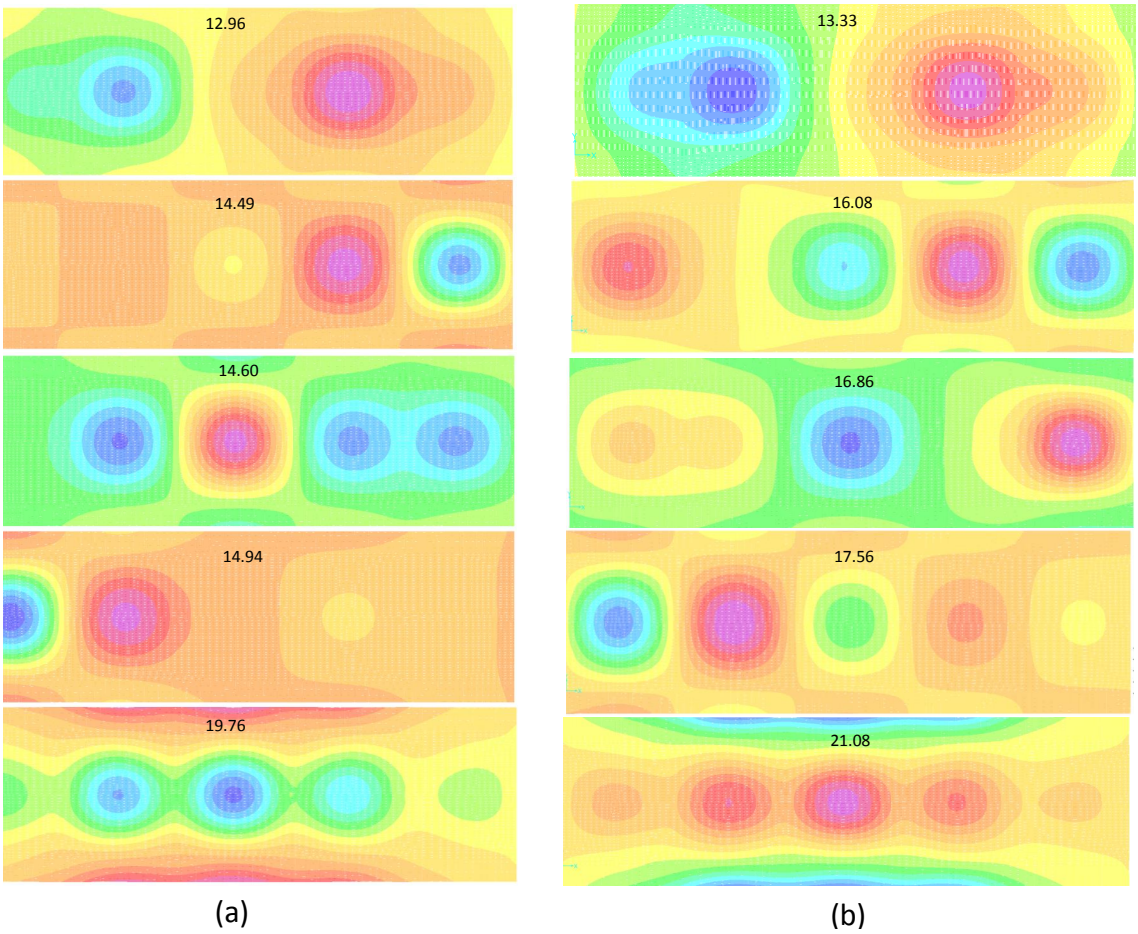

Figure 4.14: Mode shapes on the concrete slab corresponding to the updated model. On the left is the result of the constrained model updating and on the right the results of the unconstrained.

the deck. The loading is a pair point loads as indicated in the figure. These loads represent the last axle of a three axle truck. The position of the loads corresponds to the most critical, in the sense that it creates the largest bending moment. The constrained updated model presents significant differences with respect to the unconstrained model, specially in the stringer bending moments. The unconstrained

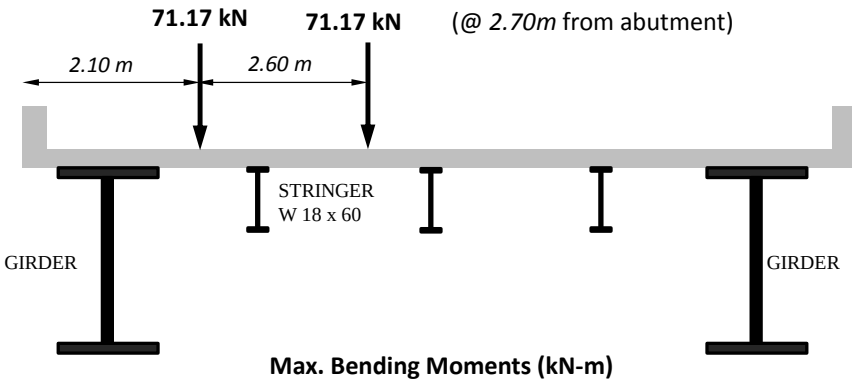

Max. Bending Moments (kN-m)

	Girder	Stringer 1	Stringer 2	Stringer 3	Girder
Initial FEM	117.50	13.59	16.74	3.62	45.79
Updated FEM Unconstr.	138.89	14.27	17.47	2.94	57.13
Updated FEM Constr.	125.42	21.84	27.20	6.72	49.70

Figure 4.15: Comparison of maximum bending moments in various elements of the bridge deck

model presents a very high level of composite action and a very low slab stiffness, this translates into a higher level of loads going into the girders with lower loads going into the stringers. In the constrained model, the slab is much stiffer in comparison with the unconstrained case and thus this means a better and more even transverse distribution of forces.

4.7.5 Validation of Updated Finite Element Model

In this section a validation of the updated finite element model (constrained FEM) is presented. The data was derived from a test conducted on the bridge deck. The

bridge was subjected to a passing truck driven on the travel lane with known axle weight and spacing (measured off site). The truck had three axles weighting $30kN$, $100kN$ and $100kN$ from front to back. The spacing of the axles was $3.00m$ and $6.00m$ respectively. The truck was driven at a constant speed of 60 mph on the travel lane. During the passing of the truck, accelerations were measured at all locations indicated in Fig. 4.10. Similarly, the updated finite element model was subjected to a set of simulated moving point loads with the same magnitude, relative spacing and speed as the actual truck. For this simulation a modal damping ratio of 0.035 for every mode was used. This is consistent with identified damping from vibration measurements on the bridge deck.

Figures 4.16 and 4.17 show a comparison between the measured acceleration, the original model and the updated model predictions. The improvement in prediction capability as a product of the model updating can be easily observed.

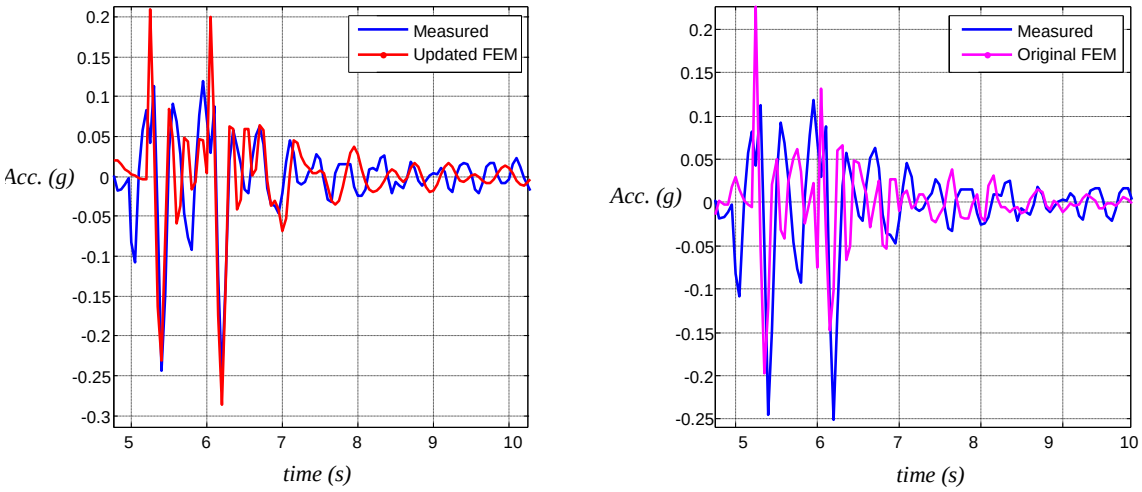

Figure 4.16: Comparison of acceleration response (updated model vs. orignal model) at stringer 1 (position P-5) when a test vehicle crosses the bridge in the travel lane at 60 mph.

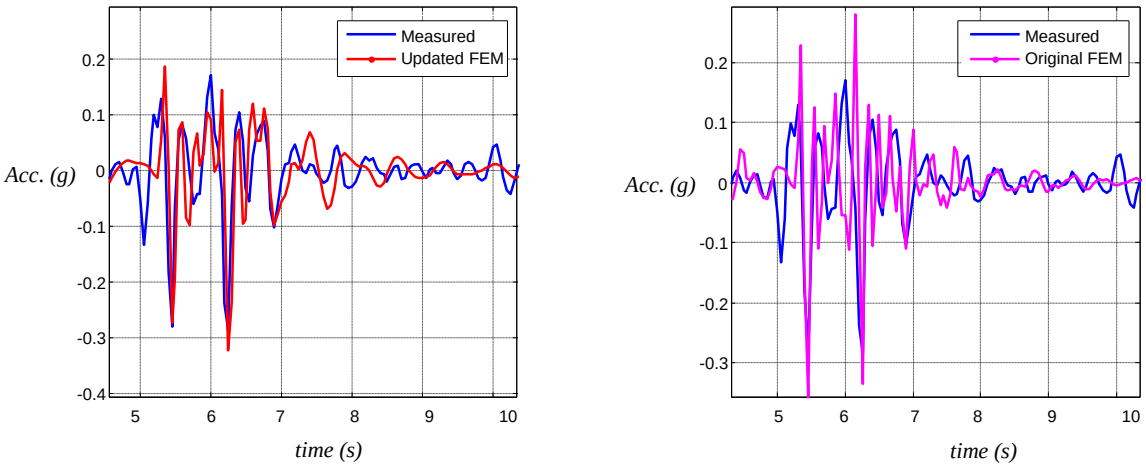

Figure 4.17: Comparison of acceleration response (updated model vs. orignal model) at stringer 2 (position P-5) when a test vehicle crosses the bridge in the travel lane at 60 mph.

4.8 Conclusions

In this paper the authors propose the use of a weighted sensitivity-based finite element model updating to determine the degree of composite behavior in operational bridge decks with unknown/uncertain installation of shear connectors. The free parameters of the model are the rigidity per unit length of the beam-slab interface and the elastic modulus of the concrete slab. The type of measurements used are vertical accelerations at various points in the span. The number of measurements required by the proposed methodology are significantly less than the ones required if the more traditional strain sensing is used, with the drawback that the estimated quantities represent the behavior of the deck in an average sense and not section-by-section.

The proposed methodology was verified by means of numerical simulations in

two models that varied in size and complexity. The first model was a 2D FEM of an isolated stringer in a bridge deck. The second model was a 3D FEM of a deck substructure. For each model, various levels of composite action were considered. In all cases, the modal features were selected as a subset of the system eigenvalues and the procedure accurately updates the model parameters related to composite action. The method was implemented in an operational and partially instrumented deck located in Vermont, USA. The variability of the identified data features was accounted in the model updating procedure by means of a weighting matrix (inversely proportional to the variance of the identified frequencies). As expected, identified modal frequencies varied significantly from summer to winter and thus two separate analysis were conducted, one with the complete data set and the other with a reduced data set which included only the summer months.

As an illustrative exercise, two model updating strategies were compared, constrained versus unconstrained. In the unconstrained case, the free parameters did not have limits or bounds, while, as the name suggests, in the constrained cases the elastic modulus of concrete was constrained to a lower bound. It was found that these two model updating solutions result in different structural behaviors of the bridge (static and dynamic). The unconstrained solution results in a very low (and physically unreasonable) value of the concrete modulus in the slab and a very high value for connection stiffness; the constrained solution provides more reasonable results and was thus adopted. The updated FEM, using the constrained approach, was further validated using measured accelerations induced by a moving test truck with known axle weight and spacing. It was found that the updated model provided an improved match between predictions and measurements in comparison with the original model.

This exercise highlights the need for sound physical understanding of the variables when performing a model updating.

A limitation of the proposed model updating approach (which is independent of the type of sensing used) is that only stiffness of the deck can be assessed and not much can be learned regarding its ultimate static capacity. This is because various types of shear connectors can provide similar stiffness but display very different post-yielding behavior. Nevertheless, if the interest is the formulation of a finite element model that can be used as a base-line model for stress analysis (say for fatigue life estimation and(or) load distribution factors) then the proposed model updating approach would prove useful.

4.9 Acknowledgments

The research presented in this paper was partially funded by the Vermont Agency of Transportation and by the National Science Foundation Grant ECC-1342190. Their support is gratefully acknowledged. The contents of this paper only reflect the views of the authors. The contents do not necessarily reflect the official view or policies of the Vermont Agency of Transportation.

4.10 Bibliography

[1] National Bridge Inventory. U.S. department of Transportation. Federal Highway Admisnistration. http://www.fhwa.dot.gov/bridge/nbi.cfm

[2] Salmon, C. and Johnson, J. (1996) Steel Structures, 4th edition. Prentice Hall. Upper Saddle River, N.J.

[3] Chen W-F, Duan, L. (1999) Bridge Engineering Handbook. CRC Press, N.Y.

[4] Breña, S., Jeffrey, A., and Civjan, S. (2013). "Evaluation of a Noncomposite Steel Girder Bridge through Live-Load Field Testing". J. Bridge Eng., 18(7), 690-699.

[5] Chakraborty, S. and DeWolf, J. (2006) "Development and implementation of a continuous strain monitoring system on a multi-girder composite steel bridge" ASCE Journal of Bridge Engineering 11(6): 753-762

[6] Kim, S. and Nowak, A.S. (1997) "Load distribution and impact factors for I-girders bridges" ASCE Journal of Bridge Engineering 2(3): 97-104.

[7] Jauregui, D. V., Yura J. A., Frank, K. H., and Wood, S. L. (2002) "Field evaluation of decommissioned non-composite steel girder bridge" ASCE Journal of Bridge Engineering 7(1): 39-49

[8] American Association of State Highway and Transportation Officials (AASHTO) (2010) LRFD bridge design specifications, Washington, D.C.

[9] Morassi, A. and Rocchetto, L. (2003) "A damage analysis of steel-concrete composite beams via dynamic methods: Part I, experimental results" Journal of Vibration and Control (9):507-527.

[10] Kwon, G., Engelhardt, M.D. and Klingner, R.E. (2009), "Strengthening bridges by developing composite action in existing non-composite bridge girders" Structural Engineering International, International Association for Bridge and Structural Engineering, 19(4): 432-437

[11] Newmark, N.M., Siess, C.P. and Viest, I.M., (1951) Test and analysis of composite beams with incomplete interaction. Proceedings of the Society of Experimental Stress Analysis 9(1): 75-92

[12] Girhammar, U.A. and Pan, D. (1993), Dynamic analysis of composite members with interlayer slip, International Journal of Solid and Structures 30(6):797-823

[13] Oehlers, D.J. and Sved, G. (1995) Composite beams with limited slip capacity shear connectors, ASCE Journal of Structural Engineering 121(6):932-938

[14] Nguyen, N.T., Oehlers, D.J. and Bradford, M.A. (1998), A rational model for the degree of interaction in composite beams with flexible shear connectors, Mechanics of Structures and Machines 26(2):175-194

[15] Oehlers, D.J., Nguyen, N.T., Ahmed, M. and Bradford, M.A. (1997) Partial Interaction in Composite Steel and Concrete Beams with Full Shear Connection, Journal of Constructional Steel Research 41(2/3):235-248

[16] Dall′Asta, A., (2001) Composite beams with weak shear connection, International Journal of Solids and Structures, 38, 5605-5624

[17] Ranzi, G., Gara, F., Leoni, G. and Bradford, M. A. (2006), Time analysis of composite beams with partial interaction using available modelling techniques: A comparative study, Computers and Structures, 84, 930-941

[18] Hernandez, E. M. and May, G. (2013), Vibration Monitoring and Load Distribution Characterization of I-89 Bridge 58N, Proceedings of the XXXI International Modal Analysis Conference (IMAC) Orange County, CA

[19] Mottershead, J. E. Link, M. and Friswell M.I. (2010), The sensitivity method in finite element model updating: A tutorial, Mechanical Systems and Signal Processing .

[20] Friswell M.I. and Mottershead, J. E. (1995), Finite Element Model Updating in Structural Dynamics. Kluwer Academic Publishers, Dordrecht, .

[21] Fox, R. L. and Kapoor, M. P. (1968), Rates of change in eigenvalues and eigenvectors. American Institute of Aeronautics and Astronautics Journal, 6(12): 2426-2429

[22] Juang, L.(1999), Applied System Identification Prentice Hall. Upper Saddle River, NJ.

[23] Zárate, B. A. and Caicedo, J. M. (2008), Finite element model updating: Multiple alternatives, Engineering Structures, 30, 3724-3730

Chapter 5

Kalman filter robustness for fatigue usage monitoring of flexible frame structures

Néstor R. Polanco[1] and Eric M. Hernández[2]

[1]Ph.D. candidate at the School of Engineering. University of Vermont, USA.

nestor.polanco@uvm.edu

[2]Assistant Professor at the School of Engineering. University of Vermont, USA.

eric.hernandez@uvm.edu

Conference: *2016 American Control Conference (ACC)*, Boston, MA, USA.

5.1 Abstract

This paper explores the robustness of the Kalman filter in structural dynamics and fatigue monitoring applications. The study is carried out using simulations and small scale experiments. We investigate robustness to non-parametric errors in the description the unmeasured excitations, measurement noise and structural model.

5.2 Introduction

Fatigue is responsible for a large portion of structural failures in flexible structures subjected to vibration effects [1]. Examples of these systems are aircraft, wind turbines, bridges, offshore structures, among many others. Fatigue damage evolves in three distinguishable phases: (1) micro-crack formation, (2) micro-crack nucleation and (3) macro-crack formation and propagation. Phases 1 and 2 encompass the majority of the fatigue life of a specimen. Once phase 3 begins and a macro-crack begins propagate, fatigue life is basically over. Monitoring fatigue in complex structures, specially as they age, has become a topic of increasing interest among academics and practicing engineers working in control, fault diagnosis, and structural health monitoring [2–6].

There are essentially two approaches to monitor fatigue in flexible structures: local and global [7]. In the local approach intense sensing such as guided waves are used to detect small cracks, delaminations, etc. The local approach is feasible if the engineer knows a priori where damage is taking place. In the global approach a more sparse array of sensors is used which typically measure response in the low-

to-medium frequency range. In this case the spatial range of detection increases but the resolution decreases. This means that fatigue can be monitored throughout the complete structure, the price to pay is that only larger cracks can be detected.

In this paper we focus on the global approach and in particular on vibration-based monitoring. However, our aim is not to detect cracks after they have occurred or are actively propagating. The objective in this paper is to monitor the accumulation of fatigue damage throughout the structure during its operational life, even before visible cracks begin to appear, i.e. phase 1 and 2. We investigate the use of the Kalman filter to estimate stress and strain fields (and their uncertainty) throughout the structure using operational acceleration measurements. The estimated stress and strain fields can be used together with mechanistic damage functions, such as the popular S-N curve and Miner rule, to estimate fatigue damage and remaining service life [8].

An investigation along these lines has been carried out by Papadimitriu et al. [2], however their study was limited to simulation. In this paper we present simulation and experimental results aimed at determining the robustness and sensitivity of the Kalman filter estimates to various sources of modeling errors. In particular we investigate the effects of errors in the stochastic description of the measurement noise and unmeasured excitations, as well as errors in the physics of the model describing the flexible structure.

5.3 System of Interest

The system of interest is a flexible, bolted steel structure shown in Fig. 5.2. The dimensions of the structure are shown in Fig. 5.1. The system was instrumented with accelerometers (PCB 333B30) and strain sensors (PCB 740B02) as shown in Fig. 5.1. The driving excitation force was delivered using an electrodynamic shaker (TMS 2060E) from the Modal Shop. The input force to the system was measured by means of a force transducer (PCB C02). The sampling frequency of all sensors was 819.2 Hz.

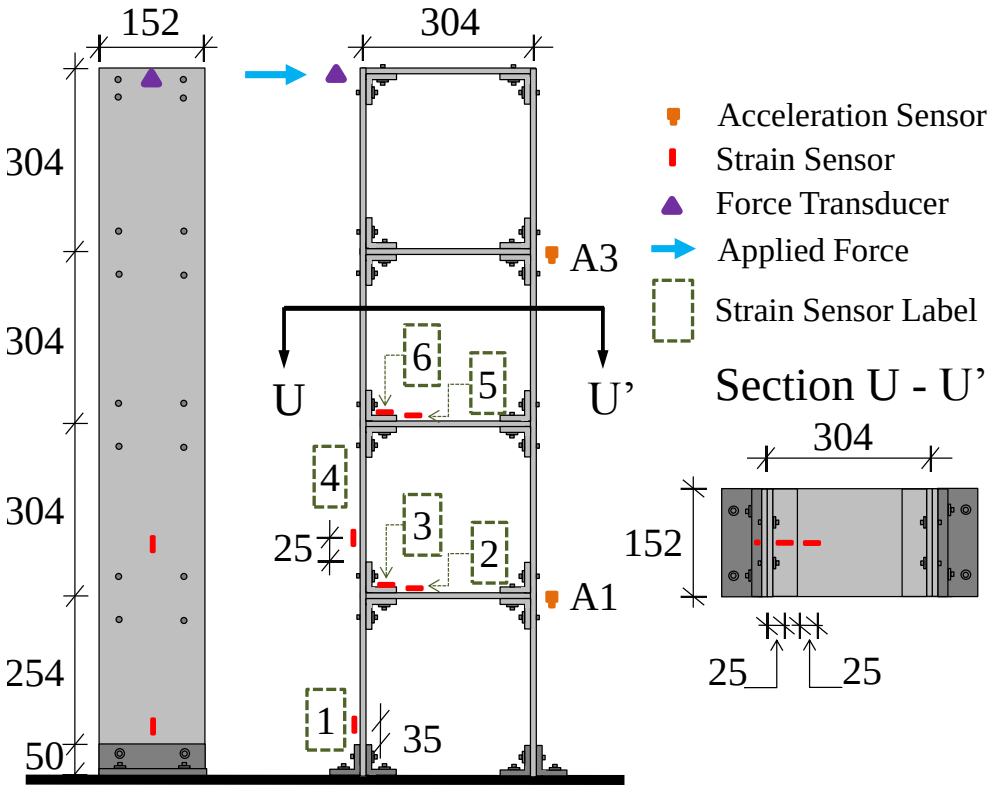

Figure 5.1: Dimensions of experimental structure (mm)

Figure 5.2: Experimental setup

5.4 Mathematical Model

The partial differential equation (PDE) that models the vibrations $y(x,t)$ of the linear elastic frame structure in Fig. 5.2 at any point x and any time t is given by

$$\rho A \frac{\partial^2 y}{\partial t^2} + c\frac{\partial y}{\partial t} + EI\frac{\partial^4 y}{\partial x^4} = p(x,t) \tag{5.1}$$

where A and I are the cross-sectional area and moment of inertia of the frame

elements, E is the elastic modulus of the material, c is the damping constant, ρ is the mass density of the material and $p(x,t)$ is the forcing function. This PDE, with its boundary conditions, can not be solved analytically (except for very simple cases). To obtain an approximate solution it is necessary to discretize in space and time. For the particular structure of interest two discretizations are investigated. These are shown in Fig. 5.3 and summarized below.

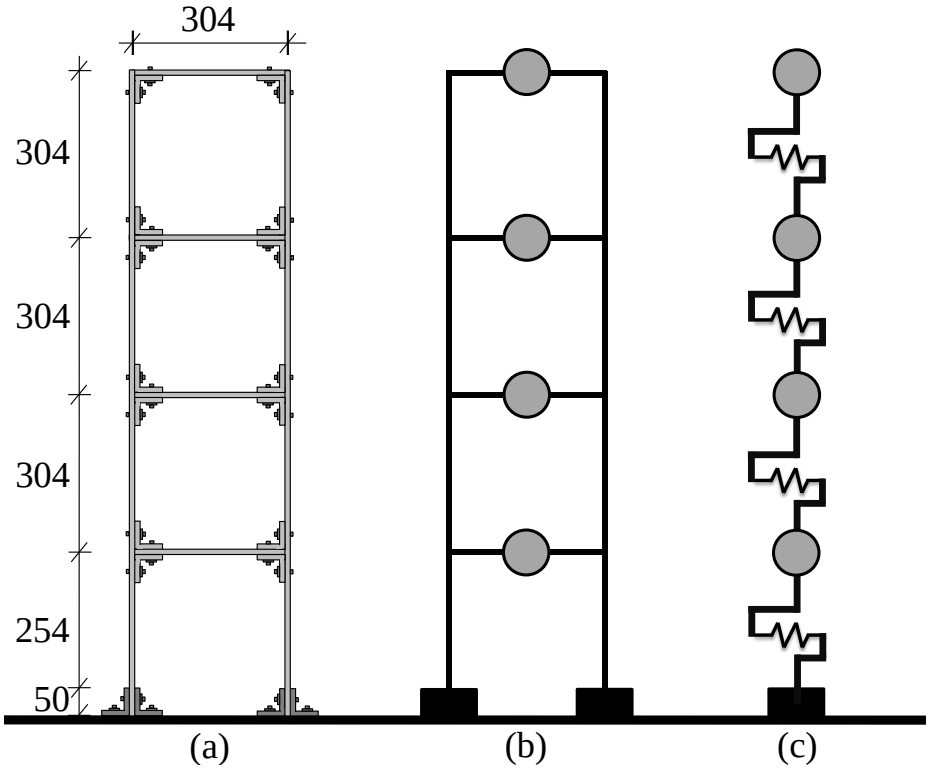

Figure 5.3: From left-to-right: (a) The system, (b) Model M1, a frame with lumped masses and (3) Model M2, a shear-beam model with lumped masses. Dimensions in mm

- **Model M1**: This model is a static condensation of the frame system to the 4 horizontal DOF at the centroid of the horizontal elements.

- **Model M2**: This model is a vertical shear-beam with concentrated masses.

Both of these models can be represented as a set of simultaneous linear ordinary differential equations of the form

$$\mathbf{M}\ddot{q}(t) + \mathbf{C_D}\dot{q}(t) + \mathbf{K}q(t) = \mathbf{b_2}p(t) \tag{5.2}$$

where $q(t) \in \Re^{4\times 1}$ is a displacement vector at time t , $\mathbf{M} = \mathbf{M}^T > 0$ is the mass matrix, $\mathbf{C_D} = \mathbf{C_D}^T > 0$ is the damping matrix and $\mathbf{K} = \mathbf{K}^T > 0$ is the stiffness matrix. The measured forces that drive the response of the system are defined by the vector $p(t)$ with $\mathbf{b_2}$ as its force distribution matrix. By setting

$$x(t) = \left\{ \begin{array}{c} \dot{q}(t) \\ \ddot{q}(t) \end{array} \right\}, \ \mathbf{A_c} = \left[\begin{array}{cc} \mathbf{0} & \mathbf{I} \\ -\mathbf{M}^{-1}\mathbf{K} & -\mathbf{M}^{-1}\mathbf{C_D} \end{array} \right]$$

$$\mathbf{B_c} = \left[\begin{array}{c} \mathbf{0} \\ \mathbf{M}^{-1}\mathbf{b_2} \end{array} \right]$$

we can write eq.5.2 as

$$\dot{x}(t) = \mathbf{A_c}x(t) + \mathbf{B_c}p(t) \tag{5.3}$$

where $x(t)$ is known as the state vector. Measurements $z(t)$ are modeled as

$$z(t) = \mathbf{C}x(t) + \mathbf{D}p(t) + v(t) \tag{5.4}$$

where $v(t)$ is the measurement noise. In the case of acceleration measurements the state-to-output matrix $\mathbf{C}$ has the following form

$$\mathbf{C} = \mathbf{c_2} \left[\; -\mathbf{M}^{-1}\mathbf{K} \quad -\mathbf{M}^{-1}\mathbf{C_D} \; \right] \tag{5.5}$$

where $\mathbf{c_2}$ indicates which degree of freedom in the model corresponds to a measurement. The direct transmission matrix $\mathbf{D}$ is given by

$$\mathbf{D} = \mathbf{c_2}\mathbf{M}^{-1}\mathbf{b_2} \tag{5.6}$$

All the previous equations are represented in continuous time. In practice, vibration signals are obtained in a digital fashion and we need to convert the continuous system matrices to discrete time. The solution to state space of the system is well known [9] and can be expressed in discrete time as

$$x_k = \mathbf{A}x_{k-1} + \mathbf{B}p_{k-1} \tag{5.7}$$

$$z_k = \mathbf{C}x_k + \mathbf{D}p_k + v_k \tag{5.8}$$

where

$$\mathbf{A} = e^{\mathbf{A}_c \Delta t} \tag{5.9}$$

where $x_k = x(t = k\Delta t)$, Δt is the time step and $\mathbf{B}$ depends on the intersample behavior of the excitation force (see [10] for more details). In this paper we operate using zero-order hold.

5.5 Kalman Filter

The Kalman filter (KF) is a sequential state estimation algorithm. The algorithm is optimal for linear systems subjected to zero-mean unmeasured excitations and additive measurement noise with covariances $\mathbf{Q}_k$ and $\mathbf{R}_k$ respectably.

The basic equations of the algorithm are given below. Eqs. 5.10 and 5.11 propagate the mean and covariance of the state estimate from time step $k-1$ to k. Eq. 5.12 is the Kalman gain matrix. Eqs. 5.13 and 5.14 are the update or correction equations for the mean and covariance of the state estimate.

$$\hat{x}_k^- = \mathbf{A}\hat{x}_{k-1}^+ \tag{5.10}$$

$$\mathbf{P}_k^- = \mathbf{A}\mathbf{P}_{k-1}^+\mathbf{A}^T + \mathbf{Q}_{k-1} \tag{5.11}$$

$$\mathbf{K}_k = \mathbf{P}_k^-\mathbf{C}^T\left(\mathbf{C}\mathbf{P}_k^-\mathbf{C}^T + \mathbf{R}_k\right)^{-1} \tag{5.12}$$

$$\hat{x}_k^+ = \hat{x}_k^- + \mathbf{K}_k\left(z_k - \mathbf{C}\hat{x}_k^-\right) \tag{5.13}$$

$$\mathbf{P}_k^+ = \left(\mathbf{I} - \mathbf{K}_k\mathbf{C}\right)\mathbf{P}_k^- \tag{5.14}$$

Expressions for the sensitivity of the KF to errors in the description of $\mathbf{Q}$ and $\mathbf{R}$ are given in [11]. However these expressions assume that the error is parametric, i.e. the measurement and process noise are zero-mean, white and Gaussian and the error

lies in the numerical description of the respective covariance matrices. In this paper we take a wider view of the problem and investigate the effect of errors that can not be simply described by parametric errors in the covariance matrices.

5.6 Strain Estimation and Uncertainty Propagation

Once the displacements have been estimated for all the DOF; the strain tensor and its uncertainty can be calculated by a linear transformation of the nodal displacements as

$$\hat{\epsilon}_i(t) = \mathbf{T}_i \hat{x}(t)$$

$$\mathbf{P}_\epsilon(t) = \mathbf{T}_i \mathbf{P}^+(t) \mathbf{T}_i'$$

where t is time and the subindex i refers to the particular structural element of interest. The estimated strain can be used to compute the stress tensor and subsequently used as input to a fatigue damage function, from where the accumulated fatigue damage, and its uncertainty, can be estimated.

5.7 Modeling Error

This section describes the experimental characterization of modeling errors in the stochastic description of the unmeasured excitation, measurement noise and physical model error.

5.7.1 Physical Model

As mentioned in a previous section we investigate two different physical models for the structure shown in Fig. 5.3. Fig. 5.4 shows the modal frequencies vs the damping ratios plot of each mode shape in the two models compared the identified values from vibration testing of the structure. As can be seen, the statistical variability in modal damping is significantly larger than the variability in modal frequency. It can also be observed that although M1 and M2 have almost the same fundamental frequency, they differ significantly at the higher frequencies. Model M1 constitutes an overall better representation of the structure than model M2.

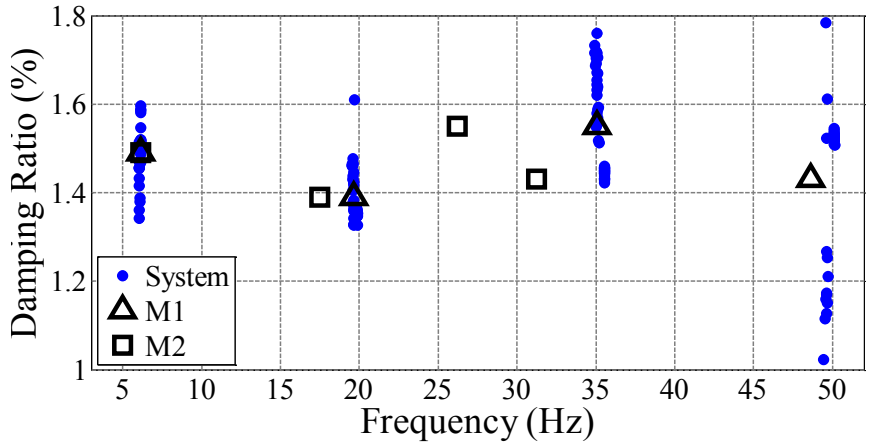

Figure 5.4: Comparison of modal frequency and damping ratio between models and identified from vibration tests in test structure.

5.7.2 Covariance matrices

A fundamental input to the Kalman filter are the covariance matrices for the unmeasured excitation and measurement noise. Off-line vibration measurements were

preformed in order to estimate these covariances. To characterize the stochastic nature of the excitation, the shaker was ran for 600s and the estimated, normalized PSD (using the Welch algorithm) was computed and shown in Fig. 5.5. To characterize the stochastic nature of the measurement noise, ambient acceleration response was measured with the structure "at rest" for 600s and its power spectral density was computed. The result is shown in Fig. 5.6.

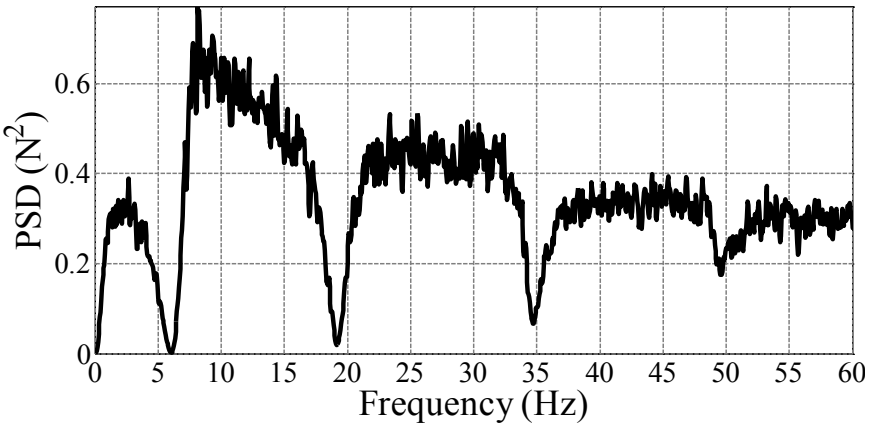

Figure 5.5: Power spectral density of the excitation (assumed unmeasured for the estimation).

As can be seen from Figs. 5.5 and 5.6 neither of the signals satisfies the whiteness assumption (essential in the derivation of the KF). We selected the following values for $\mathbf{Q}$ and $\mathbf{R}$ for the implementation of the KF.

$$\mathbf{Q}_k = \frac{1}{N-1}\sum_k (p_k - \bar{p})^2 = 53.36\ N^2 \qquad \forall k \tag{5.15}$$

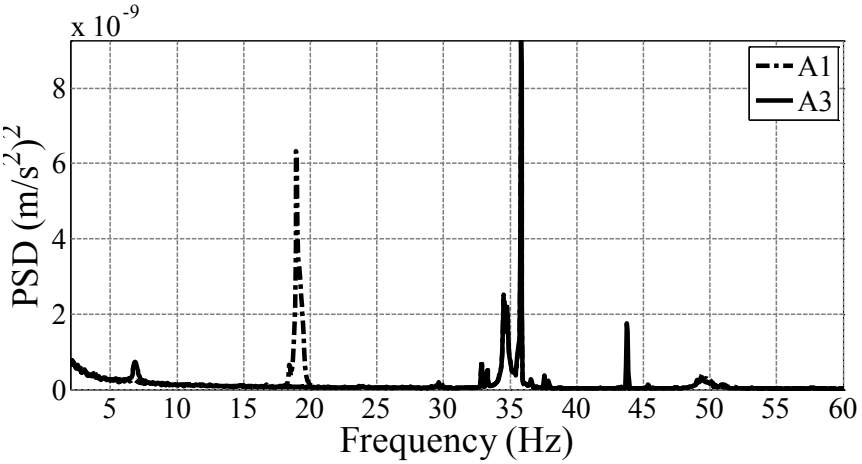

Figure 5.6: Estimated power spectral density of the acceleration measurement noise. (According to Fig. 5.1)

$$\begin{aligned}\mathbf{R}_k =& \frac{1}{N-1}\sum_k (v_k - \bar{v})(v_k - \bar{v})^T \\ =& \begin{bmatrix} 3.49 & -3.59 \\ -3.59 & 11.15 \end{bmatrix} * 10^{-8}(m/s^2)^2 \qquad \forall k \end{aligned} \tag{5.16}$$

5.8 Estimation Results

Table 5.1 summarizes all the cases examined in this study. Cases 0-2 use simulated data and case 3 uses experimental data. In case 0 the Kalman filter is simulated in an ideal setting (all assumptions are valid to within computer precisions and random number generator). Case 1 looks at the effect of only modeling error. In this case M1 is used to generate the system response and M2 is used to perform the estimation. Case 2 looks at various combined scenarios of modeling errors and finally case 3, examines the robustness of the KF in the environment of experimental data.

Figures 5.7-5.14 depict estimation results in a small window of time for each of

Table 5.1: Summary of Cases

	Excitation		Measurement noise		Response	
Case	System	Model	System	Model	System	Model
0	$\mathcal{N}(0,\mathbf{Q})$	$\mathcal{N}(0,\mathbf{Q})$	$\mathcal{N}(0,\mathbf{R}_d)$	$\mathcal{N}(0,\mathbf{R}_d)$	4 DOF$_c$	4 DOF$_c$
1	$\mathcal{N}(0,\mathbf{Q})$	$\mathcal{N}(0,\mathbf{Q})$	$\mathcal{N}(0,\mathbf{R}_d)$	$\mathcal{N}(0,\mathbf{R}_d)$	4 DOF$_c$	4 DOF$_s$
2$_a$	$\mathcal{N}(0,\mathbf{Q})$	$\mathcal{N}(0,\mathbf{Q})$	Exp	$\mathcal{N}(0,\mathbf{R}_d)$	4 DOF$_c$	4 DOF$_c$
2$_b$	$\mathcal{N}(0,\mathbf{Q})$	$\mathcal{N}(0,\mathbf{Q})$	Exp	$\mathcal{N}(0,\mathbf{R})$	4 DOF$_c$	4 DOF$_c$
2$_c$	Exp	$\mathcal{N}(0,\mathbf{Q})$	$\mathcal{N}(0,\mathbf{R}_d)$	$\mathcal{N}(0,\mathbf{R}_d)$	4 DOF$_c$	4 DOF$_c$
2$_d$	Exp	$\mathcal{N}(0,\mathbf{Q})$	Exp	$\mathcal{N}(0,\mathbf{R}_d)$	4 DOF$_c$	4 DOF$_c$
2$_e$	Exp	$\mathcal{N}(0,\mathbf{Q})$	Exp	$\mathcal{N}(0,\mathbf{R}_d)$	4 DOF$_c$	4 DOF$_s$
3	Exp	$\mathcal{N}(0,\mathbf{Q})$	Exp	$\mathcal{N}(0,\mathbf{R}_d)$	Exp	4 DOF$_c$

$_c \rightarrow$ condensed model
$_s \rightarrow$ shear model
$_d \rightarrow$ diagonal covariance matrix
Exp$\rightarrow$ measured from experiment

the cases examined. Table 5.2 present the computed values of the estimated variance of the strain estimate at the various points of strain measurement indicated in Fig. 5.1. Table 5.3 presents the computed values of the actual variance of the estimation error. As can be seen, in case 0 the match is very close, meaning that the KF provides an accurate estimate of the response and also an accurate estimate of the actual estimation uncertainty. In case 3, which includes errors in the model and the covariance matrices, the KF displays significant error in tracking and significant underestimation of the actual variance of the estimation error.

In order to disaggregate the various source of error we contrast case 0 and case 1. It can be verified that the significant drop in accuracy is solely a product of model error. This can be further confirmed by examining the results of case 2d where the model and the system coincide but there is discrepancy covariance matrices of the

measurement noise and the unmeasured excitation.

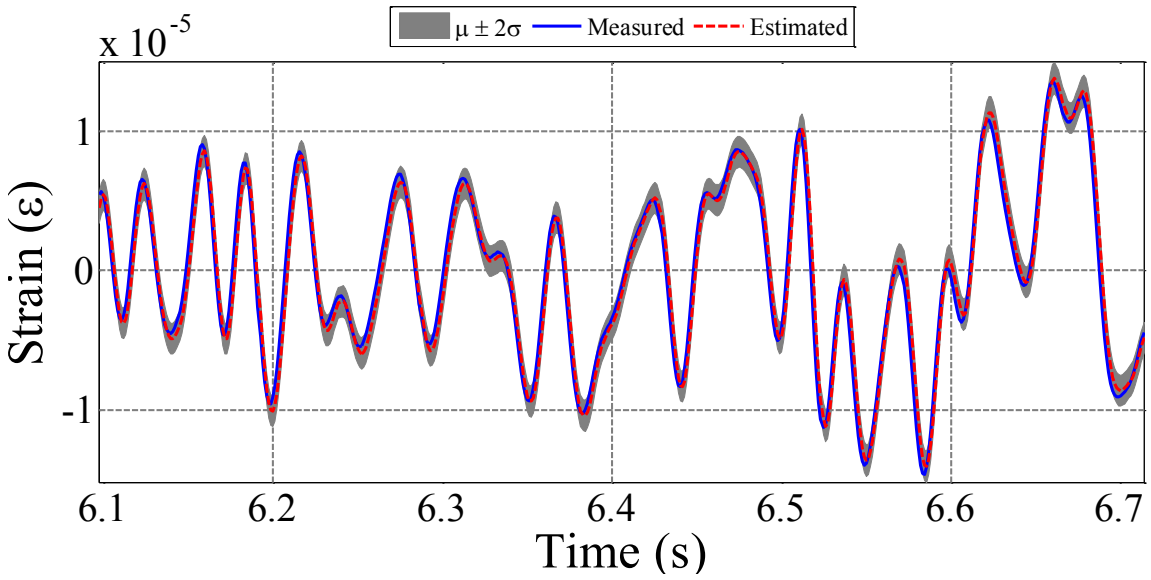

Figure 5.7: Strain estimation Case 0: Location 1

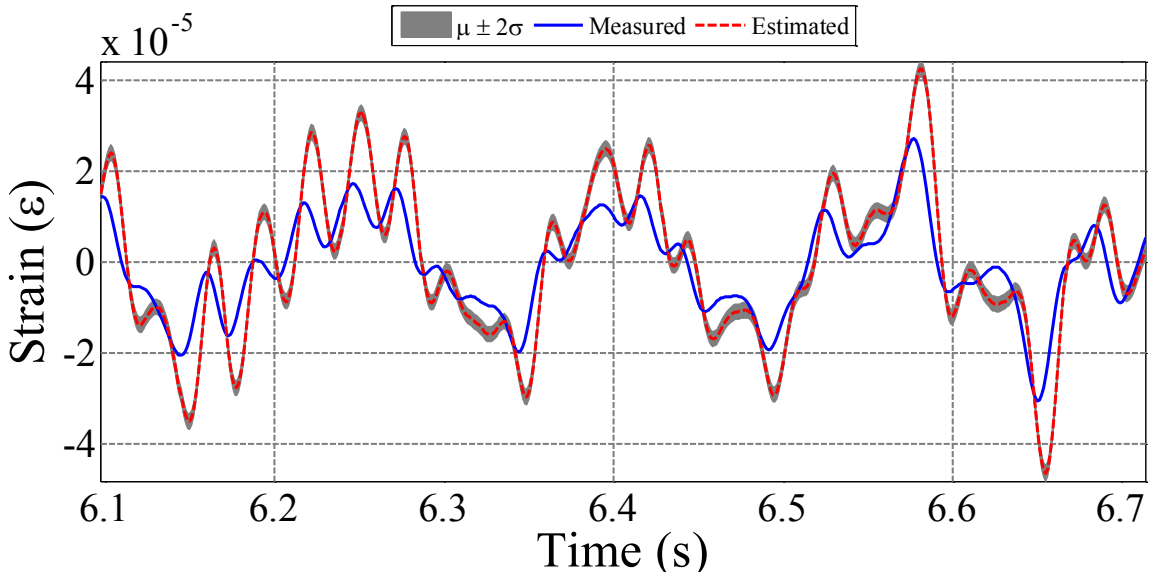

Figure 5.8: Strain estimation Case 1: Location 1

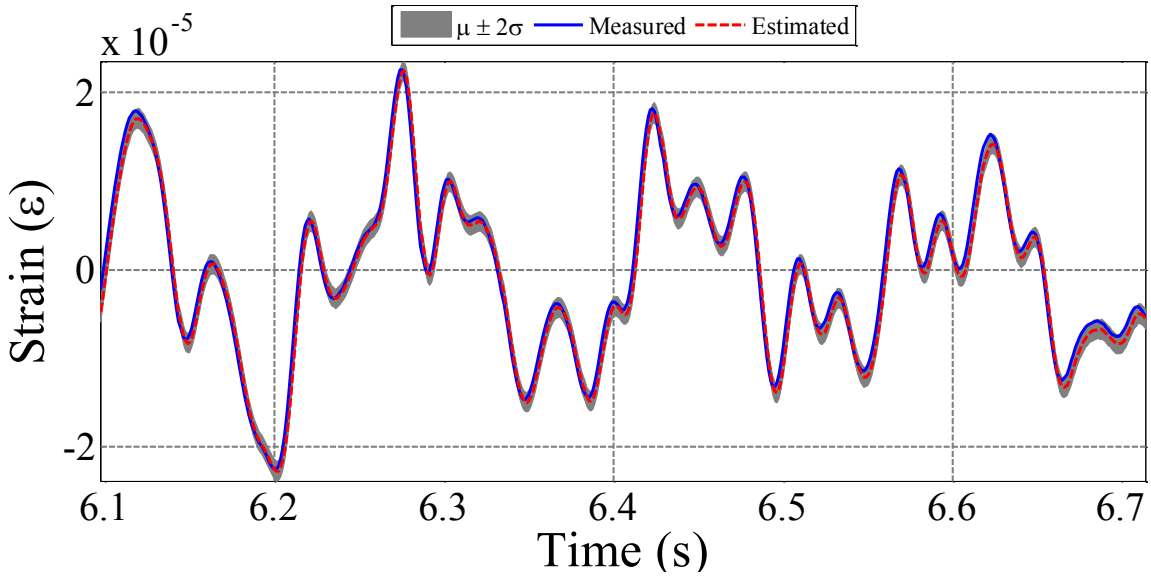

Figure 5.9: Strain estimation Case 2a: Location 1

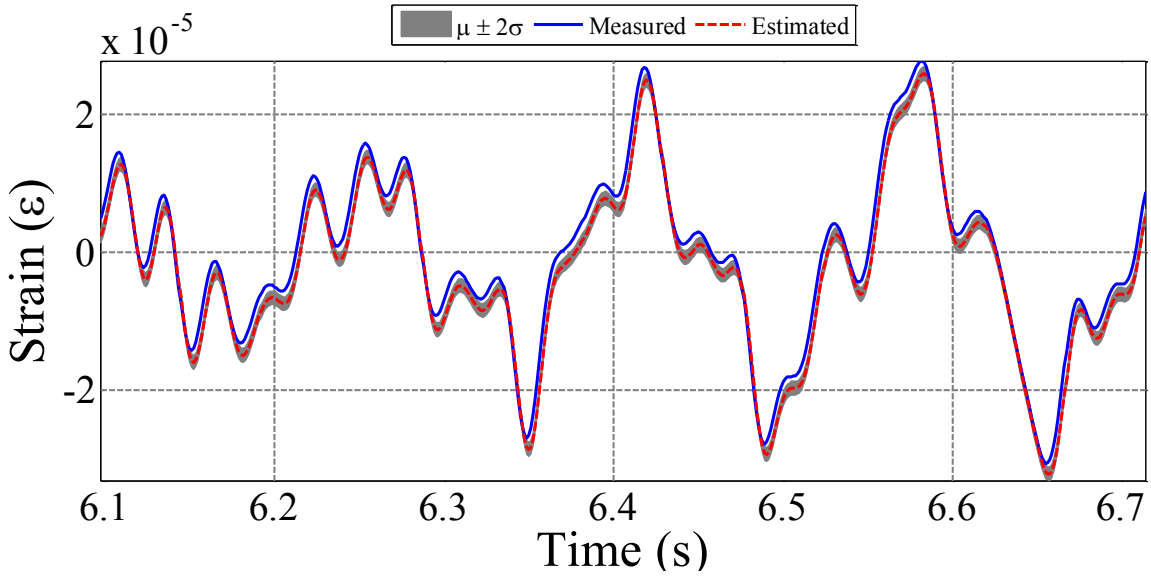

Figure 5.10: Strain estimation Case 2b: Location 1

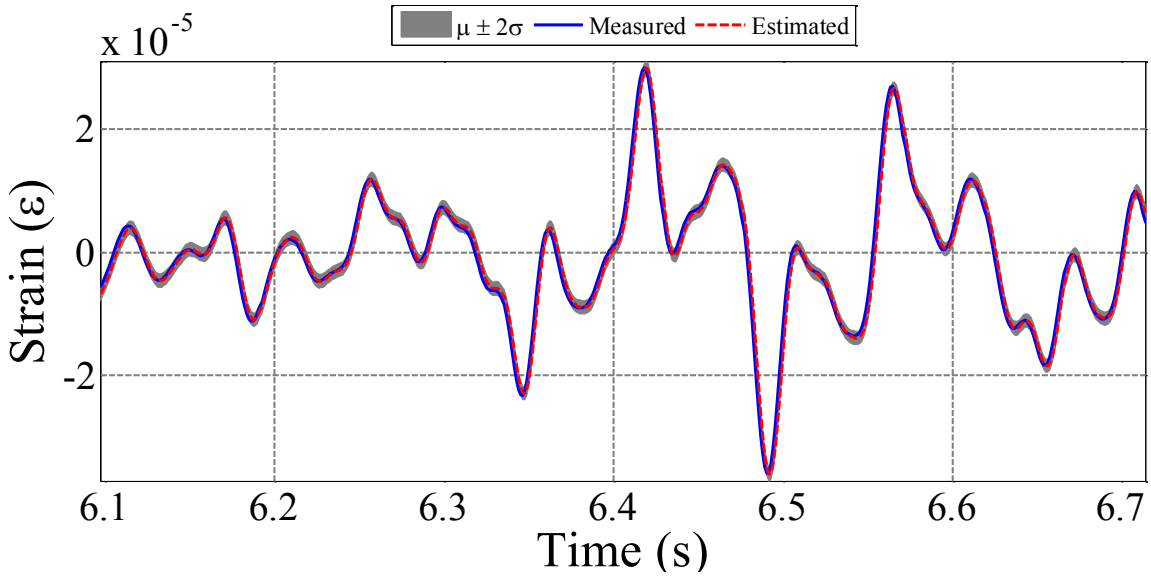

Figure 5.11: Strain estimation Case 2c: Location 1

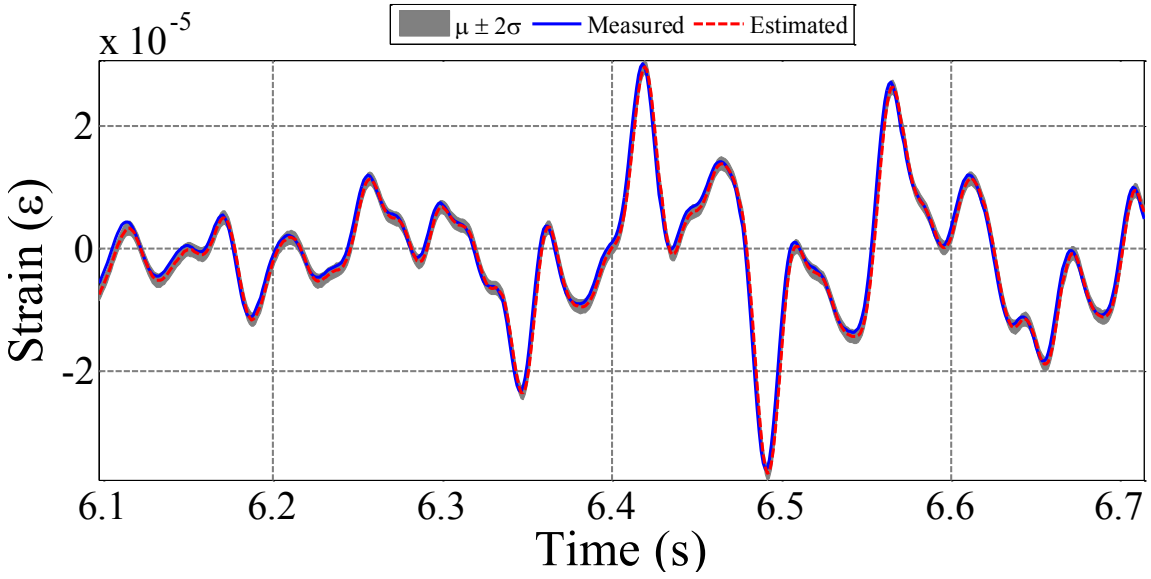

Figure 5.12: Strain estimation Case 2d: Location 1

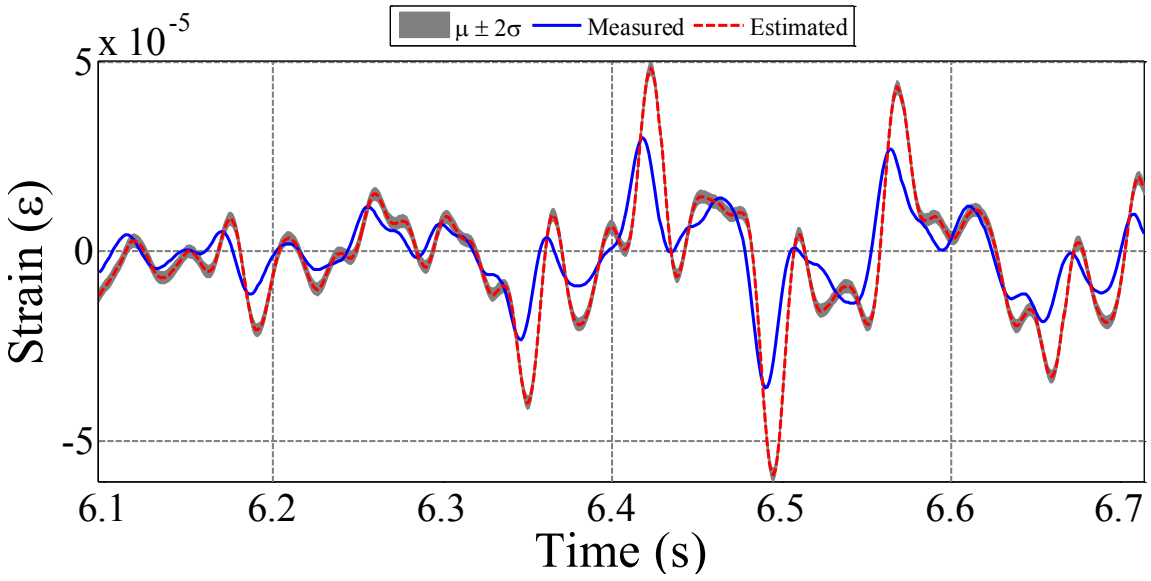

Figure 5.13: Strain estimation Case 2e: Location 1

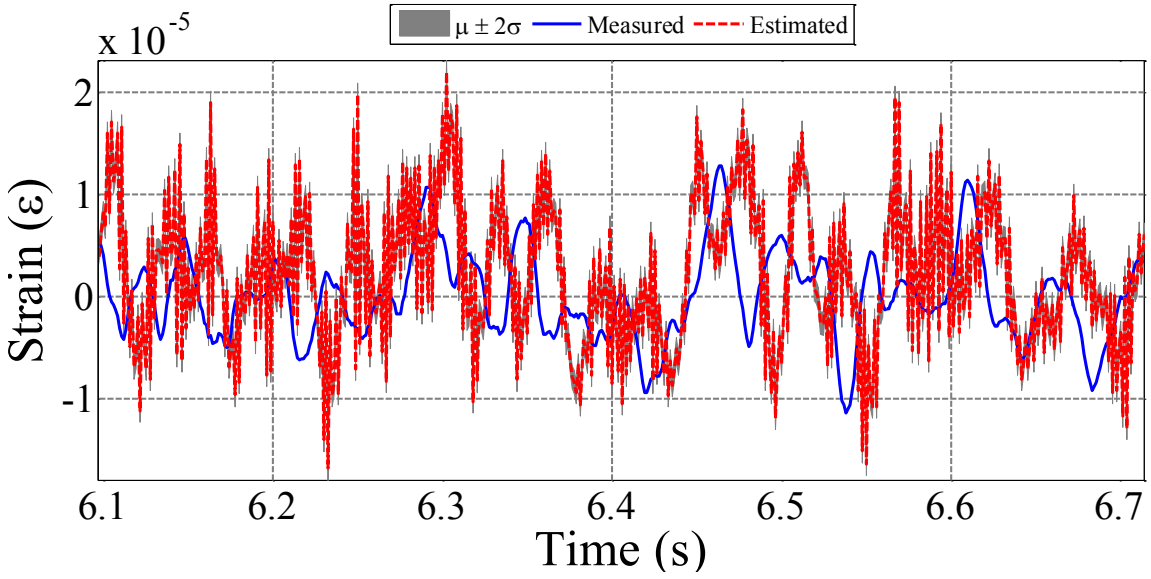

Figure 5.14: Strain estimation Case 3: Location 1

Table 5.2: Strain Error RMS

	Strain RMS error per Case ($*10^{-6}$)							
Loc.	**0**	**1**	**2**$_a$	**2**$_b$	**2**$_c$	**2**$_d$	**2**$_e$	**3**
1	0.57	8.45	0.83	1.66	0.43	0.76	9.39	8.20
2	0.67	3.44	0.97	1.96	0.51	0.90	4.71	7.11
3	1.22	6.21	1.76	3.55	0.92	1.63	8.53	14.11
4	0.42	7.60	0.60	1.21	0.31	0.56	8.69	6.28
5	0.75	5.60	1.09	2.19	0.57	1.01	5.90	9.21
6	1.39	10.34	2.01	4.05	1.05	1.86	10.90	16.93

Table 5.3: KF Estimated Variance

	$STD(\epsilon)$ **per Case ($*10^{-6}$)**							
Loc.	**0**	**1**	**2**$_a$	**2**$_b$	**2**$_c$	**2**$_d$	**2**$_e$	**3**
1	0.56	0.85	0.56	0.51	0.56	0.56	0.85	0.56
2	0.66	0.72	0.66	0.60	0.66	0.66	0.72	0.66
3	1.19	1.30	1.19	1.09	1.19	1.19	1.30	1.19
4	0.41	0.16	0.41	0.37	0.41	0.41	0.16	0.41
5	0.74	0.51	0.74	0.67	0.74	0.74	0.51	0.74
6	1.36	0.95	1.36	1.24	1.36	1.36	0.95	1.36

5.9 Conclusions

The Kalman filter was implemented for strain estimation in a flexible steel structure. The estimated strain can be used as input for fatigue damage models and fatigue

damage can be monitored using only minimal instrumentation. It was found that the KF is robust to errors in the description of the measurement noise and unmeasured excitation; however, we found that modeling errors (within the range of practical engineering models) can have significant detrimental effect in the estimation quality. It was also found that the variance predicted by the KF significantly underestimates the actual estimation variance of strains. Results presented in this paper indicate that there is a need to develop and implement robust methods for filtering vibration measurements in structural dynamics.

5.10 Acknowledgement

The research presented in this work was funded by the National Science Foundation grants CMMI-1453502 and EEC-1342190. The support is gratefully acknowledged.

5.11 Bibliography

[1] A. Halfpenny. A practical discussion on fatigue. nCode TP-0123, 2001.

[2] C. Papadimitriou, C.P. Fritzen, P. Kraemer, and E. Ntotsios, "Fatigue predictions in entire body of metallic structures from a limited number of vibration sensors using Kalman filtering",*J Structural Control and Health Monitoring*, vol. 18, num. 5, pp. 554 - 573, Aug. 2011.

[3] K. Erazo, E.M. Hernandez, "A model-based observer for state and stress estimation in structural and mechanical systems: Experimental validation", Mech. Syst. Signal Process. vol.43, num.1-2, pp. 141-152, Feb. 2014

[4] E.M. Hernandez, D. Bernal and L. Caracoglia, "On-line monitoring of wind-induced stresses and fatigue damage in instrumented structures", *J Structural Control and Health Monitoring*, vol. 20, num. 10, pp. 1291 - 1302, Oct. 2013.

[5] D.C. Lee, J.J. Lee, I.B. Kwon and D.C. Seo, "Monitoring of fatigue damage of composite structures by using embedded intensity-based optical fiber sensors", *J Smart Materials and Struct*, vol. 10, num. 2, pp. 285-292, Oct. 2001.

[6] J. Mohammadi, S.A. Guralnick and R. Polepeddi, "Use of stress range data in fatigue reliability assessment of highway bridges", in *NDT Methods Applied to Fatigue Reliability Assessment of Structures* J. Mohammadi Ed., REston, VA: ASCE, 2004, pp. 56-71.

[7] C.P. Fritzen, M. Klinkov and P. Kraemer, "Vibration-based damage diagnosis and monitoring of external loads" in *New Trends in Structural Health Monitoring* W.Ostachowicz and J.A. Guemes Eds. New York, NY: Springer, 2013, pp. 149-208.

[8] C. Lalanne, *Fatigue Damage* New York, NY: Taylor and Francis, 2002, p.351.

[9] Jer-Nan Juang (1944). Applied system identification. PTR Prentice Hall.

[10] D. Bernal, "Optimal discrete to continuous transfer for band limited inputs", *J of Eng Mechanics*, vol. 133, num. 12, pp. 1370-1377, Dec. 2007.

[11] D. Simon (2006). Optimal State Estimation. Wiley and Sons, Hoboken, NJ.

Chapter 6

Conclusions

The research in this dissertation addresses the implications of model uncertainty to system identification, parameter estimation, and state estimation. Specifically, determining the highest achievable accuracy in the presence of measurement noise, unmeasured excitations, environmental conditions, and model class selection.

6.0.1 Intellectual Contributions

- Exact expressions to compute the lowest achievable variance by any unbiased estimator of modal frequency and damping ratio from free vibration and forced vibration signals contaminated by additive Gaussian white noise. These limits are found through the Cramer-Rao lower bound theory. The results were obtained for displacement or acceleration measurements contaminated with zero-mean additive Gaussian white noise.

  The expressions were derived for single degree of freedom systems and heuristically extended to classically damped multi-degree of freedom systems with well

separated modes. It was proved that the coefficient of variation of identified modal damping ratio must be significantly higher that the coefficient of variation of identified modal frequency. The results were confirmed via simulated system identification using subspace identification methods. It was found by means of simulation that if the identified model does not explicitly account for the noise in the measurements, then in order to reach (or come close) to the CRLB it is necessary to increase the size of the identified system to a size significantly larger that the underlying size of the system of interest. It was also found that in the case of multi-degree of freedom systems, the CRLB of different modes can vary appreciably depending on the signal-to-noise ratio of the individual modes. We also derived an expression that aids in the decision to use acceleration measurements or displacements measurements.

- A model updating methodology that accounts for the variability of environmental conditions to estimate the level of composite action in a full scale operational bridge deck. We present recent developments in the feasibility of using global acceleration measurements to assess the level of composite action on operational bridge decks with unknown girder-slab connection stiffness. Our efforts focused on the 58N Bridge constructed in 1963 and located on Interstate 89 in Richmond, Vermont, United States. The Bridge has a three-span continuous deck with buildup outer girders spanning a total length of 558 feet (170.08 m). A portion of the bridge deck was monitored with uni-directional accelerometers and dynamic strain sensors distributed at various locations. Intermittently, for over two years, with measured temperatures ranging from $15°F$ to $87°F$, data was acquired. As a result, we achieved improved structural behavior was ob-

tained (static and dynamic) with an improved matching between predictions and measurements to those of the original model.

The proposed methodology was verified by means of numerical simulations in two models that varied in size and complexity. The first model was a 2D FEM of an isolated stringer in a bridge deck. The second model was a 3D FEM of a deck substructure. For each model, various levels of composite action were considered. In all cases, the modal features were selected as a subset of the system eigenvalues and the procedure accurately updates the model parameters related to composite action. We show that structural model parameters, the elastic modulus of concrete and the rigidity per linear meter of rigid links, are distinguishable based on the first five modal frequencies of the bridge deck's model. We verify this with 2D and 3D models of the deck and considering various levels of composite action.

The variability of the identified data features was accounted in the model updating procedure by means of a weighting matrix (inversely proportional to the variance of the identified frequencies). As expected, identified modal frequencies varied significantly from summer to winter and thus two separate analysis were conducted, one with the complete data set and the other with a reduced data set which included only the summer months.

A limitation of the proposed model updating approach (which is independent of the type of sensing used) is that only stiffness of the deck can be assessed and not much can be learned regarding its ultimate static capacity. This is because various types of shear connectors can provide similar stiffness but display very different post-yielding behavior. Nevertheless, if the interest is the formulation

of a finite element model that can be used as a base-line model for stress analysis (say for fatigue life estimation and(or) load distribution factors) then the proposed model updating approach would prove useful.

- The Kalman filter was implemented for strain estimation in a flexible steel structure. The estimated strain can be used as input for fatigue damage models and fatigue damage can be monitored using only minimal instrumentation. It was found that the KF is robust to errors in the description of the measurement noise and unmeasured excitation. However, we found that modeling errors (within the range of practical engineering models) can have significant detrimental effect in the estimation quality. It was also found that the variance predicted by the KF significantly underestimates the actual estimation variance of strains. Results indicate that there is a need to develop and implement robust methods for filtering vibration measurements in structural dynamics.

6.0.2 Broader Impacts

The research presented in this dissertation can be extended and has the following broader impacts:

- The Cramér-Rao Lower Bound (CRLB), obtained for modal frequency and damping ratio of structural systems, could be applied to any other second order system. This includes electrical, mechanical, and biological systems.

- The dissertation develops computational tools that will improve the fatigue life assessment of a structure by updating a high fidelity finite element model and thus reducing the uncertainty in its response to time-varying loads.

6.0.3 Future Work

The following aspects remain open for future research:

- *Uncertainty and estimation of model parameters in non-linear systems:* We focused on structural systems that can be modelled with linear time invariant equations of motion. Further studies need to be applied to parameter estimation and their uncertainty in systems that experience elasto-plastic type cyclic loading, represented with hysteresis models (like the Bouc-Wen model). Can the CRLB theory be extended to systems with nonlinear behavior?

- *Development and implementation of robust methods for filtering in structural dynamics:* Classical filters can be easily applied for state estimation in structural dynamics; yet their initial and operating conditions of are not clearly transferable. For simple cases, deviations of these can still provide adequate results. The implementation of more robust methods (extended Kalman Filter, Unscented Kalman Filter, Robust Kalman Filter, etc.) could provide a better tracking of the state estimate and its uncertainty in the presence of practical modeling errors in structural engineering. Although this aspect has been examined by some authors, significant work remains on the subject.

Bibliography

[AASHTO/AWS D1.5; 2002] Bridge Welding Code. *Report :FHWA-HIF-19-088. Infrastructure Office of Bridges and Structures*.

[AASHTO LRFD; 2010] American Association of State Highway and Transportation Officials (2010). *LRFD Bridge Design Specifications*, Washington, D.C.

[Adhikari & Woodhouse; 2001] Adhikari, S. & Woodhouse, J. (2001). Identification of Damping: Part 1, Viscous Damping. *Journal of Sound and Vibration*, 243(1):43-61.

[Adhikari et. al.; 2009] Adhikari, S., Friswell , M. I., Lonkar, K. & A. Sarkar (2009). Experimental case studies for uncertainty quantification in structural dynamics. *Probabilistic Engineering Mechanics*, 24:473-492.

[ASCE Infrastructure Report Card; 2017] merican Society of Civil Engineers. *2017 Infrastructure Report Card*. `https://www.infrastructurereportcard.org/`.

[Au; 2014] Au, S. K. (2014). Uncertainty law in ambient modal identification-Part I: Theory. *Mechanical Systems and Signal Processing*, 48(1-2) 15-33.

[Balageas et. al.; 2006] Editor(s): Balageas, D., Fritzen, C.P. & Güemes, A. (2006). *Structural Health Monitoring*. ISTE Ltd.

[Beck & Katafygiotis; 1998] Beck, J. L. & Katafygiotis, L. S. (1998). Updating models and their uncertainties I: Bayesian statistical framework. *ASCE Journal of Engineering Mechanics*, 124(4):455-461.

[Bernal; 2007] Bernal, D. (2007). Optimal discrete to continuous transfer for band limited inputs. *J of Eng Mechanics*, vol. 133, num. 12, 1370-1377.

[Bernal et. al; 2013] Bernal, D., Dohler, M., Mozaffari-Kojidi, S., Kwan, K. & Liu, Y. (2013). First mode damping ratios for buildings. *Earthquake Spectra*, doi: 10.1193/101812EQS311M.

[1] Breña, S., Jeffrey, A., & Civjan, S. (2013). Evaluation of a Noncomposite Steel Girder Bridge through Live-Load Field Testing. *J. Bridge Eng.*, 18(7), 690-699.

[Chakraborty & DeWolf; 2006] Chakraborty, S. & DeWolf, J. (2006). Development and implementation of a continuous strain monitoring system on a multi-girder composite steel bridge. *ASCE Journal of Bridge Engineering*, 11(6): 753-762.

[Chen & Duan; 1999] Chen, W-F. & Duan, L. (1999). *Bridge Engineering Handbook*. CRC Press, N.Y.

[Cook & Young; 1999] ook, R. D. & Young, W. C. (1999). *Advanced Mechanics of Materials*, 2nd Edition, Pearson.

[Dall′Asta; 2001] Dall′Asta, A. (2001). Composite beams with weak shear connection. *International Journal of Solids and Structures*, 38, 5605-5624.

[Deraemaeker et. al.; 2010] Editor(s): Deraemaeker, A. & Worden, K. (2010).. New Trends in Vibration Based Structural Health Monitoring, *Part of the CISM Courses and Lectures book series*, (CISM, volume 520).

[Doebling et. al.; 1996] Doebling, S.W., Farrar, C.R. Prime, M.B. & Shevitz, D.W. (1996). Damage Identification and Health Monitoring of Structural and Mechanical Systems From Changes in their Vibration Characteristics: A literature Review. *Los Alamos National Laboratory report LA-13070-MS*.

[Doebling et. al.; 1998] Doebling, S. W.; Farrar, C.; Prime, M.B. & Sehvitz, D.W. (1998). A Review of Damage Identification Methods that Examine Changes in Dynamic Properties. *Shock and Vibration Digest*, 30(2):91-105.

[Döhler et. al.; 2011] Döhler, M., Hille, F., Lam , X., Mevel, L. & Rucker, W. (2011). Confidence intervals of modal parameters during progressive damage test. *Proc. Soc. Exp. Mech.*, 237-250.

[Döhler et. al.; 2013] Döhler, M., Lam , X-B. & Mevel (2013). Uncertainty quantification for modal parameters from stochastic subspace identification on multi-setup measurements. *Mechanical Systems and Signal Processing*, 36(2):562-581.

[Erazo & Hernandez; 2013] Erazo, K. & Hernandez, E. M. (2013). A model-based observer for state and stress estimation in structural and mechanical systems: Experimental validation. *Mech. Syst. Signal Process*, 43(1-2):141-152.

[Eykhoff; 1974] Eykhoff, P. (1974). *System Identification: parameter and state estimation*. John Wiley and Sons Inc., New York, N.Y.

[Farrar & Lieven; 2007] Farrar, C. & Lieven, N. A. J. (2007). Damage prognosis: The future of structural health monitoring. *Philosophical transactions. Series A, Mathematical, physical, and engineering sciences*, 365(1851):623-32.

[Farrar & Worden; 2007] Farrar, C.R. & Worden K. (2007). An introduction to structural health monitoring. *Philosophical transactions. Series A, Mathematical, Physical, and Engineering Sciences*, 365(1851), 303-315.

[Fox & Kapoor; 1968] Fox, R. L. & Kapoor, M. P. (1968). Rates of change in eigenvalues and eigenvectors. *American Institute of Aeronautics and Astronautics Journal*, 6(12): 2426-2429.

[Friswell & Mottershead; 1995] Friswell, M.I. & Mottershead, J. E. (1995). Finite Element Model Updating in Structural Dynamics. *Kluwer Academic Publishers, Dordrecht.*

[Fritzen et. al.; 2013] Fritzen, C.P., Klinkov, M. & Kraemer, P. (2013). Vibration-based damage diagnosis and monitoring of external loads. *New Trends in Structural Health Monitoring* Ostachowicz, W. & Guemes, J.A. Eds. New York, NY: Springer, 149-208.

[Gersch; 1974] Gersch, W. (1974). On the achievable accuracy of structural system parameter estimates. *Journal of Sound and Vibration*, 34(1) 63-79.

[Girhammar & Pan; 1993] Girhammar, U. A. & Pan, D. (1993). Dynamic analysis of composite members with interlayer slip. *International Journal of Solid and Structures*, 30(6):797-823.

[Grebici et al.; 2008] Grebici, K., Goh, Y. M., & McMahon, C. (2008). Uncertainty and risk reduction in engineering design embodiment processes. *10th International Design Conference, Dubrovnik, Croatia, Product development models and strategies*, 143-156.

[Griffith & Carne; 2007] Griffith, D. T. & Carne, T. G. (2007). Experimental uncertainty quantification of modal test data. *Proc. of the XXV International Conference in Modal Analysis.*

[Halfpenny; 2001] Halfpenny, A. (2001). A practical discussion on fatigue. *nCode TP-0123.*

[Hernandez et. al.; 2013] Hernandez, E. M., Bernal, D. & Caracoglia, L. (2013). Online monitoring of wind-induced stresses and fatigue damage in instrumented structures. *J Structural Control and Health Monitoring*, vol. 20, num. 10, pp. 1291-1302.

[Hernandez & May; 2013] Hernandez, E. M. & May, G. (2013). Vibration Monitoring and Load Distribution Characterization of I-89 Bridge 58N. *Proceedings of the XXXI International Modal Analysis Conference (IMAC)*, Orange County, CA.

[Hernandez & Polanco; 2014] Hernandez, E.M. & Polanco, N. R. (2014). Uncertainty Quantification of Identified Modal Parameters Using the Fisher Information Criterion. *XXXII Proceedings of the International Conference in Modal Analysis - Model Validation and Uncertainty Quantification*, Volume 3, 177-184.

[Jauregui et. al.; 2002] Jauregui, D. V., Yura J. A., Frank, K. H., & Wood, S. L. (2002). Field evaluation of decommissioned non-composite steel girder bridge. *ASCE Journal of Bridge Engineering*, 7(1): 39-49.

[Juang; 1994] Juang, J-N. (1994). *Applied system identification*, PTR Prentice Hall.

[Kalman; 1960] Kalman, R. E. (1960). A new approach to linear filtering and prediction problems. *Transactions of the ASME-Journal of Basic Engineering*, 82 (Series D):35-45.

[Karlsson et. al.; 2000] Karlsson, E., Söderström, T. & Stoica, P. (2000). The Cramer-Rao lower bound for noisy input-output systems. *Signal Processing*, 80:2421-2447.

[Kay; 1993] Kay, S. M. (1993). *Fundamentals of Statistical Signal Processing: Estimation theory*. Prentice Hall. Upper Saddle River, NJ.

[Kim & Nowak; 1997] Kim, S. & Nowak, A.S. (1997). Load distribution and impact factors for I-girders bridges. *ASCE Journal of Bridge Engineering*, 2(3): 97-104.

[Kown et. al.; 2009] Kwon, G., Engelhardt, M.D. & Klingner, R.E. (2009). Strengthening bridges by developing composite action in existing non-composite bridge girders. *Structural Engineering International, International Association for Bridge and Structural Engineering*, 19(4): 432-437.

[Lalanne; 2012] Lalanne, C. (2002). *Fatigue Damage*. New York, NY: Taylor and Francis.

[Ljung; 1999] Ljung, L. (1999). *System Identification*, Prentice Hall. Upper Saddle River, NJ.

[Maia & Silva; 1997] Maia, N. M. & Silva, J. M. (Eds.). (1997). *Theoretical and Experimental Modal Analysis*. Research Studies Press Ltd. Hertfordshire, England.

[MathWorks] System Identification Toolbox. *MATLAB*. http://www.mathworks.com/products/sysid/.

[McHenry & Rolfe; 1980] McHenry, H. I. & Rolfe, S. T. (1980). *Fracture Control Practices for Metal Structures*, National Bureau of Standards Report NBSIR 79-1623.

[Mehra; 1974] Mehra, R. K. (1974). Optimal inputs or linear systems input identification. *IEEE Trans. Autom. Control*, 19(3): 192-200.

[Mehra; 1974] Mehra, R. K. (1974). Optimal input signals for parameter estimation in dynamical systems - Survey and results. *IEEE Trans. Autom. Control*, 19(6): 753-768.

[2] Mohammadi, J., Guralnick, S. A. & Polepeddi, R. (2004). Use of stress range data in fatigue reliability assessment of highway bridges. *NDT Methods Applied to Fatigue Reliability Assessment of Structures*, VA: ASCE, 2004, pp. 56-71.

[Mohsen & Cekecek; 2000] Mohsen, H. A. & Cekecek, E. (2000). Thoughts on the use of Axiomatic Design with the product development process. *First International Conference on Axiomatic Design*.

[Morassi & Rocchetto; 2003] Morassi, A. & Rocchetto, L. (2003). A damage analysis of steel-concrete composite beams via dynamic methods: Part I, experimental results. *Journal of Vibration and Control*, (9):507-527.

[Mottershead et. al.; 2010] Mottershead, J. E., Link, M. & Friswell, M. I. (2010). The sensitivity method in finite element model updating: A tutorial. *Mechanical Systems and Signal Processing*, 25, 7, 2275-2296.

[National Bridge Inventory; 2019] (2019). *National Bridge Inventory* U.S. Department of Transportation. Federal Highway Administration. https://www.fhwa.dot.gov/bridge/britab.cfm.

[NASA SP-8057; 1972] NASA SP-8057 (1972). *Structural Design Criteria Applicable to a Space Shuttle*.

[Newark et. al.;1951] Newmark, N. M., Siess, C. P. & Viest, I. M. (1951). Test and analysis of composite beams with incomplete interaction. *Proceedings of the Society of Experimental Stress Analysis*, 9(1): 75-92.

[Nguyen et. al.; 1998] Nguyen, N. T., Oehlers, D. J. & Bradford, M. A. (1998). A rational model for the degree of interaction in composite beams with flexible shear connectors. *Mechanics of Structures and Machines*, 26(2):175-194.

[Oehlers & Sved; 1995] Oehlers, D. J. & Sved, G. (1995). Composite beams with limited slip capacity shear connectors. ASCE Journal of Structural Engineering, 121(6):932-938.

[Oehlers et. al.; 1997] Oehlers, D. J., Nguyen, N. T., Ahmed, M. & Bradford, M.A. (1997). Partial Interaction in Composite Steel and Concrete Beams with Full Shear Connection. *Journal of Constructional Steel Research*, 41(2/3):235-248.

[Overschee & De Moor; 1996] Van Overschee, P. & De Moor, B. (1996). *Subspace Identification for Linear Systems: Theory.* Kluwer Academic Publications.

[Papadimitriou et. al.; 2011] Papadimitriou, C., Fritzen, C. P., Kraemer, P. & Ntotsios, E. (2011). Fatigue predictions in entire body of metallic structures from a limited number of vibration sensors using Kalman filtering. *J Structural Control and Health Monitoring*, vol. 18, num. 5, pp. 554-573.

[Pintelon & Schoukens; 1996] Pintelon, R. & J. Schoukens (1996). *System Identification: A frequency domain approach*, 2^{nd} Edition.

[Pintelon et. al.; 2007] Pintelon, R., Guillaume, P. & Schoukens, J. (2007). Uncertainty calculation in operational modal analysis. *Mechanical Systems and Signal Processing*, 21(6) 2359-2373.

[Poncelet; 1870] Poncelet, J. V. (1870). *Introduction à la mécanique industrielle physique ou expérimentale*, Paris:Gauthier-Villars.

[Proakis & Salehi; 2005] Proakis, J. G. & Salehi, M. (2005). *Fundamentals of Communication Systems*. Pearson, Prentice Hall. Upper Saddle River, NJ.

[Lee et. al.; 2001] Lee, D. C., Lee, J. J., Kwon, I. B. & Seo, D. C. (2001). Monitoring of fatigue damage of composite structures by using embedded intensity-based optical fiber sensors, *J Smart Materials and Struct*, vol. 10, num. 2, pp. 285-292.

[Ranzi; 2006] Ranzi, G., Gara, F., Leoni, G. & Bradford, M. A. (2006). Time analysis of composite beams with partial interaction using available modelling techniques: A comparative study. *Computers and Structures*, 84, 930-941.

[Report $MN/RC-2001-10$] (2001). Minnesota Department of Transportation. Fatigue Evaluation of the Deck Truss of Bridge 9340 (Report). *Report* $MN/RC-2001-10$, Minnesota Local Road Research Board.

[Reynders et. al.; 2008] Reynders, E., Pintelo, R. & De Roeck, G. (2008). Uncertainty bounds on modal parameters obtained from stochastic subspace identification. *Mechanical Systems and Signal Processing*, 22(4) 948-969.

[Rytter; 1993] Rytter, A. (1993). Vibration based inspection of civil engineering structures. *Ph.D. Dissertation*, Department of Building Technology and Structural Engineering, Aalborg University, Denmark.

[Salmon & Johnson; 1996] Salmon, C. & Johnson, J. (1996). *Steel Structures*, 4th edition. Prentice Hall. Upper Saddle River, N.J.

[Schultz et al.; 2010] Schultz, M. T., Mitchell, K. N., Harper, B. K., & Bridges, T. S. (2010). *Decision Making Under Uncertainty*, ERDC TR-10-12. US Army Corps of Engineers - Engineer Research and Development Center.

[Shannon ; 1948] Shannon, C.E. (1948). A Mathematical Theory of Communication. *The Bell System Technical Journal*, 27:379-423.

[Simon; 2006] Simon, D. (2006). *Optimal State Estimation*. Wiley and Sons, Hoboken, NJ.

[Sohn, et. al.; 2004] Sohn, H., Farrar, C. R., Hemez, F. M., Shunk, D. D., Stinemates, D. W., Nadler, B. R., & Czarnecki, J. J. (2004). *A Review of Structural Health Review of Structural Health Monitoring Literature 1996-2001*, United States.

[Söderström & Stoica; 1989] Söderström, T. & Stoica, P. (1989). *System Identification.* Prentice-Hall, Englewood Cliffs.

[Staszewski & Worden; 2009] Staszewski, W. J. & Worden. K. (2009). *Encyclopedia of Structural Health Monitoring*. Editors: Boller, C. Chang, Fu-Kuo. & Fujino, Y. John Wiley & Sons, Ldt.

[Stelling et. al.; 2004] Stelling, J., Sauer, U., Szallasi, Z., Doyle, F.J. 3rd, & Doyle, J. (2004). Robustness of cellular functions. *Cell*, 118(6):675-85.

[Sundararajan; 1995] Sundararajan, C. (1995). *Probabilistic Structural Mechanics Handbook: Theory and Industrial Applications*. Chapman & Hall.

[Udwadia; 1994] Udwadia, F. E. (1994). Methodology for Optimum Sensor Locations for Parameter Identification in Dynamic Systems. *ASCE Journal of Engineering Mechanics*, 120(2):368-390.

[Vander Heyden et al.; 2001] Vander Heyden, Y., Nijhuis, A., Smeyers-Verbeke, J., Vandeginste, B. G., & Massart, D. L. (2001).Guidance for robustness/ruggedness tests in method validation. *Journal of pharmaceutical and biomedical analysis*, 24(5-6), 723-753.

[Wigren & Nehorai; 1991] Wigren, T. & Nehorai, A. (1991). Asymptotic Cramer-Rao bounds for estimation of the parameters of damped sine waves in noise. *IEEE Transactions on Signal Processing*, 39(4) 1017-1020.

[Wolfram Research, Inc.; 2010] Wolfram Research, Inc. (2010). *Mathematica*, Version 8.0, Champaign, IL (2010).

[Worden & Dulieu-Barton; 2004] Worden, K. & Dulieu-Barton, J. M. (2004). An overview of intelligent fault detection in systems and structures. *Structural Monitoring*, 3, 85-98.

[Zárate & Caicedo; 2008] Zárate, B. A. & Caicedo, J. M. (2008). Finite element model updating: Multiple alternatives. *Engineering Structures*, 30, 3724-3730.